ISAS - INTERNATIONAL SCHOOL FOR ADVANCED STUDIES

CNG and HCN channels: a structure-function analysis

Thesis submitted for the degree of "Doctor Philosophiae"

CANDIDATE
Paola Roncaglia

SUPERVISOR
Prof. Vincent Torre

SISSA - SCUOLA INTERNAZIONALE SUPERIORE DI STUDI AVANZATI
TRIESTE
Via Beirut 2-4

TRIESTE

A Stefano, e a Mara:

alla vita che ci ha uniti.

Declaration

The work described in this dissertation was carried out at the International School for Advanced Studies, Trieste, between October 1997 and December 2000. All work reported, with the exceptions listed below, arise solely from my own experiments and this work has not been submitted in whole or in part to any other University.

The molecular biology experiments regarding the preparation of the cyclic nucleotide-gated channel mutants were carried out in collaboration with Dr Katia Gamel; their electrophysiological characterization was performed in collaboration with Andrea Becchetti.

The plasmids for expressing the wild type forms of the α subunit of the bovine rod cyclic nucleotide-gated channel and of the SpHCN channel were a kind gift of Prof. U.B. Kaupp.

Paola Roncaglia
March 2001

Acknowledgements

Many thanks go to my colleagues Andrea Becchetti and Katia Gamel, for their helpfulness and collaboration in carrying out many experiments; and to Prof. Vincent Torre, for introducing me to electrophysiology and supporting my research with new ideas always.

Also, I'm indebted to many people who have helped me with scientific support, interesting discussions and technical help: my colleagues Alessandro Bisso, Riccardo Brancaleon, Andrea Cavalli, Monica Mazzolini, Giulietta Pinato, Marco Punta, Davide Zoccolan, and Mr Claudio Becciani and Ms Laura Giovanelli at the Galileo Galilei building laboratory and at the SISSA main building; and Jessica Franzot, Roberto Marzari, Gabriella Rossi, Michela Visintin and Paola Zacchi at the SISSA laboratory hosted by ICGEB. My experiments, and the writing of this dissertation, would have been far more difficult without their help.

Very special thanks go to my family and friends, and above all to my parents. They have given me the possibility of improving my abilities, and much of what I've reached in life is owed to them.

But all my deepest gratitude goes to my husband: he has always, constantly, blindly trusted me, and supported me strongly throughout the difficulties of life in general... including the hard times during my PhD research when the experiments were not too collaborative. Thank you for having been at my side for all these years.

TABLE OF CONTENTS

ABBREVIATIONS USED IN THE TEXT

CaM: calmodulin
cAMP: cyclic 3', 5'-adenosine monophosphate
CAP: catabolite activator protein
cDNA: complementary DNA
cGMP: cyclic 3', 5'-guanosine monophosphate
CNBD: cyclic nucleotide-binding domain
CNG: cyclic nucleotide-gated
CNS: central nervous system
CO: carbon monoxide
DAG: diacylglycerol
DAT: digital audio tape
DEPC: diethylpirocarbonate
EAG: ether-à-go-go
EEG: electroencephalogram
EST: expressed sequence tag
GARP: glutamic-acid-rich protein
GCAP: guanylate cyclase-activating protein
GDP: 3', 5'-guanosine diphosphate
GMP: 3', 5'-guanosine monophosphate
GTP: 3', 5'-guanosine triphosphate
HCN: hyperpolarization-activated and cyclic nucleotide-gated
HEPES: (N-2-hydroxyethyl)piperazine-N'-(2-ethanesulfonic acid)
I_{AR}: anomalous rectifying current
I_f: "funny" current
I_h: hyperpolarization-activated current
IP_3: inositol 1, 4, 5-triphosphate
IPSP: inhibitory postsynaptic potential
I_q: "queer" current
I_R: inward rectifying current
IRBP: interphotoreceptor retinol-binding protein
LG: ligand-gated
MTS: methanethiosulfonate
MTSEA: 2-aminoethyl methanethiosulfonate
MTSET: 2-trimethylammonioethyl methanethiosulfonate
NO: nitric oxide
PCM: pulse code modulation
PCR: polymerase chain reaction

PDE: phosphodiesterase
PKA: protein kinase A
PLC: phospholipase C
P_o: open probability
PTDM: protein domain topography model
RPA: RNase protection assay
RPE: retinal pigment epithelium
SCAM: substituted-cysteine accessibility method
SpHCN: *Strongylocentrotus purpuratus* hyperpolarization-activated, cyclic nucleotide-gated channel
VCR: video cassette recorder
VG: voltage-gated
V_{rev}: reversal potential

ABSTRACT

In recent years, growing importance has been given to the studies of genomics and proteomics, the disciplines that collect available knowledge about genomes and proteins and whose main aim is to exploit the usefulness of this information to understand how organisms work and possibly foresee how eventual diseases can be cured. The research on proteins, meant as the essential molecular tools for cellular functioning, has a key role, and can be conducted at various levels, corresponding to the degrees of structural complexity; but the ultimate clue to the comprehension of the molecular mechanisms of polypeptides, from enzymes to receptors and ion channels, resides in their three-dimensional structure. Until recently, for ion channels, due to the difficulties of obtaining crystals, only indirect investigations were possible (e.g., mutagenesis and electrophysiological characterization). Then, in 1998, the structure of the K^+ channel KcsA was determined by x-ray chrystallography (Doyle et al., 1998), and the molecular principles of its conduction and selectivity were explained.

The present research focuses on channels that share relevant features with K^+ channels like KcsA, but differ from them for some important characteristics. Cyclic nucleotide-gated (CNG) channels display a pore region that is homologous to that of K^+ channels, but they are not as selective in the permeation of cations, and their gating is insensitive to voltage, while it requires the direct binding of a ligand (cAMP or cGMP). Hyperpolarization-activated and cyclic nucleotide-gated (HCN) channels, on the other hand, have an even higher affinity in their pore region with K^+ channels, and their selectivity towards cations is intermediate between that of K^+ and CNG channels; like the former, they are voltage-dependent, and their gating is modulated by cyclic nucleotides. CNG channels are fundamental in phototransduction and olfactory transduction where simple electrical stimuli are transferred as flow of information; HCN channels are at the basis of rhythmic activities including the pacemaker mechanisms of cardiac cells, the repetitive firing of neurons and the swimming behaviour of sperm. Within the more general investigation of ion channels structure and function, the aim of my thesis is to elucidate the structure of the pore regions of these proteins, to establish whether these pore regions are similar or not to the one of KcsA, and to gain insights about the molecular characteristics at the origin of the differences with K^+ channels.

In more detail, I have investigated the pore regions of the α-subunit of the CNG channel from bovine retinal rods (brCNGCα) and the HCN channel

from the sperm of the sea urchin (SpHCN). I have used tools of molecular biology (site-directed mutagenesis) and electrophysiology (patch-clamp), and I have heterologously expressed the above mentioned channels in *Xenopus laevis* oocytes. My investigation and the results obtained can be summarized as follows.

1) The topology of the pore region of brCNGCαhas been studied by testing the accessibility to Cd^{2+} of serially substituted cysteine residues, thus extending and completing a previous investigation (Becchetti et al., 1999) and gaining a clearer understanding of the position of important residues close to the selectivity filter possibly involved in gating, and whose localization within the pore loop was not precisely defined yet. My results allow to sketch a three-dimensional model of the brCNGCα pore region which is different from a previously proposed one (Sun et al., 1996).
2) In brCNGCα, the substitution of the glutamate residue in position 363 with a neuter alanine induces desensitization of the channel in presence of a steady ligand concentration (Bucossi et al., 1996). In view of understanding whether channel gating in ligand-gated channels occurs through both local interactions between amino acid residues and global channel rearrangement, this artificial CNG channel desensitization offers useful general clues to study the energetic interactions occurring between residues involved in channel gating. Accordingly, I have investigated eventual major rearrangements in the pore region topology of the mutant channel E363A, by means of the substituted cysteine accessibility method (SCAM). I found that the pore region topology was not disrupted by the mutation, and that the nature of the residues immediately close to position 363 influences the structural rearrangements leading to desensitization.
3) In the pore region of HCN channels, some residues in key positions are different from the homologous ones in most K^+ channels. In particular, the GYG triplet which is the signature sequence of K^+-selective channels is followed by a basic or neuter residue, in place of an acidic one. Also, N-terminal to the same triplet, all HCN channels bear a cysteine residue, in place of a larger threonine or serine. In view of understanding whether these differences may account for the poor cation selectivity of HCN channels and for their regulation by external chloride, the topology of residues C428 and K433 in the SpHCN channel has been investigated. My results indicate that the

pore loop topology resembles the one of KcsA, with residue C428 facing the intracellular side of the membrane and thus being responsible for the block by internal Cd^{2+}, and residue K433 located extracellularly, but with its side chain pointing towards the lipid phase, and being alone not responsible for ion selectivity and for regulation by external chloride.

1) INTRODUCTION

1.1 Cyclic nucleotide-gated (CNG) channels

1.1.1 CNG channels from identification to cloning

Vertebrate rod and cone photoreceptor cells respond to light by closing cation-selective channels in the plasma membrane of their outer segments. Before the mid-1980s, these channels were thought to be regulated only indirectly by cyclic nucleotides, through the action of cyclic nucleotide-dependent protein kinases and channel phosphorylation; then it was found out that in retinal rods cyclic GMP exerts its action in phototransduction upon direct binding to these cation channels (Fesenko et al., 1985; Yau and Nakatani, 1985b). Shortly after, similar findings were done in cone photoreceptors (Cobbs et al., 1985; Haynes and Yau, 1985) and in olfactory receptors (Nakamura and Gold, 1987); in the latter case, channels responded similarly to cAMP and cGMP.

These physiological findings were further confirmed with the isolation, from bovine retina, of a 63 kDa polypeptide (Cook et al., 1987) which forms functional cGMP-gated channels when reconstituted into phospholipid vesicles (Cook et al., 1986) or artificial planar bilayers (Hanke et al., 1988), and above all with the first cloning of the same channel and its heterologous expression (Kaupp et al., 1989). This protein was termed α-subunit and structurally consists in six hydrophobic regions later shown to span the membrane (Henn et al., 1995; for details on CNG channels structure, see section 1.1.4).

It is now clear that ion channels directly activated by cyclic nucleotides are not unique to neurons involved in visual and olfactory transduction: after being cloned from olfactory epithelium (Dhallan et al., 1990; Ludwig et al., 1990; Goulding et al., 1992) and cone photoreceptors (Bonigk et al., 1993), they were also identified in aorta (Biel et al., 1993), kidney (Biel et al., 1994), testis (Weyand, 1994), keratinocytes (Oda et al., 1997) and taste buds (Misaka et al., 1997). CNG channels have also been cloned from invertebrates like mollusks (Sudlow et al., 1993), *D. melanogaster* (Baumann et al., 1994) and *C. elegans* (Coburn and Bargmann, 1996). Moreover, ancillary subunits have been cloned for the rod and olfactory channels. Based on sequence homology to the α-subunit of the rod cGMP-gated channel, a "second" subunit was cloned from the human rod (Chen et al., 1993); this subunit appeared to exist in two different forms of

respectively 70 and 102 kDa, but none of these was found in retinal rod channel preparations. Later, a 240 kDa polypeptide was identified as the authentic β-subunit and was shown to have a bipartite structure (Körschen et al., 1995). The two parts consist in a cytoplasmic amino-terminal segment similar to a glutamic-acid-rich proteins (GARP), with the second part being homologous to the polypeptide previously described (Chen et al., 1993). Like the α-subunit, the second portion of the β-subunit is made of six transmembrane segments, with a pore region, a calmodulin binding site and the cGMP-binding site. Recently, a third subunit was cloned from rat olfactory epithelium (Sautter et al., 1998); it represents an alternative splice form of the β-subunit of the rod CNG channel. Table 1 summarizes the results of the cloning effort so far and provides references for papers.

1.1.2 Role of CNG channels in phototransduction

Light is transferred into electrical signals by rods and cones, which are specialized retinal neurons also called photoreceptors. These are not able to generate action potentials, but respond to light by gradually modifying their membrane potential. Both rods and cones (fig. 1a) have an outer segment, in which phototransduction takes place, an inner segment, containing nucleus and organelles, and a synaptic ending, which contacts bipolar and horizontal cells, using glutamate as a neurotransmitter. The external segments contain many discs which are stacked membranous structures containing the visual pigment rhodopsin; in rods, the discs are enclosed by the plasma membrane, while in cones they consists of infoldings of the plasma membrane (fig. 1a). A rhodopsin molecule is made of a chromophore, the retinal, and a protein component, the opsin. The outer segment membrane contains the cGMP-gated channels and the Na^+/Ca^{2+} exchangers; the presence of cGMP-gated channels has also been admitted in the inner segment as well as in the synaptic endings (Watanabe and Matthews, 1988; Rieke and Schwartz, 1994). The inner segment membrane contains Na^+/K^+ pumps.
The process of phototransduction is illustrated in figs. 1b and 1c. In darkness, the cGMP-gated channels in the outer segment are open and allow a steady "dark current" to enter the photoreceptor cells (Hagins et al., 1970; Baylor et al., 1979): Ca^{2+} and Na^+ ions are entering the cells through the cGMP-gated channels, and Ca^{2+} ions are leaving them via the Na^+/ Ca^{2+} exchangers. Consequently, intracellular Ca^{2+} concentration is around 550 nM (Gray-Keller and Detwiler, 1994). The cells are kept slightly depolarized

Nature of the channel	Species and short name	References
Retinal rod photoreceptor cGMP-gated channel	Bovine rod α	Kaupp et al., 1989
	Chicken rod α	Bönigk et al., 1993
	Human rod α	Dhallan et al., 1992; Pittler et al., 1992
	Mouse rod α	Pittler et al., 1992
	Rat rod α	Barnstable and Wei, 1995
	Dog rod α	Zhang et al., 1997
Retinal cone photoreceptor CNG channel	Bovine cone α	Weyand et al., 1994; Biel et al., 1994
	Chicken cone α	Bönigk et al., 1993
	Human cone α	Yu et al., 1996; Wissinger et al., 1997
Retinal rod photoreceptor cGMP-gated channel, secondary subunit	Bovine rod β	Körschen et al., 1995
	Human rod β	Chen et al., 1993
Olfactory cAMP-gated channel	Bovine olf α	Ludwig et al., 1990
	Mouse olf α	Ruiz et al., 1996
	Rat olf α	Dhallan et al., 1990
	Catfish olf α	Goulding et al., 1992
Olfactory cAMP-gated channel, secondary subunit	Rat olf β	Bradley et al., 1994; Liman and Buck, 1994
Drosophila CNG channel		Baumann et al., 1994
Rabbit aorta CNG channel		Biel et al., 1994
C. elegans CNG channel TAX-2		Coburn and Bargmann, 1996
C. elegans CNG channel TAX-4		Komatsu et al., 1996
Rat taste CNG channel gust α		Misaka et al., 1997
Rat pineal gland CNG channel		Sautter et al., 1997
Lizard parietal eye CNG channel		Finn et al., 1997
Human fetal heart CNG channel		Gong et al., 1998
Limulus CNG channel		Chen et al., 1999

Tab. 1
CNG channels cloned so far.

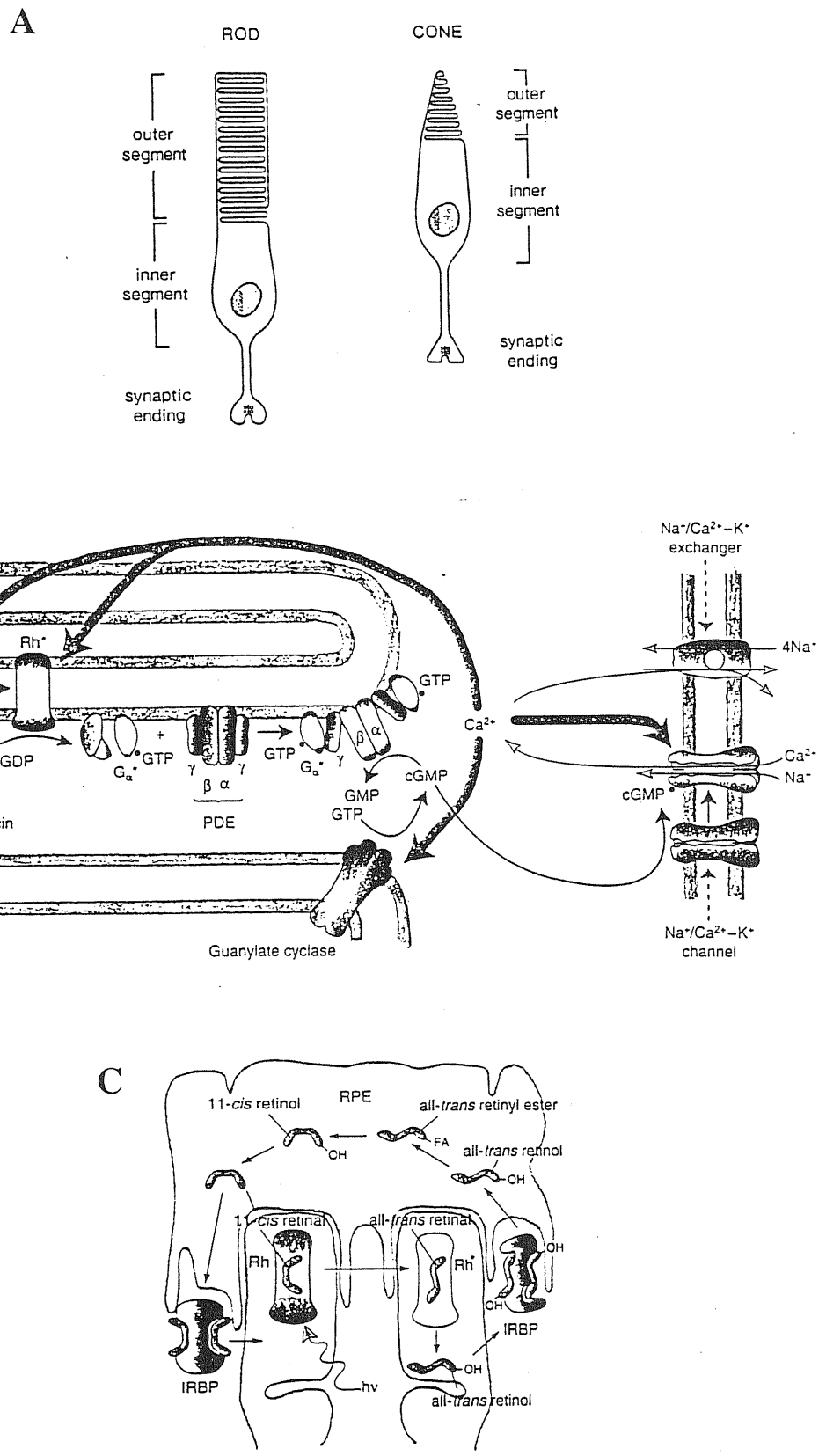

Fig. 1A-C
Photoreceptor cells and phototransduction process.
A Schematic drawing of rod and cone photoreceptor cells (Yau and Baylor, 1989).
B Overview of phototransduction in vertebrates (Fain et al., 1996).
C The visual cycle (Fain et al., 1996).
See the text for detailed descriptions.

with a membrane potential of –40 mV and glutamate is continuously released from the synaptic endings. The absorption of a photon by a rhodopsin molecule causes the conversion of the retinal chromophore from its 11-*cis* stereisomer to its all-*trans* form (Yoshizawa and Wald, 1963; Baylor, 1996). The opsin component of the rhodopsin is subsequently converted to metarhodopsin II (Emeis et al., 1982). This form of phosphorylated rhodopsin exchanges with GTP the GDP which is bound to the α-subunit of a G protein called transducin. In parallel, metarhodopsin II binds to arrestin, a protein which competitively inhibits the binding of transducin to rhodopsin in order to let the transducin free to bind GTP. The substitution of GDP with GTP leads to the transfer of the GTP-α to one of the inhibitory γ-subunit of the phosphodiesterase (PDE), an enzyme which is then able to hydrolyse cGMP into GMP. This reaction is at the origin of the closure of the cGMP-gated channels and thus causes a decrease in the intracellular Ca^{2+} concentration (Yau and Nakatani, 1984).
In saturating light, intracellular Ca^{2+} concentration declines to a minimum value of about 50 nM (Gray-Keller and Detwiler, 1994). The membrane is hyperpolarized and the rate of glutamate release is reduced. In order for a bleached rhodopsin molecule to be able to absorb an eventual other photon, the response to light has to terminate and this involves several steps. Most part of the metarhodopsin II is first converted to metarhodopsin III and the chromophore part of the rhodopsin molecule separates from the opsin component and is converted into retinal. The arrestin which was bound to the metarhodopsin II is removed as well as the phosphate groups. The chromophore is also regenerated: it is transported by an interphotoreceptor retinol-binding protein (IRBP) to the retinal pigment epithelium (RPE) where the retinal, following various enzymatic steps, is converted into 11-*cis* retinal. The chromophore is transported back to the photoreceptor, where it associates with the dephosphorylated form of opsin to give the functional rhodopsin. The transducin molecule regenerates also thanks to an endogenous GTPase activity of the α-subunit which then allows the reunion of the α-subunit to the βγ complex. Without the GTP-α transducin the PDE inactivates and the guanilate cyclase can transform GMP in cGMP and restore the cGMP concentration present in darkness, before the light-triggered cGMP cascade (see Yau and Baylor, 1989; Fain et al., 1996). Recently, glutamic-acid-rich proteins (GARP), which exist as two soluble forms (GARP1 and GARP2) and as a cytoplasmic domain of the rod channel

β-subunit, were shown to interact with the cGMP signaling pathway. GARP2 was shown to potently inhibit PDE (Körschen et al., 1999).
To fulfill their function, photoreceptors must be able to register small changes in light intensity. Thus, it is important to prevent the closure of all cGMP-gated channels when moderate changes of the background light occur. This role is played by Ca^{2+} ions which are involved in a fairly complex mechanism of feedback (Baylor, 1996; Koutalos and Yau, 1996). First, guanilate cyclase is inhibited by Ca^{2+} so that, when the intracellular Ca^{2+} concentration falls down in the presence of light, the hydrolysis of cGMP by PDE is counterbalanced (Lolley and Racz, 1982; Koch and Stryer, 1988). The same role is played by a Ca^{2+}-binding protein termed GCAP for guanylate cyclase-activating protein (Koch and Stryer, 1988; Gorczyca, 1994). Second, at low Ca^{2+} concentration, the shut-off of rhodopsin by phosphorylation is favoured by recoverin (another Ca^{2+}-binding protein) which prevents inhibition of phosphorylation (see Gray-Keller et al., 1993). This action may have an influence on the different steps occurring downstream in the light-triggered cascade (Lagnado and Baylor, 1994). Finally, the cGMP-gated channel is itself a target for Ca^{2+}-dependent feedback through the action of calmodulin (for a review, see Molday, 1996): when activated by Ca^{2+}, calmodulin binds to the N-terminal part of the cGMP-gated channel β-subunit (Weitz et al., 1998) and the apparent affinity of the CNG channel for its ligand decreases. Thus, when intracellular Ca^{2+} concentration decreases in the presence of light, some of the cGMP gated channels tend to reopen. Despite the complexity of Ca^{2+}-dependent channel modulation, the contribution of this feedback process to the overall light adaptation is thought to be rather small (Nakatani et al., 1995).

1.1.3 Role of CNG channels in olfactory transduction

(For a recent review, see Gold, 1999.)
The olfactory epithelium is made of three different cell types: supporting cells, basal cells and olfactory receptor cells (fig. 2a). The supporting cells are involved in the so-called secretion transduction, a mechanism stimulated by odorants and that generates a field potential before the large response occurring in the olfactory receptors. The supporting cells are also involved in the oxidation of odorant molecules in order to make them less membrane permeable. The basal cells are dividing cells that lead to receptor cells upon differentiation. Olfactory receptor cells, whose function is to transduce odorant molecules into membrane depolarization, are bipolar neurons with a

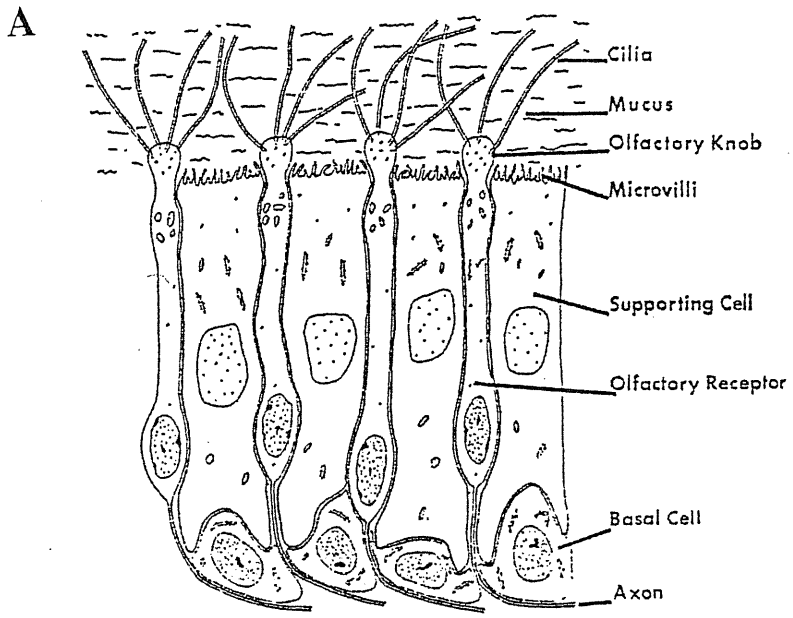

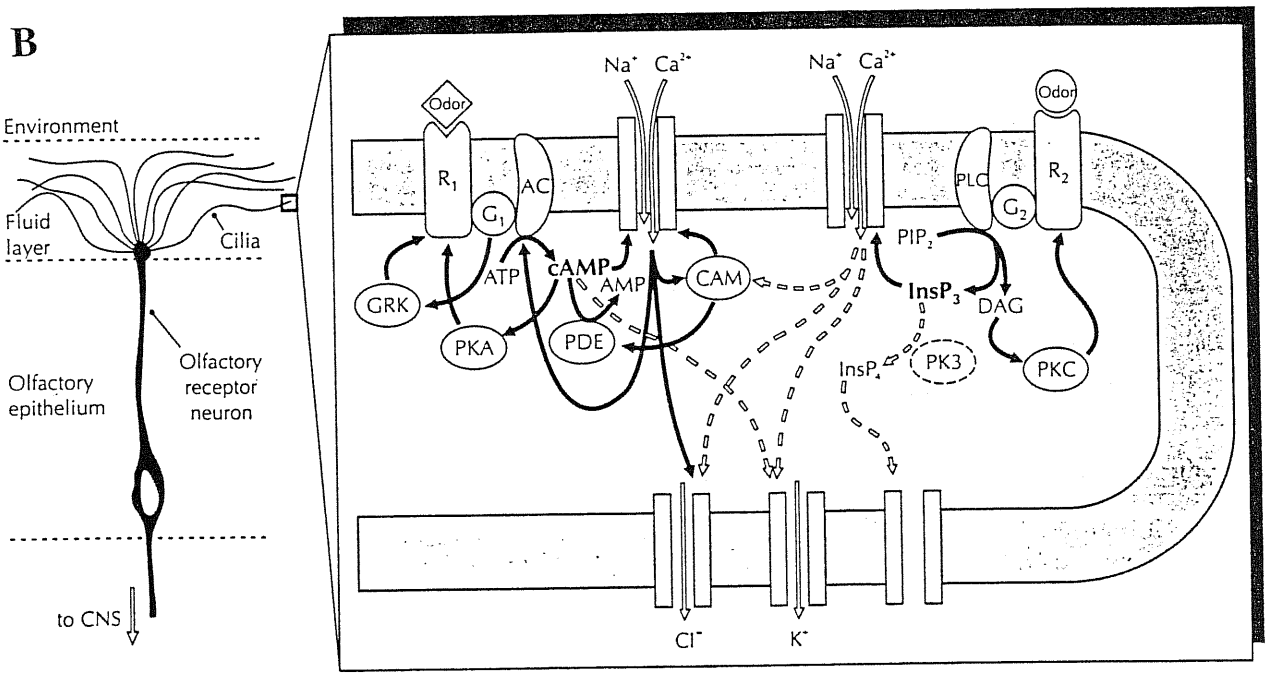

Fig. 2A-B
Olfactory sensory neurons and olfactory transduction.
A Schematic drawing of the olfactory epithelium with its various cell types, including olfactory receptors (Gold, 1999).
B Scheme of the olfactory transduction process (Ache and Zhainazarov, 1995).
See the text for detailed descriptions.

single dendrite that extends to the apical surface of the olfactory epithelium. The tip of the dendrite is the olfactory knob, from which many (10-30) cilia extend into the mucus that covers the olfactory epithelium. The cell body contains the nucleus and is physically not clearly separated from the dendrite; it is then prolonged by a single axon that projects into the olfactory bulb.

In vertebrates, olfactory transduction occurs in the olfactory cilia, which extend in a thin layer of mucus covering the olfactory epithelium and that is exposed to the environment, i.e. to the odorant molecules. This transduction process is generally thought to take place via two different second-messenger pathways (Sklar et al., 1986; for a review, see Ache and Zhainazarov, 1995): the cyclic 3', 5'-adenosine monophosphate (cAMP) transduction pathway and the inositol 1, 4, 5-triphosphate (IP_3) pathway (fig. 2b). According to the cAMP-second messenger model (Buck and Axel, 1991), a subset of odorants activates a subset of receptor proteins which are coupled to the G protein G_{olf}, coupled in turn to adenylate cyclase. The activation of adenylate cyclase leads to a rise in cAMP concentration and to the subsequent opening of CNG channels, and thus to a current of Na^+ and Ca^{2+} ions flowing through these channels. The entry of Ca^{2+} in the olfactory cells results in the activation of a Ca^{2+}-dependent chloride current, which amplifies the primary odour-induced cation current. Mechanisms of odorant adaptation and inactivation in the olfactory receptor cells were first studied *in vitro*, and several possibilities were proposed: phosphorylation of the odour-receptor by protein kinase A (PKA) (Boekhoff and Breer, 1992; Boekhoff et al., 1992), activation of a phosphodiesterase to reduce the cAMP concentration (Borisy et al., 1992), ion channel regulation (Kramer and Siegelbaum, 1992; Chen and Yau, 1994; Lynch and Lindermann, 1994; Balasubramanian et al., 1996). The nature of the olfactory adaptation was later investigated in intact olfactory cells of the newt (Kurahashi and Menini, 1997), and the main mechanism of adaptation was identified as being a regulation of the cAMP-gated channels by a Ca^{2+}-feedback via Ca^{2+}-calmodulin. According to the IP_3 hypothesis (Sklar et al., 1986; Boekhoff et al., 1990; Breer and Boekhoff, 1991), a different subset of odorant molecules would activate a different subset of receptors that couple to phospholipase C (PLC) via a different G protein; PLC then cleaves the membrane phospholipid phosphatidyl inositol, leading to diacylglycerol (DAG) and IP_3. IP_3, which is water soluble, would then activate IP_3-gated Ca^{2+} channels in the ciliary membrane that then mediate Ca^{2+} influx and membrane depolarization. A recent review (Gold, 1999) favors the cAMP-triggered cascade and suggests that this is the only transduction mechanism in

olfactory cells; the author criticizes the sensitivity of the biochemical assays and cilia preparations used when the IP_3 second possible pathway was postulated. A previous study (Lowe et al., 1989) showed that differences observed in the magnitude of cyclase activity (Sklar et al., 1986) was simply reflecting the number of cells activated by each odour. Moreover, knockout mice have been bred for both the cAMP-gated channels (Brunet et al., 1996) and for G_{olf} (Belluscio et al., 1998). In the former case, both the cAMP and IP_3 odorants responses were abolished, suggesting that olfactory transduction depends in any case on the activation of cAMP-gated channels. In the newborn G_{olf} knockout mice, the G protein G_s could substitute the lacking G_{olf}, but G_s expression declines after birth and by the third week of age the responses induced by both cAMP and IP_3 odorants were about 25% of the wild-type ones, arguing for the cAMP-cascade as a majoritary transduction pathway. It has also been suggested that gaseous second messengers such as carbon monoxide (CO; Zufall and Leinders-Zufall, 1997) and nitric oxide (NO; Broillet and Firestein, 1997) produce cGMP and prolong the responses to odorants triggered by cAMP. However, data for CO were obtained for the salamander, and the generalization to humans is controversial; and regarding the NO pathway, the way of activation of NO synthase is still unclear (see Gold, 1999). In brief, the mechanism of olfactory transduction and its modulation are still matter of debate.

1.1.4 Structural features and functional properties of CNG channels: an overview

Ionic channels are assigned to the superfamily of either ligand-gated (LG) channels or voltage-gated (VG) channels depending on their transmembrane organization, quaternary structure and functional properties. CNG channels are activated upon direct binding of either cGMP (Fesenko et al., 1985; Yau and Nakatani, 1985b) or cAMP (Nakamura and Gold, 1987), and are to be considered, functionally, LG channels. However, each subunit of LG channels is composed of four transmembrane segments (Barnard, 1992), instead of the six of CNG channels (Henn et al., 1995), and CNG channels share their overall topology with VG channels, as suggested by sequence homology. In fact, both CNG (fig. 3) and VG channels have six membrane spanning domains with cytoplasmic amino- and carboxi-termini, a positively charged S4 segment, and a pore region located between the fifth and sixth transmembrane domain (see sections 1.1.5 and 1.1.6). As for the quaternary structure, VG channels are homotetrameric assemblies of subunits in the case of K^+ channels, or pseudotetrameric structures in the case of Na^+ and

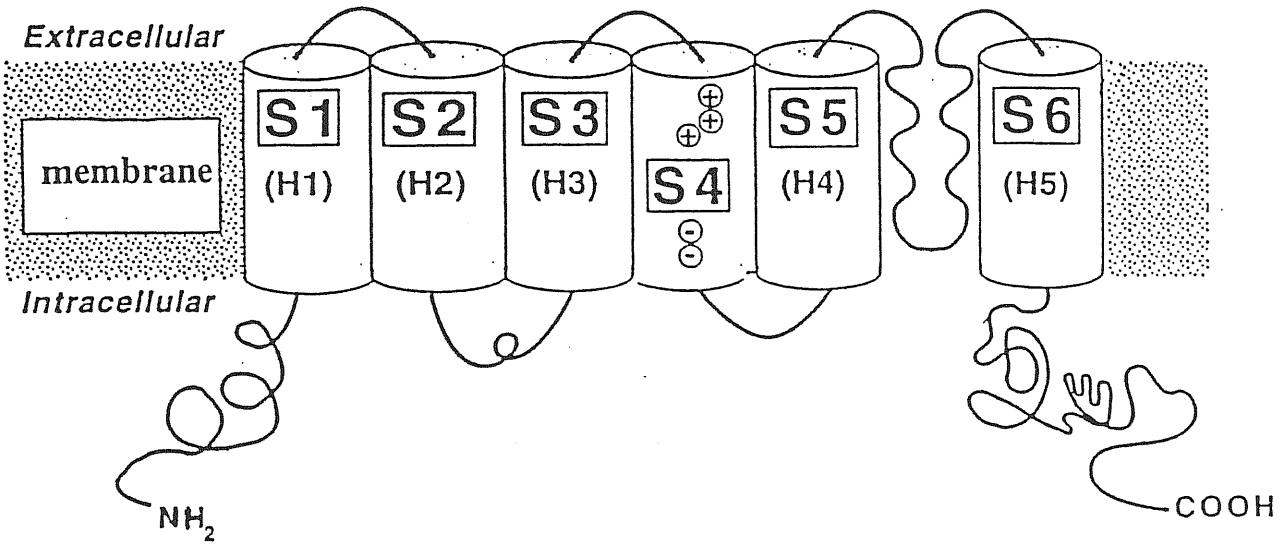

Fig. 3
Generalized monomeric protein domain topography model (PTDM) for a cyclic nucleotide-gated nonselective cation channel α-subunit (adapted from Conley, 1996). Domain nomenclatures (S1-S6) analogous to those used for Kv channel α-subunits are indicated in boxes. Other domain names (H1-H5), frequently used in old literature, are shown in brackets.
See the text (sections 1.1.4 to 1.1.7) for details on CNG channel structure.

Ca^{2+} channels (the same topological motif of six membrane-spanning domains is repeated four times in the same polypeptidic chain) (for a review, see Guy and Durell, 1995). Even if the stoichiometry of native CNG channels hasn't been determined precisely, it has nevertheless been shown that the expressed α-subunits assemble into a homotetrameric channel (Liu et al., 1996b; Varnum and Zagotta, 1996), while β-subunits alone do not lead to functional homomeric channels (Liman and Buck, 1994; Bradley et al., 1994). The cooperativity observed for calmodulin modulation of the channel suggests that the native rod channel consists of two α-subunits and two β-subunits (Bauer, 1996); the same conclusion was drawn from studies using tandem dimers containing α- and β-subunits of the olfactory CNG channel (Liu et al., 1998; Shapiro and Zagotta, 1998). Moreover, the analysis of the dose-response relations of macroscopic currents of CNG channels indicates that a multiple binding event is at the origin of channel activation: the Hill coefficient, which is a measure of apparent cooperativity, usually falls between 1.7 and 3.5 (Zimmermann and Baylor, 1986; Yau and Baylor, 1989). Analysis of channel gating (Ruiz and Karpen, 1997) using photoaffinity cGMP analogue that covalently binds to cGMP-activated channels showed that these channels open maximally when four ligands are bound. This result is also consistent with CNG channel being organized into tetramers, similarly to VG channels. In conclusion, CNG channels, due to their transmembrane organization and quaternary structure, are assigned to the superfamily of VG channels (Jan and Jan, 1990, 1992).

1.1.5 The S4 segment

In VG channels, the fourth transmembrane domain is characterized by a regularly repeated motif of a positively charged residue followed by two mainly hydrophobic ones. This S4 segment is considered to be the voltage sensor in VG channels, as they are thought to activate due to a voltage-driven movement of the positively charged motif, which would lead to a conformational change that propagates itself through the membrane (Guy and Conti, 1990; Durell and Guy, 1992). This model has been confirmed by site-directed mutagenesis experiments (Yang and Horn, 1995; Aggarwal and MacKinnon, 1996; Yang et al., 1996; Yusaf et al., 1996). In CNG channels, the fourth transmembrane domain strongly resembles a voltage sensor, and this similarity with VG channels effectively served as one of the bases for the classification of CNG channels (see North, 1995). Even if the net charge of the motif is reduced by the presence of additional negatively charged

residues, the presence of such an S4 segment is somehow unexpected in channels that do not respond to voltage changes, while being activated by ligand binding, and could represent a residual portion of a common ancestor of VG and CNG channels. Experiments involving the construction of chimeras have shown that if the S4 motif of the rat olfactory CNG channel is transferred into the sequence of the *Drosophila ether-à-go-go* (eag) VG channel this still retains significant sensitivity to voltage changes; if the S3-S4 loop is also transferred, the resulting channel becomes voltage-insensitive, possibly because the loop increases the stability of the open conformation (Tang and Papazian, 1997). Maybe, in CNG channels the S4 segment is no longer functional due to the presence of some surrounding portions of the protein. To date, no voltage-sensitive chimeras of CNG channels have been reported.

1.1.6 The pore region

In CNG channels, the putative pore forming (P) region, a stretch of about 20 amino acids located between the fifth and sixth transmembrane domains, exhibits approximately 30% sequence identity with the homologous segment in VG channels. The most remarkable difference is the presence, in most K^+ VG channels, of a tyrosine and a glycine residues (the YG motif). Remarkably, when these conserved residues are deleted from the Shaker pore region, the channel loses its selectivity among cations (Heginbotham et al., 1994), arguing for a role in the selectivity filter. No addition of the YG motif in the CNG pore region resulting in a functional channel has ever been reported.
A first three-dimensional model for the CNG channel pore implies that the stretch of residues lines the wall of the aqueous pore by forming a hairpin that spans the membrane twice (Eismann et al., 1993). A second model, resulting from substituted-cysteine accessibility method (SCAM; Karlin and Akabas, 1998) experiments, sees the P region loops of the CNG tetramer extending towards the central axis of the pore, forming the blades of an iris-like structure (Sun et al., 1996).

1.1.7 The C-terminal portion: C-linker and cyclic nucleotide-binding domain

The C-linker is a segment about 90 amino acids long that links the last transmembrane region to the cyclic nucleotide-binding domain, and is highly conserved among CNG channels. Some of its residues were shown to play

an important role in coupling ligand binding to channel gating (Zong et al., 1998; Paoletti et al., 1999). Moreover, the histidine residue in position 420 of the α-subunit of the bovine rod CNG channel is a binding site for Ni^{++}, which potentiates CNG current, suggesting that the histidine residue is involved in gating mechanisms (Gordon and Zagotta, 1995). The C-linker is also involved in a direct interaction between the N- and C-terminal domains of CNG channels through a cysteine residue (in position 481 of the α-subunit of the bovine rod CNG channel) (Gordon et al., 1997).
The cyclic nucleotide-binding domain (CNBD) was first identified as a stretch of about 120 amino acids by sequence homology with the corresponding region of the *E. coli* CAP (catabolite activator protein; Shabb and Corbin, 1992) and with the regulatory subunits of cAMP-dependent or cGMP-dependent protein kinases. Crystal structures of CAP and a regulatory subunit of bovine protein kinase A (PKA) were solved (McKay and Steitz, 1981; Weber and Steitz, 1987; Su et al., 1995), and, because most of the residues forming the nucleotide-binding pocket of CAP are conserved in the CNBD of CNG channels, the tertiary structure might be similar. The cGMP-binding site for the α-subunit of the bovine rod CNG channel was localized more precisely to residues 515 to 580 (Brown et al., 1995). The function of the CNBD will be discussed in section 1.1.11.

1.1.8 Effects of subunit composition

Heterologous expression of the α-subunit of the bovine rod CNG channel results in channel activity largely resembling the native one. However, the former gives rise to distinct rectangular currents (Kaupp et al., 1989; Nizzari et al., 1993), whereas the latter displays a rapid flickering behavior indicating very brief open and closed times (Haynes et al., 1986; Zimmermann and Baylor, 1986; Matthews and Watanabe, 1988; Quandt et al., 1991; Torre et al., 1992; Sesti et al., 1994). Moreover, the native channel is more sensitive to the ion channel blocker *l-cis*-diltiazem (Stern et al., 1986; Quandt et al., 1991; Haynes, 1992), less sensitive to block by external divalent cations (Root and MacKinnon, 1993; Eismann et al., 1994), and is subject to negative modulation by Ca^{2+}/calmodulin, a feature that is absent in α-homomeric channels (Chen et al., 1994). These discrepancies suggested the requirement of additional subunit(s) to form a native channel, and some β-subunits have actually been identified (see section 1.1.1). Although the rod photoreceptor β-subunit does not lead to functional channels when expressed on its own, when coexpressed with the corresponding human α-subunit

(Dhallan et al., 1992; Körschen et al., 1995) it introduced rapid flickers to the channel openings. In addition, the heteromeric channel is highly sensitive to *l-cis*-diltiazem (McLatchie and Matthews, 1992), its current is diminished by Ca^{2+}/calmodulin (Körschen et al., 1995), and its sensitivity to block by external divalent cations is similar to that of the native channel (Körschen et al., 1995). This result is consistent with the presence, in the β-subunit, of a glycine residue at a position corresponding, in the bovine rod α-subunit, to the glutamate 363, which is involved in block by divalent cations (Root and MacKinnon, 1993; Eismann et al., 1994; see section 1.1.10).
As for CNG channels expressed in the olfactory epithelium, a second subunit was discovered that has a shorter N-terminus than the α-subunit (a feature in common with the rod β-subunit), and is phylogenetically closer to the α-subunits than to the rod β-subunit (Kaupp, 1995). If the two olfactory subunits are coexpressed, the sensitivity to cAMP increases, but it still remains twofold lower than observed for native channels. Moreover, these heteromeric channels still display an increased sensitivity to external divalent cations; the position corresponding to the glutamate 363 in the bovine rod α-subunit is occupied by a glutamate in the α-subunit, and by an aspartate in the second subunit. A third subunit, an alternative splice form of the β-subunit expressed in rods, was then cloned from rat olfactory epithelium (Sautter et al., 1998). If all three olfactory subunits are coexpressed, the resulting channels display a cAMP sensitivity that resembles the native one (Bönigk et al., 1999). Moreover, *in situ* hybridization and RNase protection assays confirmed the presence of all three subunits mRNAs in the olfactory epithelium, and subsequent immunoprecipitation experiments made on preparation of solubilized olfactory cilia suggested that all three subunits co-assemble in the cilia to form the native channels. Single channel and macroscopic currents were then studied on patches excised from rat olfactory neurons, and the best match to functional characteristic of native channels was obtained when all three subunits are present (Bönigk et al., 1999).
In cone photoreceptors, only one α-subunit has been identified so far (Bönigk et al., 1993).

1.1.9 Ionic permeation

The pore-forming region is known to be the major determinant of ion permeation in VG (Heinemann et al., 1992; Yang et al., 1993; Heginbotham

et al., 1994) as well as in CNG channels (Goulding et al., 1993). Despite the sequence homologies displayed by the pores of VG K^+ and CNG channels, ions do not permeate in the same manner. Indeed, while VG K^+, like VG Na^+ channels, are highly selective, CNG channels do not discriminate well among the different monovalent alkali cations, as was demonstrated both in intact retinal rods (Capovilla et al., 1983; Menini et al., 1988; Nakatani and Yau, 1988) and in excised patches (Fesenko et al., 1985; Nunn, 1987; Furman and Tanaka, 1990; Menini, 1990). With respect to the native bovine rod CNG channel, the heterologously expressed α-subunit is more selective for Na^+ than for Li^+ (Kaupp et al., 1989). Surprisingly, CNG channels share many permeation properties with VG Ca^{2+} channels, despite different amino acid sequences in their pore regions. Both channels are permeable to Ca^{2+} and monovalent cations (Yau and Nakatani, 1985a), and Ca^{2+} also blocks the flow of current carried by monovalent ions (for photoreceptor channels, see Yau and Baylor, 1989; Zimmermann and Baylor, 1992; for olfactory receptor channels, see Zufall et al., 1994; for Ca^{2+} channels, see Almers and McCleskey, 1984; Hess and Tsien, 1984). In CNG channels, Ca^{2+} permeation is very subtle, since, depending on the cyclic nucleotide concentration, Ca^{2+} ions either permeate or block the channel (Colamartino et al., 1991). The ratio of Na^+ and Ca^{2+} ions crossing the pore is then determinant for the sensitivity of the visual and olfactory systems (Picones and Korenbrot, 1995a; Kolesnikov et al., 1990). Similarly to Ca^{2+} channels, CNG channels are also sensitive to external proton concentration in that a subconductance state due to a blocking effect is observed when the pH is decreased (for CNG channels, see Goulding et al., 1992; Zufall and Firestein, 1993). Ionic selectivity of CNG channels to non physiological cations has also been investigated in order to understand the permeability rules at the molecular level and to give an estimate of the pore size (Picco and Menini, 1993). The study of permeation of ammonium and guanidinium derivatives indicates that the pore of CNG channels is permeable to at least thirteen organic cations. While Na^+ and K^+ VG channels exclude all methylated cations, the salamander rod cGMP-gated channel is permeable to many cations containing a methyl group. Following this study of ionic permeation, the cross section of the narrowest part of the pore was estimated to be at least as large as 0.38 x 0.5 nm. This suggests that the pore of CNG channels is bigger than the ones of Na^+ and K^+ channels but smaller than the one of the Ca^{2+} channel from skeletal muscle, in accordance with the estimation obtained in a recent study of statistical mechanics (Laio and Torre, 1999), in which the physical origins of ionic selectivity were investigated. The selectivity for monovalent alkali cations is likely to depend

on geometrical properties of the inner core of the channel without any critical contribution from charged or polar groups that would interact electrostatically with the permeant ions. This hypothesis might explain the differences in ionic selectivity among channels having similar pore residues and *vice-versa* the similarities in ionic selectivity between channels having different pore residues.

1.1.10 The functional role of a conserved glutamate

Some residues in the pore region of CNG channels might be more important than others in controlling the flow of ions. Indeed, a conserved glutamate which is found at position 363 in the α-subunit of the bovine rod CNG channel is involved in the block by external Mg^{2+}, Ca^{2+} and protons (Root and MacKinnon, 1993; Eismann et al., 1994). Because substitution of E363 by a neutral amino acid reduced external divalent cations block but maintained the channel sensitivity to internal blockage, it was suggested that this glutamate was localized inside the pore, close to the external surface. The β-subunit bears a glycine residue at the corresponding position. Interestingly, coexpression of α- and β-subunits led to a reduced sensitivity to external divalent cations (Körschen et al., 1995) analogue to the level reported for the native channel, and in consistency with the role played by E363 in divalent cations block. Indeed, it has been proposed that in homotetrameric channels the four glutamate residues form the high affinity Ca^{2+} binding site. Since the glutamate residue is conserved in all CNG channels α-subunits known so far, additional residues or factors must participate in the binding of divalent cations and account for the different sensitivity to Ca^{2+} blockage observed in various homomeric CNG channels (Frings et al., 1995). It was recently shown that the S5-P-S6 region defines a particular dielectric environment that sets the state of protonation of the glutamate residues and consequently determines the affinity of the Ca^{2+} binding site inside the pore (Seifert et al., 1999a).
A study in which the anomalous mole fraction effect was tested with mixtures of Li^+ and Cs^+ showed that E363 is also responsible for the multi-ion nature of the pore of CNG channels (Sesti et al., 1995). The anomalous mole fraction effect is characteristic of a pore containing multi ion-binding sites and was observed in both native and homomeric channels, but it was absent when E363 was replaced by a neutral amino acid, and was only reduced when E363 was mutated into an aspartate. These results suggest that the coordination of several negative residues is necessary to form the

molecular structure that can bind one or two monovalent cations. This structural organization is reminiscent of the coordination of four glutamate residues in the four different repeats of Ca^{2+} channels that constitutes a binding site for one or two small cations (Armstrong and Neyton, 1992).
Another interesting observation was made regarding channel gating in the α-subunit of the bovine rod CNG channel (Bucossi et al., 1996). By mutating E363 into an alanine, a serine or an asparagine, a current decline reminiscent of the desensitization of LG channels was observed, suggesting that E363 is involved in gating properties, in addition to its role in the selectivity filter. It was also shown that when E363 is mutated into the smaller serine residue, the channel is permeable to dimethylammonium, contrarily to the w.t. channel. This suggests that E363 is located close to the narrowest part of the pore.

1.1.11 Function of the cyclic nucleotide-binding site

The apparent ligand sensitivity of the cyclic nucleotide-binding sites differs depending on the channel considered. Nevertheless, all CNG channels are more sensitive to cGMP than to cAMP. The constant for half activation $K_{1/2}$ for native and cloned bovine rod channels are similar: 10-50 μM for cGMP and 1.2-1.5 mM for cAMP. For the native salamander photoreceptor channel, $K_{1/2}$ is 4 μM for cGMP and 20 μM for cAMP (for a review, see Eismann et al., 1993). For the cone photoreceptor channel, $K_{1/2}$ is around 34-70 μM for cGMP and 1 mM for cAMP. For the olfactory CNG channels, the $K_{1/2}$ values for both cyclic nucleotides are in general closer: for the cloned bovine olfactory receptor channel, $K_{1/2}$ is 1.4 μM for cGMP and 54 μM for cAMP; for the native rat olfactory receptor channel, $K_{1/2}$ is 1 μM for cGMP and 2.5 μM for cAMP. Although the olfactory CNG channel is slightly more sensitive to cGMP than to cAMP, its physiological ligand is cAMP.
The binding site is formed by eight-stranded antiparallel β-rolls flanked by a short N-terminal α-helix (A helix) and two C-terminal α-helices (B and C helices). Based on sequence comparison among different cyclic nucleotide binding proteins, a model of binding was proposed (for a review, see Zagotta and Siegelbaum, 1996), and some amino acids were identified as key residues in the interaction with the cyclic nucleotides. A set of highly conserved glycines in the β-rolls are important for the proper folding of the binding pocket. Using a photoaffinity radioactive analogue of cGMP able to label specifically both subunits of the bovine rod CNG channel, the cGMP binding site was localized more precisely and the residues lining the binding

pocket were identified (Brown et al., 1995). The specific labeling of the α-subunit was localized to a 66-amino acid region (Tyr 515-Met 580) entirely contained in the 120-amino acid segment previously supposed to form the binding site. Within this fragment, residues Val 524, Val 525 and Ala 526 are likely to line the binding pocket. The specific labeling was also confirmed repeating these experiments on the β-subunit. Conserved residues of the β7 strand were also investigated. Molecular modeling on cGMP-dependent protein kinase suggested that the hydroxyl group of the threonine residue of the β7 strand formed a hydrogen bond with the amino group attached to the C2 of cGMP (Weber et al., 1989). Since this amino group is missing in cAMP, the same threonine residue might account for ligand discrimination. Mutation of the first alanine in the β7 roll into a threonine in the cAMP dependent kinase actually increased the binding of cGMP, but this mutation had little effects on the cAMP binding (Shabb et al., 1990). It was later established that the hydroxyl group of Thr 560 (rod channel) and Thr 537 (olfactory channel) form a hydrogen bond with cGMP but not cAMP (Altenhofen et al., 1991). However, since all CNG channels contain a threonine at this position, this residue could not account for the molecular basis of ligand discrimination between the retinal and olfactory channels. Moreover, the hydrogen bond can only be formed when cGMP is in a syn conformation, while in CAP the binding occurs in the anti conformation (see Zagotta and Siegelbaum, 1996). Based on the observation that two residues in the C-helix of CAP (T127 and S128) make two hydrogen bonds with the C6-amino group of cAMP (Weber and Steitz, 1987), chimeras of bovine rod and catfish olfactory channels were studied, and it was concluded that the C-helix is both necessary and sufficient to account for ligand specificity (Goulding et al., 1994). In another study, mutations were performed on the residue D604 of the bovine rod channel, which corresponds to T127 of CAP (Varnum et al., 1995). The nucleotide selectivity was significantly altered when the aspartate was mutated into a glutamine (corresponding residue in the fish olfactory channel), and completely inverted if the aspartate was substituted by a methionine. These changes might be due to an alteration in the relative ability of the bound agonist to trigger the allosteric conformational changes necessary for the channel opening. It was also suggested that D604 forms two hydrogen bonds with N1 and N2 of the guanine ring in the anti configuration.

The functional role of aromatic residues in the CNBD was also analyzed (Li and Lester, 1999). By replacing tyrosine 565 of the rat olfactory CNG channel with an alanine, a 10-fold increase in sensitivity to both cAMP and

cGMP was observed. This tyrosine lies in the hinge between helices B and C, and is thought to facilitate gating transitions that occur after ligand binding.

1.1.12 Properties of the macroscopic current

To activate CNG channels and observe macroscopic currents, patches of membrane are excised from cells that express these channels (natively or heterologously) and exposed to micromolar concentration of cyclic nucleotides. Figs. 4A-B show the macroscopic currents obtained from inside-out membrane patches excised from salamander photoreceptors, at +60 mV and in the presence of different cGMP concentrations. The currents observed are dependent on the cGMP concentration: at saturating concentration (about 100 μM), currents as large as 1-2 nA can be obtained (fig. 4A), while only small currents are measured at low cGMP concentration (fig. 4B). The relationship between the current and the cGMP concentration can be described as

$I=I_{max}[g^n/(g^n+K^n)]$

where I_{max} is the maximal current activated by cGMP, g is the cGMP concentration, K the cGMP concentration activating half of the maximal current and n the Hill coefficient. Experimentally, n is between 1.7 and 3.5 (Zimmermann and Baylor, 1986; Yau and Baylor, 1989), and K has a value of 10 or 50 μM (for CNG channels of salamander photoreceptors, see Zimmermann and Baylor, 1986; Colamartino et al., 1991; for CNG channel of bovine rods, see Luehring et al., 1990). CNG channel activation is also slightly voltage-dependent: hyperpolarization increases the rate constant of channel closing (Karpen et al., 1988). In the presence of low cGMP concentration, an outward rectification is observed, which is primarily due to an increase in the open probability at positive voltages, as resulting from the analysis of single channel activity at positive and negative voltages (Sesti et al., 1994). A very small outward rectification is also present in currents of CNG channels from olfactory receptors (Dhallan et al., 1990; Goulding et al., 1992). Also these channels physiologically respond to the binding of an agonist, cAMP. For the cloned channel, the half saturating concentration value (at +40 mV) is higher for cAMP (38-68 μM) than for cGMP (1.2-2.4 μM) (Dhallan et al., 1990); for the native channel, a bimodal value was found (K=2 and 40 μM for cAMP; Nakamura and Gold, 1987).The Hill coefficient is around 1.9 (Dhallan et al., 1990).

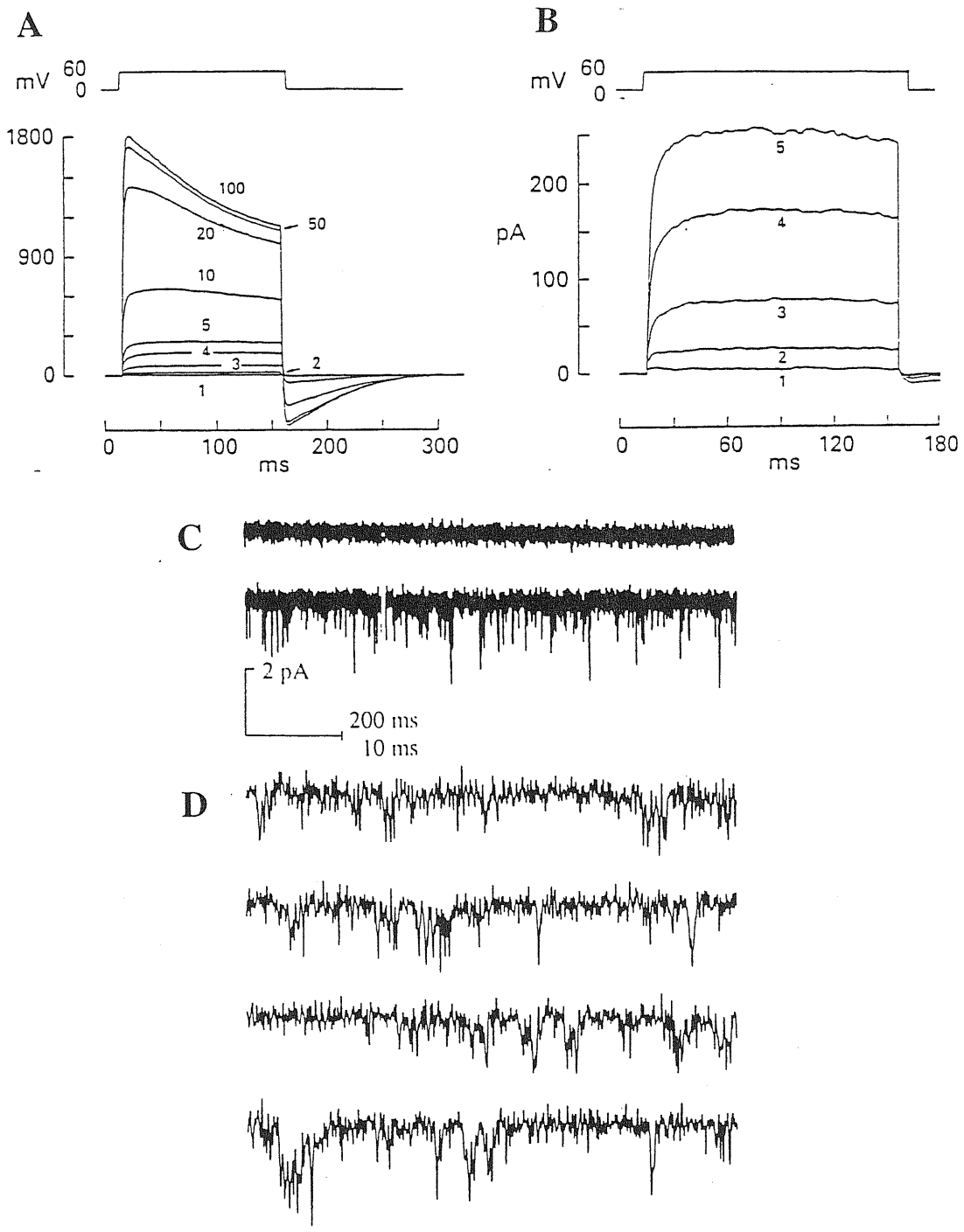

Fig. 4A-D

A-B Stoichiometry of the activation of the macroscopic CNG current in inside-out membrane patches from salamander rod outer segments. Voltage steps were from 0 to +60 mV.

A Current recordings activated by 1, 2, 3, 4, 5, 10, 20, 50 and 100 μM cGMP.

B Current recordings activated by 1, 2, 3, 4 and 5 μM cGMP.

C-D Single-channel CNG current recordings in inside-out membrane patches from vertebrate rod outer segments. Holding potential was –60 mV (cytoplasmic side).

C Current recordings activated by 0 (top) or 2 (bottom) μM cGMP. No transient currents were observed in the absence of cGMP (top).

D Raw current recordings with 2 μM cGMP, on a faster time base and filtered at 4kHz. (Torre and Menini, 1994)

1.1.13 Single channel properties

The first attempts to record single channel currents induced by cGMP were unsuccessful (Fesenko et al., 1985; Nakamura and Gold, 1987). Noise measurements revealed a very small single channel conductance of less than 0.1 pS, inconsistent with an aqueous pore but more fitting to the case of membrane carriers (Fesenko et al., 1985). Alternatively, such a small unitary current could be explained with a blockage of the channel pore. Indeed, the first measurements of single channels were obtained in excised rod membrane patches using divalent cation-deprived solutions (Zimmermann and Baylor, 1986; Haynes et al., 1986; Matthews and Watanabe, 1987, 1988). The reduction in single-channel conductance by divalent cations could be physiologically important in reducing the signal-to-noise ratio of sensory transduction (Yau and Baylor, 1989). A great variability in the mean open time ranging from 0.1 to 1 msec and a single-channel conductance between 20 and 60 pS were obtained (Yau and Baylor, 1989; Torre et al., 1992; Sesti et al., 1994; Zufall et al., 1994). The typical traces for single-channel recordings from excised patches of rod outer segments (fig. 4C-D) reveal a continuous flickering between the closed and open state; analysis of the amplitude histograms gives an estimate of the mean open time of maximally 35 μsec (Torre and Menini, 1994). The density of cGMP-activated channels in the membrane of the rod outer segment is high (126 μm^{-2}, Karpen et al., 1992), and single channel openings can only be obtained using very small concentrations of cGMP. However, cGMP-gated channels are not so dense in the inner segment, making single-channel recordings easier (Matthews and Watanabe, 1988). Surprisingly, in some rare recordings the application of cGMP induced well-defined openings (Torre et al., 1992; Sesti et al., 1994), without the flickering behaviour which is particularly notable in recordings from the inner segments. The properties of these single-channel recordings in terms of conductance (25-30 pS) and open probability (half activation of this channel occurred at about 18 μM cGMP) were reminiscent of the ones observed when expressing the α-subunit of the bovine rod channel (Kaupp et al., 1989). Depending on the nature of the preparations, the properties of CNG channels are quite different. In fact, the α-subunit of channels from catfish olfactory sensory neurons are characterized by three different open states with respective conductances of 25, 50 and 80 pS (Goulding et al., 1992; Root and MacKinnon, 1994). The α-subunit of the channel from rat olfactory neurons has a conductance of about 40 pS and doesn't present subconductance states

(Li and Lester, 1999). On the whole, collected data are consistent with the existence of different conducting levels in the CNG channel, leading to the appearance of well-resolved open states in homomeric channels and to flickering behaviour in heteromeric channels (Bucossi et al., 1997).

1.1.14 Role of the C-linker in coupling ligand binding to channel gating

In the investigation of the molecular mechanisms underlying the coupling of ligand binding to channel opening, a histidine residue in the C-linker of the bovine rod CNG channel was identified as responsible for potentiation by internal Ni^{2+} ions (a phenomenon previously described by Ildefonse et al., 1992) through stabilization of the open conformation (Gordon and Zagotta, 1995a). Another histidine in the rat olfactory CNG channel accounted for channel inhibition by preferential binding of the Ni^{2+} to the closed states, stabilizing them and thus reducing the efficiency of channel activation (Gordon and Zagotta, 1995b). A conserved cysteine residue in the C-linker L2 region was then identified as a site of potentiation through the modification by sulfhydryl-reactive chemicals (Broillet and Firestein, 1996; Brown et al., 1998). It was suggested that the C-linker undergoes a movement during channel activation which is essential for coupling ligand binding to channel gating (Brown et al., 1998). Experiments on chimeric channels between the cone photoreceptor and the olfactory receptor allowed the identification of three amino acids in the C-linker that account for the differences in cAMP efficacy and are major determinants in channel gating (Zong et al., 1998). A similar study, in which the very high cAMP efficacy of a *Caenorhabditis elegans* sensory neuron channel (TAX-4) was conferred to the bovine rod CNG channel (which is usually poorly activated by cAMP), indicated that three other residues in the C-linker L2 region are involved in gating processes (Paoletti et al., 1999). The exchange of the two different C-linker L2 regions did not alter the spontaneous open probability of the channel, despite a large effect on gating. This suggests that the C-linker might have a role in determining the differences in agonist interaction between the closed and open state. The C-linker effectively favors the stability of the ligand binding in the open state, stabilizing the interactions between the ligand and its binding site. Since this stabilization occurs in the same way for both cGMP and cAMP, the C-linker must interact with the cyclic nucleotide in a part of the molecule which is common to both cGMP and cAMP. The C-linker could act as a rigid arm that couples a change in the structure of the core of the channels to a movement of the ligand-binding site, which favors the binding of the cyclic nucleotide in the open

conformation and the interactions among subunits, thus stabilizing the open state. The cyclic nucleotide-binding site itself has been proposed to play an important role in coupling ligand binding to channel allosteric conformational change (see also section 1.1.11).

1.1.15 Kinetic models of gating

The gating kinetics of CNG channels were studied by Karpen and coworkers (Karpen et al., 1988), who, as already mentioned, showed the cGMP-dependence of channel activation, the saturation of the opening rate at high cGMP levels, and the slight voltage sensitivity of these channels, whose opening can be increased by depolarization. Accordingly, a model was proposed with three ligand-binding steps followed by a closed-to-open transition which is favored by depolarization and occurs when the channel is fully liganded. This model accounts for the almost linear current-voltage relation observed at saturating concentrations of cGMP, i.e. when nearly all channels are open even at negative voltages. At low cGMP concentrations, the open probability is low, so that the role of voltage changes in the closed-to-open equilibrium is major for increasing the open probability.

1.1.16 Allosteric models of gating

Spontaneous openings of CNG channels in the absence of ligand have been reported (Picones and Korenbrot, 1995b; Tibbs et al., 1997). In view of this observation, an allosteric model has been proposed (Stryer, 1987), in which the affinity of cGMP is higher for the open conformation than for the closed one, the change of conformation is concerted between the different subunits, the binding of the ligand to each subunit is independent from the other bound subunits and the more cGMP molecules bind, the more stable the conformational change. Experiments with chimeras between the bovine retinal and rat olfactory channels allowed the identification of two different domains, the N-S2 domain of the N-terminal region and the C-helix of the C-terminal domain, which are important for channel opening; the N-S2 region is probably a site for contacts among subunits. These contacts are enhanced during channel activation and thus lead to changes in subunit orientation, that in turn, coupled to a movement of the C-helix, triggers channel opening (Goulding et al., 1994). This interpretation is based on a simple tetrameric allosteric model, that, like the model proposed by Stryer, implies that the ligand prefers the open conformation. The N-terminal region of the olfactory channels seems to be particularly important (Chen and Yau,

1994; Gordon and Zagotta, 1995b). This feature has been exploited to analyze the kinetic behavior of single bovine retinal channels in which mutations in the binding domain (at position 604, see section 1.1.11 and Varnum et al., 1995) have been introduced and/or the rat olfactory channel N-terminal domain substituted to the original one of the bovine retinal channel (Sunderman and Zagotta, 1999b). The authors refined the previously proposed model (Gordon and Zagotta, 1995b; Varnum et al., 1995) in which the cyclic nucleotide is supposed to bind to the closed state through interactions with the β-roll of the binding site, and this binding leads to a movement of the β-roll relative to the C-helix and to a subsequent strengthening of cGMP binding through hydrogen bond with residue D604. The formation of the hydrogen bonds is important for the allosteric transition leading to channel opening, while dissolution of these bonds is required for channel closing. The action exerted by the N-terminal portion occurs just before the allosteric transition and then following it, for stabilizing the interactions between the ligand and the aspartate residue of the binding domain. The same authors studied in detail the mechanisms of allosteric transition performing single-channel analysis of the α-subunit of the bovine rod CNG channel expressed in *Xenopus* oocytes (Sunderman and Zagotta, 1999a). They determined that two closed and one open state are required to explain the gating at saturating ligand concentration. Two distinct models would then be possible: C<-->C<-->O or C<-->O<-->C. The first could describe the activation of a channel composed of two functional dimers which should both adopt the activated conformation to allow channel opening (concerted transition). A similar scheme was previously proposed (Liu et al., 1998). According to the second hypothetical model, a single concerted allosteric conformational change could underly the C<-->O transition, while the O<-->C, being cyclic nucleotide-independent, would rely on an open-channel block or closure of a secondary gate (multiple conformational changes). While the real mechanism is undoubtedly more complex than two closed and one open state, the second model was favored. The effect of Ni^{2+} was also studied, concluding that this ion induces and stabilizes the allosteric transition of liganded channels (Sunderman and Zagotta, 1999a). This hypothesis also implies that the conformational changes occurring spontaneously are based on a different mechanism which doesn't involve the movement of residue H420, in accordance with recent findings (Paoletti et al., 1999) showing that alterations in the C-linker do not affect spontaneous opening. In the past, kinetic studies were impaired by the fact that the ligand binds and unbinds continuously from the binding site, but

this problem was overcome with the use of a photoaffinity cGMP analogue that binds covalently to CNG channels (Ruiz and Karpen, 1997). This allowed the finding that CNG channels can be locked in four liganded states, and that in each state channels open in two or three different conductance states. More recently, opening mechanisms have been studied in further detail (Ruiz and Karpen, 1999) performing analysis of single channels locked in each liganded state. The authors concluded that the channels exhibit at least nine different states for each doubly, triply and fully liganded channel. This implies that the channels exhibit the same series of conformational changes at each possible liganded state. Such a complex behavior cannot be explained with simple concerted or sequential allosteric models. A general allosteric model is proposed in this study: channels with zero and one activated subunit are closed, channels with two adjacent activated subunits lead to an open state (O1), channels with diagonally activated subunits are closed, channels with three or four activated subunits are open (states O2 and O3). In the fully liganded channels, additional states are required: an additional conformational change can be added for a modification in the interaction between two liganded subunits that are adjacent. There are some evidences for such a conformational change that occurs between pairs of subunits: the open state is stabilized by such intersubunit interactions through Ni^{2+} coordination (Gordon and Zagotta, 1995c); activation properties are different for adjacent subunits with respect to diagonally opposed ones (Varnum and Zagotta, 1996). A mechanism based on interactions between adjacent subunits was also proposed (Liu et al., 1998).

1.1.17 Modulation of CNG channels

(For a review, see Wei et al., 1998.)
The effect of calcium-calmodulin (Ca-CaM) on CNG channels has been introduced in section 1.1.2 (for a review, see Molday, 1996). The effect on the rod CNG channel was found to be a suppression of the cGMP-activated current at subsaturating concentrations of cGMP in rod outer segments. The net action of calcium and CaM is to shift the dose-response curve to the right without changing maximal channel activity and cooperativity. It was found that CaM modulates ligand affinity, which in turn affects channel activity. This action can be blocked by a CaM inhibitor, mastoparan (Hsu and Molday, 1993, 1994). From studies on cloned and heterologously coexpressed CNG channels, it resulted that CaM specifically and directly binds to the α-subunit of the olfactory CNG channel and the β-subunit of the

rod CNG channel. These detailed physiological studies suggest that CaM plays an important role in olfactory adaptation, because olfactory CNG channels are highly permeable to Ca^{2+}. In contrast, it may have a minor role in the photorecovery of rod photoreceptors. Some experiments have shown no effect of CaM on dark current or light responses in intact rods. Although the cone CNG channel is also highly permeable to Ca^{2+}, CaM still has no significant effect on native cone CNG channel (Molday, 1996; Haynes and Stotz, 1997). Using a series of deletion mutants, glutathione-*S*-transferase-fusion peptides and synthetic peptides, the CaM binding site was localized to residues 62-87 at the N-terminus of the rat olfactory CNG channel α-subunit. The binding showed a dissociation constant (K_d) of 3.4 nM (Liu et al., 1994). A CaM binding site in the rod CNG channel β-subunit was found at the C-terminus, although the N-terminus is also involved in CaM regulation of channel activity (Chen et al., 1994; Molday, 1996). Other studies have identified an endogenous Ca^{2+}-binding protein in rod outer segments that exhibits a similar effect on the CNG channel; it is either a novel protein or a different form of CaM with altered binding properties (Kramer and Siegelbaum, 1992; Gordon et al., 1995a).
Other modulators of CNG channels include nickel ions (discussed in sections 1.1.14 and 1.1.16; Gordon and Zagotta, 1995a,b,c), gaseous second messengers such as carbon monoxide (CO; Zufall and Leinders-Zufall, 1997) and nitric oxide (NO; Broillet and Firestein, 1997) (see section 1.1.3), the proteolytic enzyme papain (Shen et al., 1995), nicotine (McGeoch et al., 1995), and ATP and GTP (Filatov et al., 1989; Watanabe and Shen, 1997).

1.2 Hyperpolarization-activated, cyclic nucleotide-gated (HCN) channels

1.2.1 HCN channels from identification to cloning

Many processes in living organisms are characterized by repetitions of events over characteristic time intervals, ranging from seconds to hours: beating of the heart, cycles of sleep and wakefulness, release of hormones, breathing, swimming behavior of sperm are all examples of rhythmic activity of single cells or multicellular networks. The first and possibly the most studied case of a rhythmic event was heart beating, following the observation that specialized myocites, termed pacemaker cells, located in restricted areas, are able to beat spontaneously even when separated from the rest of the cardiac muscle (del Castillo and Katz, 1955; West, 1955;

Vassalle, 1966; Noma and Irisawa, 1976; Brown et al., 1977). Pacemaker currents responsible for this behavior were identified during the late 1970s and early 1980s in sinoatrial node cells, and were termed I_h (h for hyperpolarization activated) or I_f (f for "funny") (Brown et al., 1979; Brown and DiFrancesco, 1980; Yanagihara and Irisawa, 1980; DiFrancesco 1981a,b).

Among neurons, I_h current was first characterized in rod photoreceptors as a cesium-sensitive slow inward current activated by hyperpolarization and having a role in the response of the cell to bright flashes of light (Fain et al., 1978; Bader et al., 1979; Attwell and Wilson, 1980; Bader et al., 1982). An equivalent current was reported in hippocampal pyramidal cells (Halliwell and Adams, 1982; Maccaferri et al., 1993), where membrane hyperpolarization induced the activation of a slow inward current. Currents with similar properties were later found in a wide variety of neuronal and non-neuronal cells, and were recognized as an ubiquitous phenomenon within cells of the nervous system. They were alternatively termed I_q (q for "queer") in view of their odd electrophysiological behavior and undefined functional significance, I_f, I_{AR} (anomalous rectifier) or I_R (inward rectifier); however, to differentiate them from the classical K^+ inward rectifier current, the term hyperpolarization-activated current (I_h) was preferred for use in the nervous system (Hille, 1992).

Features that were recognized characteristic for channels underlying I_f, I_h, I_q are summarized here and will be further discussed in the next sections:

1) activity is dependent on membrane voltage, but unlike most other voltage-dependent channels that are activated on depolarization, pacemaker channels require hyperpolarization of the membrane to open;
2) pacemaker channels are selective for K^+ ions, but they lack the exquisite K^+ selectivity of other K^+ channels; consequently, they carry a Na^+ inward current that slowly depolarizes the membrane;
3) the relative ion permeability P_{Na}/P_K depends on the extracellular K^+ concentration;
4) current can be blocked by a low concentration of extracellular Cs^{2+} ions;
5) permeation of cations is regulated by extracellular Cl^- ions;
6) activity is directly and positively modulated by cAMP and cGMP.

This last feature led to the idea that I_f, I_h, I_q and CNG channels might be related, but despite the first cloning of a CNG channel in 1989 (Kaupp et al., 1989), the first I_f and I_h channels have only been cloned in the past three years. This delay was probably due to the small (28%) identity that I_f and I_h

channels sequence bears to that of CNG channels. In 1988, three groups reported independently the cloning of several cDNAs encoding pacemaker channels. A protein-protein interaction screen, performed using the SH3 domain of the neural form of Src tyrosine kinase as bait, allowed the detection of a brain cDNA clone, called BCNG-1, which was thought to encode a cyclic nucleotide-modulated K^+ channel based on sequence alignments (Santoro et al., 1997). Functional expression of BCNG-1 demonstrated that it formed a member of a family of hyperpolarization-activated cation channels (Santoro et al., 1998). A more direct approach to clone pacemaker channels derived from the idea that I_f and I_h channels, like CNG channels or cyclic nucleotide-dependent protein kynases, would contain a cyclic nucleotide-binding domain (CNBD). Screening the expressed sequence tag (EST) database for sequences related to the CNBD of CNG channels identified an EST sequence which was then used to isolate three homologous full-length cDNAs (HAC1-3) from mouse brain (Ludwig et al., 1998). In a third approach, a nonmammalian channel called SPIH was identified when a sea urchin sperm library was screened with degenerate primers of the cyclic nucleotide-binding region (Gauss et al., 1998). By that time, a unifying nomenclature for pacemaker channels was proposed (Clapham, 1998; Biel et al., 1999b) and they were termed HCN channels for Hyperpolarization-activated, Cyclic Nucleotide-gated. The species from which the cDNA was cloned is indicated by a preceding lowercase letter. To date, several HCN channels have been cloned from different vertebrates (mouse, rat, human, rabbit) and invertebrates (sea urchin, silkmoth, fruitfly). Table 2 summarizes the results of the cloning effort so far, tries to clear up the different nomenclatures used in the past, and provides references for papers.

1.2.2 Role of HCN channels in heart

(For a review, see DiFrancesco, 1993; Gauss and Seifert, 2000.)
In the heart of vertebrates, pacemaker activity originates from the sinoatrial node, a remnant of the sinus venosus, where a group of specialized muscle cells (the pacemaker itself), small and weakly contractile, is able to generate action potentials spontaneously. Electrical activity that starts in the pacemaker region can spread over the heart and trigger the contraction of the cardiac muscle. There are other cardiac cells capable of pacemaker activity (e.g., in the atrioventricular node, bundle of His, Purkinje fibers), but since all cells in heart are electrically coupled, the cell or group of cells with the

Name	Original name	Species	References
HCN1	mBCNG-1/HAC2	mouse	Santoro et al., 1997; Ludwig et al., 1998
	hBCNG-1 (*)	human	Santoro et al., 1998
	HCN1 (*)	rat	Shi et al., 1999
	HCN1 (*)	rabbit	Shi et al., 1999
HCN2	mBCNG-2/HAC1	mouse	Santoro et al., 1998; Ludwig et al., 1998
	hBCNG-2 (*)/hHCN2/hHCN2	human	Santoro et al., 1998; Ludwig et al., 1999b; Vaccari et al., 1999
	HCN2 (*)	rat	Shi et al., 1999
	HCN2 (*)	rabbit	Shi et al., 1999
HCN3	mBCNG-4 (*)/ HAC3	mouse	Santoro et al., 1998; Ludwig et al., 1998
	HCN3 (*)	rat	Shi et al., 1999
	HCN3 (*)	rabbit	Shi et al., 1999
HCN4	mBCNG-3 (*)	mouse	Santoro et al., 1998
	hHCN4	human	Ludwig et al., 1999b; Seifert et al., 1999b
	HCN4 (*)	rat	Shi et al., 1999
	HCN4 (**)/ HCN4 (*)	rabbit	Ishii et al., 1999; Shi et al., 1999
SpHCN	SPIH	sea urchin	Gauss et al., 1998
HvHCN	HvCNG	silkmoth	Krieger et al., 1999
DmHCN	DMIH	fruitfly	Marx et al., 1999

(*) Partial cDNA sequence.
(**) Probably represents a partial clone that is lacking part of the N-terminal region.

Tab. 2
HCN channels cloned so far (modified from Gauss and Seifert, 2000).

fastest intrinsic activity, in normal conditions, stimulates the contraction of the whole muscle and determines the heart rate.

At first, the timing of the pacemaker depolarization was thought to be controlled by a slow decline in conductance during diastole (Weidmann, 1951) that was K^+ selective. Early models of the action potential incorporated this concept of a slowly declining K^+ channel conductance into the I_{K2} current (Noble and Tsien, 1968). Since closing K^+ channels does not depolarize cells above action potential threshold, the explanation of pacing required additional inward background currents that were time invariant. The first significant revision of these early ideas about pacemaking currents stemmed from the observation of a hyperpolarization-activated inward current in rabbit sinoatrial (SA) nodal cells (Noma and Irisawa, 1976). A nonselective inward current was shown to mediate part of adrenaline's acceleration of SA nodal cell firing (Brown et al., 1979). This current was named I_f (f for "funny") or I_h (h for hyperpolarization activated), and replaced I_{K2} in pacing models (DiFrancesco and Noble, 1979).

Presently, to explain rhythmic repetitions of action potentials in the sinoatrial node cells, the involvement of four different ion channels is considered. First, T-type Ca^{2+} channels open, followed by L-type Ca^{2+} channels, which cause a large depolarization of the cell. Then the cell is repolarized by the opening of K^+ channels. At the end of each action potential, the membrane voltage approaches the K^+ equilibrium potential (about -80 mV) due to the open K^+ channels. At this hyperpolarized voltage, the pacing channels open and produce a Na^+ inward current that slowly depolarizes the membrane, until the threshold for a new action potential is reached. The lapse of time between two action potentials is determined by this pacemaker depolarization. Thus, pacemaker channels are responsible the generation of rhythmic activity, and have a role in the control of firing frequency.

Cardiac pacemaker channels are positively regulated by cAMP, and this regulation does not depend on the action of protein kinases, but on the direct binding of cAMP to the channel (DiFrancesco and Tortora, 1991). Control of channel activity by intracellular levels of cAMP (or cGMP) is of utmost physiological importance because it is the base for heartbeat acceleration upon sympathetic stimulation. Stimulation of cardiac cells by agonists of β-adrenergic receptors triggers the activation of an adenylyl cyclase, which increases the concentration of intracellular cAMP. This binds to the channel and enhances its activity. Consequently, the depolarization mediated by the pacemaker channels is accelerated, and the time interval between heartbeats is shortened (Brown et al., 1979a,b). The opposite situation occurs upon

parasympathetic stimulation, that is, with acetylcholine: the concentration of intracellular cAMP decreases, pacemaker currents decline, and the heart rate is thus diminished (Hageman et al., 1977; Prystowsky et al., 1979; DiFrancesco et al., 1998).

1.2.3 Role of HCN channels in brain

(For a review, see Pape, 1996; Lüthi and McCormick, 1998b; Santoro and Tibbs, 1999; Gauss and Seifert, 2000.)

I_h has been characterized in many neurons, and this fact can be better understood upon consideration of the role that rhythmicity may play in the central nervous system (CNS). While rhythmic activity in some lower brainstem regions, such as those involved in the generation of breathing cycles, is obviously important, it has been postulated that, at the other end of the cognitive spectrum, the rhythmic patterns observed in electroencephalograms (EEGs) reflect underlying mechanisms used in encoding and controlling the flow of information in the CNS (Steriade et al., 1993; Pare and Llinas, 1995; Singer and Gray, 1995; McCormick and Bal, 1997). For example, synchronization of the activity of neuronal populations in higher cortical regions may serve to bind together the separate analyzed components of a perceptual representation into a coherent representation of the external world (Singer and Gray, 1995).

Perhaps the best-studied example of the generation of rhythmic and tonic activity at the cellular level, and of the contribution of this to higher-order neural function, is the rhythmic bursts of action potential in the relay cells of the thalamus (Crunelli et al., 1987; McCormick and Pape, 1988; Bal et al., 1995a,b; Bal and McCormick, 1996; Lüthi and McCormick, 1998a, 1999). The thalamus is a major gateway for the flow of sensory information toward the cerebral cortex, and it is the first station at which incoming signals can be blocked. During sleep, the rapid activity patterns characteristic of the aroused state are replaced by the low-frequency, synchronized rhythms of neuronal activity. The physiological significance of oscillatory modes is uncertain, but they may play a role in controlling the flow of information through the thalamus.

During early stages of quiescent sleep, thalamocortical neurons produce synchronized network oscillations of slow periodicity, called spindle waves. The waves of electrical activity at 7-14 Hz increase and decrease within a period of 1 to 3 seconds and recur periodically once every 3-20 seconds (Steriade and Deschênes, 1984; Steriade et al., 1993; Bal and McCormick, 1996). Spindle waves are produced by the reciprocal interaction between

GABAergic neurons of the thalamic reticular nucleus and excitatory thalamic relay neurons (Steriade and Deschênes, 1984; Steriade et al., 1993; von Krosigk et al., 1993; Bal et al., 1995a,b). The barrages of inhibitory postsynaptic potentials (IPSPs) evoke Ca^{2+} rebounds by deinactivation of T-type Ca^{2+} channels, which then, through the generation of trains of action potentials, reexcite the reticular cells (Bal et al., 1995a,b; Bal and McCormick, 1996). During the late stages of sleep, spindle waves are progressively replaced by oscillations with frequencies of 0.5-4 Hz. In contrast to the origin of spindle oscillations in synaptic networks, the slow-frequency rhythm can be generated in single cells (reviewed in Steriade et al., 1993). HCN channels contribute to the different patterns of rhythmic activity of thalamocortical neurons in two ways. First, the interplay between low-threshold T-type Ca^{2+} channels and HCN channels confers the autonomous 0.5-4 Hz rhythm onto thalamocortical relay cells (McCormick and Pape, 1990; Soltesz et al., 1991; Dossi et al., 1992; McCormick and Huguenard, 1992). Activation of Ca^{2+} channels results in Ca^{2+} spikes and often in a high-frequency burst of Na^+/K^+ action potentials. Inactivation of Ca^{2+} channels terminates the Ca^{2+} spike, followed by hyperpolarization of the neuron and activation of hyperpolarization-activated channels, which provide the depolarizing I_h current. Second, persistent activation of I_h during a spindle wave epoch shifts the membrane potential by up to 5 mV to more positive values (Bal and McCormick, 1996). This afterdepolarization stops oscillations probably by inactivation of the T-type Ca^{2+} channels (Bal and McCormick, 1996). There is now good evidence that this afterdepolarization is due to an increase in HCN channel activity, probably via Ca^{2+}-calmodulin-stimulated adenylate cyclase activation and cAMP production (Lüthi and McCormick, 1998a, 1999). The duration of the refractory period between spindle wave epochs (3-20 seconds) is probably determined by the time course of HCN channel deactivation (Bal and McCormick, 1996).

Besides "pacing" rhythmic activity, HCN channels also help determine other electrical properties of non-pacemaking neurons. I_h currents contribute to the facilitation of repetitive activity, most importantly in sensory pathways such as the auditory system, where the number and timing of incoming action potentials must be accurately transmitted even at high imput rates to ensure fidelity in stimulus coding (Banks et al., 1993). I_h currents also produce rebound depolarization after hyperpolarizing responses, in the rod photoresponse to bright light for example (Fain et al., 1978; Wollmuth and Hille, 1992), and can generate rebound action potentials following inhibitory inputs (Solomon and Nerbonne, 1993). In the visual process, I_h might play an important role in the transfer of signals from photoreceptors to second

order neurons by suppressing the slow components originated in the phototransductive cascade, thus enhancing the light response in a range of temporal frequencies relevant to vision (Gargini et al., 1999). Finally, I_h channels have been shown to impact the shape and propagation of subthreshold voltage potentials in dendritic trees, and thus to regulate the integration of synaptic inputs (Magee, 1998).

1.2.4 Role of HCN channels in fertilization

HCN channels have been identified in both invertebrate and vertebrate testis. The channel called SpHCN or SPIH was cloned from sea urchin testis (Gauss et al., 1998); a channel with similar properties had already been described in the sperm of the same species (Labarca et al., 1996). Northern blotting showed that SpHCN mRNA is present at high levels only in male gonads; no message was found in female tissue, and Western blots and immunocytochemical studies with an antibody directed against this channel located it specifically in the sperm flagellum, where it could have a role in the control of flagellar beating and thus in the mechanisms of fertilization (Gauss et al., 1998). In fact, sea urchin eggs attract sperm through chemotactic peptides, which evoke complex changes in membrane voltage and in the concentration of cyclic AMP, cyclic GMP and Ca^{2+} ions (for a review, see Ward and Kopf, 1993). Although the intracellular signaling pathways and their cellular targets are largely unknown, hyperpolarization induced by a chemotactic peptide called speract (Babcock et al., 1992) and a concomitant rise in cAMP levels (Hansbrough and Garbers, 1981) could activate the spHCN channel.
As for vertebrates, it has been found that the mRNA of HCN4 is expressed in human testes (Seifert et al., 1999b), but not in murine ones (Santoro et al., 1998). Northern blotting shows that mRNA for hHCN4 gives a strong hybridization signal in testis (Seifert et al., 1999b), thus suggesting expression of the channel in mature spermatozoa or their precursor cells. In this respect, hHCN4 may represent the mammalian equivalent to SpHCN, and could be involved in the generation of rhythmic activity that controls the waveform of flagellar beating. It is worth noting that spermatogenic cells and bursting neurons share a very similar assortment of channels: a low-threshold T-type Ca^{2+} channel and a pH-sensitive K^+ channel, which belongs to the family of Ca^{2+}-dependent K^+ channels, have been described in mammalian spermatogenic cells (Arnoult et al., 1996; Liévano et al., 1996; Schreiber et al., 1998). In hyperactive hamster spermatozoa, oscillations of intracellular Ca^{2+} have been reported (Suarez et al., 1993), demonstrating

that spermatozoa are capable to sustain rhythmic patterns of activity. The motility of spermatozoa is also controlled by intracellular pH (for a review, see Ward and Kopf, 1993). In this respect, it is of particular physiological significance that intracellular alkalization shifts the $V_{1/2}$ of the thalamocortical HCN channel by 4-5 mV to more positive values (Munsch and Pape, 1999). Therefore, in mammalian spermatozoa, both pH-dependent K^+ channels and HCN4 channels may mediate the physiological responses triggered by a change in intracellular pH. In conclusion, similar molecular components may underlie rhythmic activity of cells as diverse as bursting neurons and swimming spermatozoa.

1.2.5 Regional expression of mammalian HCN channels

(For a review, see Santoro and Tibbs, 1999; Gauss and Seifert, 2000.)
The localization of the four different mammalian HCN channel subtypes has been determined by Northern blotting, in situ hybridization, RNase protection assay (RPA), and various polymerase chain reaction (PCR) techniques. Following is a summary of the results, which in some cases are still controversial.
The HCN1 message was clearly found in brain (Santoro et al., 1997; Ludwig et al., 1998; Santoro et al., 1998; Shi et al., 1999). *In situ* hybridization of mouse brain sections revealed that HCN1 is mainly expressed in the neocortex, the CA1 region of the hippocampus, the superior colliculus, and the molecular cell layer of the cerebellum (Ludwig et al., 1998; Moosmang et al., 1999). While, according to some authors, Northern blotting indicated no HCN1 message in heart (Ludwig et al., 1998; Santoro et al., 1998), others describe a substantial amount of HCN1 message in the sinoatrial node and detectable expression in the Purkinje fibers of the rabbit heart (Shi et al., 1999).
Expression of HCN2 was found in brain (Ludwig et al., 1998; Santoro et al., 1998; Shi et al., 1999) and in heart (Ludwig et al., 1998; Santoro et al., 1998; Ludwig et al., 1999b; Shi et al., 1999; Vaccari et al., 1999). *In situ* hybridization of mouse brain sections shows that HCN2 mRNA is widespread within the brain (Ludwig et al., 1998; Moosmang et al., 1999). The highest expression is found in the olfactory bulb, the cerebral cortex, hippocampus, thalamus, amygdala, superior and inferior colliculi, cerebellum, and brainstem (Moosmang et al., 1999). Within the heart, HCN2 was described as present in the ventricle and atrium (Ludwig et al., 1999b), but others found HCN2 at a very low level in the sinoatrial node and the left

ventricle of rabbit heart while it appeared in moderate and abundant level in rat neonatal and adult ventricle, respectively (Shi et al., 1999).
The HCN3 message was found in brain (Ludwig et al., 1998; Santoro et al., 1998; Shi et al., 1999). *In situ* hybridization reveals only weak expression throughout the brain, with somewhat higher expression in the olfactory bulb (Moosmang et al., 1999). High amounts of message were reported in liver, lung and kidney (Santoro et al., 1998), but these findings were not always confirmed (Ludwig et al., 1998).
Message of HCN4 has been found in brain (Ludwig et al., 1998; Santoro et al., 1998; Seifert et al., 1999b; Shi et al., 1999). Main expression has been described in the olfactory bulb, habenula, and thalamus (Moosmang et al., 1999); others report significant message in the substantia nigra, in addition to the highest expression in the thalamus (Seifert et al., 1999b). HCN4 mRNA is also present in high levels in heart (Ludwig et al., 1998; Santoro et al., 1998; Ishii et al., 1999; Ludwig et al., 1999b; Seifert et al., 1999b; Shi et al., 1999). Strong expression of HCN4 has been described in the sinoatrial node of the rabbit, and much less in the Purkinje fibers (Shi et al., 1999; Ishii et al., 1999); moderate amounts of HCN4 message can be detected in the rat neonatal and adult ventricle, and in the homologous human tissue (Shi et al., 1999; Ludwig et al., 1999b). Furthermore, HCN4 message was found in lung and skeletal muscle (Santoro et al., 1998), but this result is controversial (Ludwig et al., 1999b; Seifert et al., 1999b). HCN4 mRNA has been reported in human testes (Seifert et al., 1999b), but not in murine ones (Santoro et al., 1998).

1.2.6 Structural features and functional properties of HCN channels: an overview

(For a review, see Biel et al., 1999b; Ludwig et al., 1999a; Gauss and Seifert, 2000.)
Native I_h currents have undergone extensive physiological characterization, but their molecular bases have remained unexplained for a long time. In this search, as seen in section 1.2.1, a central role was played by the hypothesis that channels underlying I_h currents could be members of the voltage-gated K^+ channel superfamily and distantly related to CNG channels. The hypothesis proved correct: sequence alignment of HCN, voltage-gated K^+ and CNG channels allows the prediction of a common overall structure. Similarities and differences among the three groups will be extensively discussed in sections 1.2.7 to 1.2.10, but it is useful to summarize them here. HCN channels display the six membrane-spanning domain topology typical

of voltage-gated channels, and common to CNG channels as well (see fig. 3), as opposed to that of ligand-gated channels, with seven hydrophobic domains. There is a voltage sensor located in the S4 segment, which is typical of voltage-gated channels, but is partially conserved also in CNG channels, that do not display voltage dependency. Interestingly, while being both dependent on voltage, HCN channels require hyperpolarization of the membrane to activate, while voltage-gated K^+ channels open upon depolarization of the membrane. The pore region is located between segments S5 and S6, and while this feature is common to all three groups, there are a few differences in the amino acid composition that might account for the different ionic selectivities: while K^+ voltage-gated channels are extremely selective, HCN and CNG channels display weak cation selectivity (respectively, for K^+ and Na^+). Finally, HCN channels share with CNG channels the characteristic of a cyclic nucleotide-binding domain (CNBD), located at the C-terminus, and absent in voltage-gated K^+ channels. While CNG channels strictly require cyclic nucleotides to open, the same compounds in HCN channels have a positive modulatory effect.
All HCN channels cloned so far can be functionally expressed as homomers, and, presumably, four subunits assemble to form a functional channel. The presence of ancillary subunits, although not demonstrated yet, cannot be excluded, and could partially explain the overlapping expression patterns of the four HCN transcripts in heart and brain (see section 1.2.5).

1.2.7 The HCN gene family

(For a review, see Santoro and Tibbs, 1999.)
The amino acid sequence similarity between channels HCN1-4 from mouse, SpHCN from sea urchin (here called SPIH, according to the old nomenclature) and HvHCN from silkmoth (see section 1.2.1; here called HVIH) is presented, as percentage, in fig. 5A. The four mammalian channels are very closely related to each other, with an overall similarity in the protein sequences of 56-60% and a similarity within the core sequence (domains S1 through the CNBD) of 80-90%. In contrast, the N- and C-termini vary considerably in their length and share only modest homology. The overall protein sequence similarity between SpHCN and the murine HCN gene products is 38-40%, with a similarity of 52-54% in the core region of the proteins. The overall protein sequence similarity of HVIH to the murine HCN channels is 46-49% (51% to the sea urchin channel), and the similarity in the core region is 58-61% (65% to SpHCN). The inferred

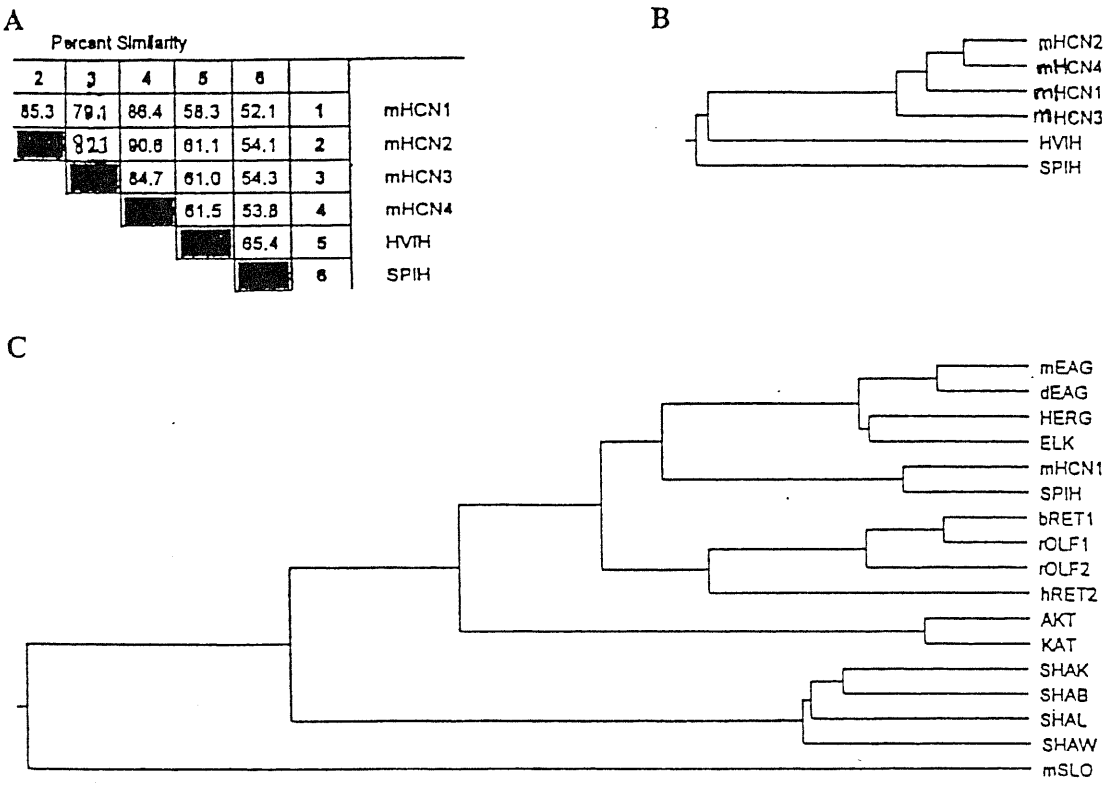

Fig. 5A-C
See legend on following page.

Fig. 5A-C
A Percent amino acid sequence similarity between mouse HCN1-4, SpHCN (here called SPIH, according to the old nomenclature) and HvHCN (here called HVIH) channels. Similarities were calculated from an alignment of the region included between transmembrane domain S1 and the CNBD.
B Phylogenetic tree deduced from sequence analysis in **A**.
C Phylogenetic tree of representatite members of the K channel superfamily. The dendrogram was derived from an alignment of the hydrophobic core of the proteins, including transmembrane domains S1 through S6.
For **A-C**, the following sequences were used:
mHCN1-4 and SPIH (SpHCN): see table 2;
HVIH (HvHCN): HCN related gene from the silkmoth *Heliothis virescens* (Krieger et al, 1999);
mEAG: mouse Eag protein (Warmke and Ganetzky, 1994);
dEAG: *Drosophila* Eag protein (Warmke et al., 1991);
HERG: human Erg protein (Warmke and Ganetzky, 1994);
ELK: *Drosophila* Elk protein (Warmke and Ganetzky, 1994);
bRET1: α-subunit of bovine retinal CNG channel (Kaupp et al., 1989);
rOLF1: α-subunit of rat olfactory CNG channel (Dhallan et al., 1990);
rOLF2: β-subunit of rat olfactory CNG channel (Liman and Buck, 1994);
hRET2: β-subunit of human retinal CNG channel (Chen et al., 1993);
AKT: *Arabidopsis* AKT1 protein (Sentenac et al., 1992);
KAT: *Arabidopsis* KAT1 protein (Anderson et al., 1992);
SHAK: *Drosophila* Shaker protein (Papazian et al., 1987);
SHAB: *Drosophila* Shab protein (Wei et al., 1990);
SHAL: *Drosophila* Shal protein (Wei et al., 1990);
SHAW: *Drosophila* Shaw protein (Wei et al., 1990);
mSLO: mouse slo protein (Pallanck and Ganetzky, 1994).
(**A-C** adapted from Santoro and Tibbs, 1999.)

phylogenetic relationship between mHCN1-4, SpHCN, and HvHCN genes is presented in fig. 5B. At present, there is little evidence that the HCN family includes any other immediate member; however, the presence of closely related or more distantly related members cannot be ruled out.

The phylogenetic relationship between the HCN gene family (represented by mHCN1 and SpHCN) and other representative members of the K^+ channel superfamily is presented as a dendrogram in fig. 5C. From this it is clear that mHCN1, its homologues, and SpHCN form a new subfamily within the K^+ channel superfamily. Not surprisingly, the HCN and SpHCN channels are most closely related to other K^+ channels that contain a CNBD, such as the EAG-related channels, the CNG channels, and the plant inward rectifiers related to KAT1. Nonetheless, HCN and SpHCN form a new branch within this group. A comparison of the hydrophobic core region (domains S1 through S6) of HCN1 and SpHCN with the corresponding region in other CNBD-containing channels shows that the highest sequence similarity occurs with the EAG and HERG proteins, albeit this amounts to only ~22%. The lowest similarity is to the α-subunit of bovine rod CNG channel (17%). However, if the CNBDs of these channels are compared, the one in HCN is found to be most similar to the one of the α-subunit of bovine rod CNG channel (28%), while the corresponding domains of HERG or KAT1 are less similar to HCN (22% or 15%, respectively). This observation is congruous with the fact that HCN channels display a voltage-dependent inward rectification reminiscent of HERG or KAT1, but a cyclic nucleotide regulation that is not seen in any other channels except the CNG channels.

It is interesting to speculate on the evolutionary relationship among the various members of the K^+ channel superfamily. It has been suggested that the fusion between an ancestral K^+ channel and an ancestral CNBD might have occurred before the evolutionary separation of plant and animals (Warmke and Ganetzky, 1994). Interestingly, among all channels bearing a CNBD, the one in HCN shows the closest homology to those present in protein kinases and most remarkably to that of the yeast cAMP-dependent protein kinase (25% similarity). At the same time, the hydrophobic core region of mHCN1 retains a relatively high similarity to that of voltage-gated K^+ channels, Shaker in particular (14%). Thus, the HCN genes might be a closer representation of the genealogical link that existed between voltage-gated and CNG channels, that any of the channels known so far.

1.2.8 The S4 segment and the activation by hyperpolarization

The transmembrane core of HCN channels contains a positively charged motif that corresponds to the S4 segment of voltage-gated cation channels, where regularly spaced lysines and arginines allow the formation of an α–helix in which these positively charged residues are lining next to each other; the S4 segment has been shown to serve as a voltage sensor that moves toward the extracellular surface after depolarization of the cell membrane and thus opens the channel (Catterall, 1986; Guy and Seetharamulu, 1986; Numa, 1989; Guy and Conti, 1990). In this respect, the presence of a similar voltage sensor in HCN channels is somewhat surprising, since these channels are activated by hyperpolarization. Fig. 6 shows the amino acid sequence alignment of the S4 segments of HCN channels characterized so far and of other members of the K^+ channel superfamily. Among mammalian HCN channels, the S4 motif is perfectly conserved, and contains 9 positive charges in the canonical pattern of one charge every third residue, in place of the 5 charges in CNG channels, 7 in Shaker, DmEAG, HERG, and 8 in KAT1. In SpHCN, the S4 motif is also well conserved with respect to the mammalian homologues, with the notable exception of a negative charge in place of the first positive one.
A mechanism of the activation of HCN channels was proposed (Gauss et al., 1998; Santoro et al., 1998; Biel et al., 1999b) based on studies on mutated Shaker channels (Miller and Aldrich, 1996) and on the HERG K^+ channel (Trudeau et al., 1995; Smith et al., 1996). According to this model, the three states of a voltage-gated channel, namely closed, open and inactive, are shifted in HCN channels pronouncedly to negative membrane voltages. Therefore, at resting potential, HCN channels are in the inactivated state even though the S4 segments forming the activation gates may be in the open configuration. Hyperpolarization would then open the channels by reversing the inactivation reaction. The structure of this "inactivation gate" is not known at present; however, a first clue towards an understanding of HCN activation is provided by a recent study on the inwardly rectifying K^+ channel KAT1 from *Arabidopsis thaliana* (Marten and Hoshi, 1998). KAT1 resembles HCN channels in that it is both activated by hyperpolarization and also contains a positively charged S4 segment. By investigating the effect of N-terminal deletions and an S4 mutation, it was concluded that in the KAT1 channel the hyperpolarizing shift in the activation curve is due to the interaction of the cytoplasmic N-terminus with the S4 segment. It is not known if a similar interaction takes place in HCN channels.
Given that HCN and KAT1 channels appear to have distinct gating behavior,

```
mHCN1     238-KTARALRIVRFTKILS-LLRLLRLSRLIR
mHCN2     291-KTARALRIVRFTKILS-LLRLLRLSRLIR
mHCN3     201-KTARALRIVRFTKILS-LLRLLRLSRLIR
hHCN4     369-KTARALRIVRFTKILS-LLRLLRLSRLIR
SpHCN     326-EVSRALKILRFAKLLS-LLRLLRLSRLMR
KAT1      168-RILSMLRLWRLRRVSSLFARLEKDIRFNY
Shaker    344-NQAMSLAILRVIRLVR-VFRIFKLSRHSK
DmEAG     341-SLFSALKVVRLLRLGR-VVRKLDRYL
HERG      519-ELIGLLKTARLLRLVR-VARKLDRYSEYG
brCNGCa   263-WNYPEIRLNRLLRISR-MFEFFQRTETRT
```

Fig. 6
S4 motif: amino acid sequence alignment of HCN channels and other members of the voltage-gated K^+ channel superfamily. Arginine (R) or lysine (K) residues are shown in bold; the serine (S) reside, which divides the S4 motif into two domains in HCN and in KAT1 channels, is underlined.
From top to bottom:
mHCN1-3, hHCN4, SpHCN: see table 2;
KAT1: hyperpolarization-activated K^+ channel from *Arabidopsis thaliana* (Anderson et al., 1992);
Shaker: K^+ channel encoded by the *Drosophila Shaker b* gene (Pongs et al., 1988);
DmEAG: *Drosophila* ether-à-go-go (eag) channel (Warmke et al., 1991);
HERG: channel encoded by the human eag-related gene (Warmke and Ganetzky, 1994);
brCNGCα: α-subunit of the CNG channel from bovine rod photoreceptors (Kaupp et al., 1989).

it is curious to note a small but potentially significant similarity in the sequences of the S4 motifs of all these inward rectifiers: in the middle of the voltage sensor, the regular repetition of positive residues is interrupted by a serine in place of an expected positive charge. Interestingly, this serine is flanked by the three residues that, when mutated in the Shaker channel, make it an inward rectifier (Miller and Aldrich, 1996). The presence of this serine, that divides the voltage sensor in two domains, is a feature that sets HCN and KAT1 channels apart from the depolarization-activated Shaker channel, and might play a role in the activation upon hyperpolarization.
A more recent step towards the understanding of the activation mechanism in HCN channels, and in agreement with the model presented above, comes from mutagenesis experiments on the mouse type 2 HCN channel (mHCN2) (Vaca et al., 2000). Single and sequential mutations in the S4 segment were introduced in an attempt to identify the structural motifs responsible for the channel voltage dependence. Neutralization of the first three positively charged residues, by replacement with glutamine, resulted in an increment of the channel voltage dependence by shifting the midpoint activation constant to more negative values, in the measure of about –20 mV shift/amino acid towards more hyperpolarizing potentials; this effect was additive for sequential mutations of these three residues. Instead, mutations of the last six positively charged amino acids resulted in silent channels, suggesting that these residues cannot be altered without impairing channel function. Moreover, none of the above amino acid substitutions resulting in functional channels had any measurable effect on the time course of channel activation, suggesting that the S4 domain of HCN channels critically controls the voltage dependence of channel opening but is not involved in regulating activation kinetics.

1.2.9 The pore region and the ion selectivity

I_h current is carried by both Na^+ and K^+, with the native I_h channels being fourfold selective for K^+ over Na^+ (Wollmuth and Hille, 1992; Ho et al., 1994); the ion selectivity of heterologously expressed HCN channels is in agreement with that of native channels (for a review, see Santoro and Tibbs, 1999). Amino acid sequence alignment, shown in fig. 7, demonstrates that the pore region of HCN channels is related to that of K^+-selective channels (Doyle et al., 1998; Choe and Robinson, 1998), despite the fact that K^+ channels are no less than hundredfold selective for K^+ versus Na^+. The pore region of K^+ channels is localized between the fifth and sixth putative transmembrane segments, and consists of a pore helix and the selectivity

```
SpHCN     416-TWALFKALSHMLCIGYGKFPPQS-438
mHCN1     335-SYALFKAMSHMLCIGYGAQAPVS-357
mHCN2     388-SFALFKAMSHMLCIGYGRQAPES-410
mHCN3     298-SHALFKAMSHMLCIGYGQQAPVG-320
hHCN4     466-SYALFKAMSHMLCIGYGRQAPVG-488
KAT1      248-VTALYWSITTLTTTGYGDFHAEN-270
Shaker    418-PDAFWWAVVTMTTVGYGDMTPVG-440
DmEAG     441-VTALYFTMTCMTSVGFGNVAAET-463
HERG      612-VTALYFTFSSLTSVGFGNVSPNT-634
brCNGCα   348-VYSLYWSTLTLTTIG--ETPPPV-368
KcsA       63-PRALWWSVETATTVGYGDLY-PV-84
```

Fig. 7
Pore region: amino acid sequence alignment of HCN channels and other members of the K^+ channel superfamily. Residues identical to the corresponding positions in SpHCN are in bold characters.
From top to bottom:
SpHCN, mHCN1-3, hHCN4: see table 2;
KAT1: hyperpolarization-activated K^+ channel from *Arabidopsis thaliana* (Anderson et al., 1992);
Shaker: K^+ channel encoded by the *Drosophila Shaker b* gene (Pongs et al., 1988);
DmEAG: *Drosophila* ether-à-go-go (eag) channel (Warmke et al., 1991);
HERG: channel encoded by the human eag-related gene (Warmke and Ganetzky, 1994);
brCNGCα: α-subunit of the CNG channel from bovine rod photoreceptors (Kaupp et al., 1989);
KcsA: K^+ channel from the yeast *Streptomyces lividans* (Schempf et al., 1995).

filter (Doyle et al., 1998). The GYG triplet is the signature sequence for K^+-selective channels (Heginbotham et al., 1994), and forms the main and narrowest part of the selectivity filter, contributing to two of the K ion binding sites (Doyle et al., 1998). In some channels, like the *Drosophila ether-à-go-go* (eag) channel and its human homologue HERG, the tyrosine residue is replaced by phenylalanine. CNG channels lack the YG motif; indeed, when these residues are deleted from the Shaker channel pore region, the ion selectivity is lost (Heginbotham et al., 1994), but all attempts to add the YG motif in the pore of CNG channels have resulted in non functional proteins. Surprisingly, HCN channels contain a GYG sequence, although they pass both Na^+ and K^+. Hence, other amino acids, in addition to the GYG sequence, must determine selectivity for K^+. In K^+-selective channels, the narrowest part of the pore is formed by the carbonyl oxigens from the main chain of the signature sequence, providing a ring of sites suitable for coordinating precisely a dehydrated K^+ ion. A sheet of aromatic amino acids, formed between the tyrosine side chains of the signature sequence and the aromatic amino acids of the pore helix, works like a ring of springs holding the pore open at its correct diameter (Doyle et al., 1998). The pore of HCN channels contains several amino acid substitutions compared to the pore of selective K^+ channels, notably:

1) 1 or 2 positively charged residues and a histidine, in place of neutral amino acids;
2) absence of the cluster of threonine residues that codetermine K^+ selectivity (Heginbotham et al., 1994);
3) the amino acid position following the GYG motif is particularly interesting: this residue is aspartic acid in almost all known K^+ channels (although, it's neuter asparagine in *Drosophila* and human eag channels); however, in HCN channels, it is either a positively charged or a neutral amino acid;
4) just N-terminal to the GYG sequence, a cysteine replaces conserved threonine or serine residues.

Therefore, if the result of these mutations in HCN channels is to make a less rigid carbonyl backbone and a smaller pore that can coordinate either hydrated Na^+ or K^+ ions, the channel may have lost its selectivity.

Potassium is not only a permeating ion of HCN channels, it also regulates the permeation of Na^+. Both the current amplitude and the P_{Na}/P_K ratio of HCN channels depend on the extracellular K^+ concentration, i.e. an increase in extracellular K^+ concentration results in a strongly increased current amplitude and in a slightly reduced selectivity for K^+ over Na^+ (Frace et al., 1992b; Wollmuth and Hille, 1992; Brown and Ho, 1996). The

interdependence of Na^+ and K^+ permeation in HCN channels is illustrated by the finding that the channels conduct little, if any, Na^+ in the absence of K^+ ions. Thus, K^+ is required for the channel to carry any current in spite of the fact that Na^+ constitutes the major inward cation current in HCN channels at physiological membrane potentials. The structural basis of this phenomenon is not known at present. However, it seems reasonable to assume that the pore of HCN is, like that of CNG channels (Sesti et al., 1995) and Ca^{2+} channels (Hess and Tsien, 1984), a multi-ion pore possessing at least two cation binding sites: one at the external mouth of the channel having a higher affinity for K^+, and another having a higher affinity for Na^+ (Wollmuth, 1995).
HCN channels are not only regulated by K^+, but also by external Cl^-. Substitution of external chloride ions by larger anions such as isethionate or gluconate results in a pronounced reduction of the current amplitude of both native (Frace et al., 1992a) and expressed channels (Santoro et al., 1998). Thus, the pore of HCN channels is likely to contain an extracellular binding site for Cl^-, which may be related to the presence of positively charged residues in this region. The physiological function of the chloride-dependence of HCN channels is not understood yet. It was speculated that Cl^- may perform a screening role for cations bound at external sites of the multi-ion channel and thereby represent a necessary step in channel permeation by cations (Frace et al., 1992a).

1.2.10 The cyclic nucleotide-binding domain and the modulation by cyclic nucleotides

Pacemaker channels are gated not only by hyperpolarization but also by cyclic nucleotides, which exert a dual effect, namely a 2- to 15-mV shift of the activation curve towards more positive membrane potentials and an acceleration of the channel activation. Cyclic nucleotides regulate HCN channels by a direct binding to a cyclic nucleotide binding domain (CNBD), a region of approximately 80-100 amino acids near the C-terminus of the channel, which is highly homologous to the CNBDs of other cyclic nucleotide-regulated proteins like the catabolite activator protein (CAP) of *Escherichia coli* and the cAMP-regulated guanine nucleotide exchange factors cAMP-GEFs/Epac (Kawasaki et al., 1998; de Rooij et al., 1998). Studies on the CAP crystal structures (Weber and Steitz, 1987) show that the CNBD is made of 3 α-helices (αA-C) and 8 β-sheets (β1-8). Amino acids which have been determined to lie close to the cAMP molecule in CAP (Weber and Steitz, 1987) are well conserved in HCN channels, and have

been shown to be responsible for forming the hydrophobic ligand-binding pocket and specific contacts with the ligand also in cAMP-dependent protein kinases and cyclic nucleotide-gated channels (Weber et al., 1987; Taylor et al., 1990; Kaupp, 1991; Kumar and Weber, 1992). In comparing the CNBDs of HCN and CNG channels, two elements, in particular, are noteworthy:

1) the threonine residue found in the β7 strand of HCN1-4 channels is also found in the α subunit of the bovine rod CNG channel (brCNGCα), where it is important for selecting cGMP over cAMP (Altenhofen et al., 1991; Scott et al., 1996). It is interesting to note that SpHCN has a valine at the respective position, which might explain the different ligand selectivity of that channel; in fact, while native and cloned mammalian HCN channel are almost equally sensitive to cAMP and cGMP (DiFrancesco and Tortora, 1991; Ludwig et al., 1998), cGMP was found to be a very poor agonist for the SpHCN channel (Gauss et al., 1998);
2) at the position of the isoleucine residue in the αC helix of HCN channels, brCNGCα carries an aspartate residue that plays an important role in promoting the binding signal into an allosteric transition (Varnum et al., 1995; Gordon et al., 1996). The negative charge of aspartate at this position makes an unfavorable electrostatic interaction with the free electron pair of the N1 position of cAMP, which makes cAMP a poor agonist in this particular CNG channel. A study involving single-point mutations at this amino acid position showed that cAMP can be a fine agonist (even better than cGMP) of this channel when aspartate at this position is replaced by a hydrophobic amino acid (Varnum et al., 1995). Thus the isoleucine residue found in all HCN channels is important for their preference for cAMP.

1.2.11 Correlation between native and cloned HCN channels

(For a review, see Biel et al., 1999b; Gauss and Seifert, 2000.)
As for neuronal HCN channels, four different types have been identified in brain (see also section 1.2.5). *In situ* hybridization indicates that HCN2 is the most widely expressed channel type in brain. Transcripts of HCN2 are nearly ubiquitously distributed in brain, whereas HCN1 expression is more limited to specific parts of the brain like hippocampal CA1 neurons, superior colliculus, cerebral cortex and cerebellum. The partially overlapping expression pattern of HCN1 and HCN2 suggests that these channels may

form heteromers in subset of neurons. At present, the expression of HCN3 and HCN4 has not been mapped at high resolution in brain, however the rather faint signal observed in Northern blots indicates that at least HCN3 is restricted to specific parts of the brain and/or expressed at much lower density than HCN1 and HCN2. The presence of multiple HCN channels in brain is in good agreement with properties of I_h currents in different types of neurons. The various I_h currents significantly differ in terms of activation kinetics, modulation by cAMP, and voltage-dependence of activation (for a review, see Pape, 1996). The region-specific expression of HCN channels, possibly in combination with the formation of heteromeric channels, could well explain the observed current diversity. This notion is supported by the expression of HCN1 (Santoro et al., 1998) and HCN2 (Ludwig et al., 1998) channels in heterologous expression systems. The expressed channels reveal the principal properties of native I_h channels like activation by hyperpolarization, permeability for Na^+ and K^+, and blockage by extracellular Cs^+, but also significantly differ from each other in terms of their activation kinetics and modulation by cAMP. HCN1, which is expressed in hippocampal neurons, resembles the native hippocampal channel (Maccaferri et al., 1993; Pedarzani and Storm, 1995) in that it activates relatively rapidly upon hyperpolarization (with an activation time constant varying from 100 to 300 ms at –130 to –100 mV, it is the fastest subtype characterized so far) and is only weakly shifted by cAMP (~2 mV) to more positive potentials. $V_{1/2}$ is roughly –100 mV. In contrast, HCN2, which is highly expressed in thalamic neurons, resembles channels characterized in these neurons (McCormick and Pape, 1990; Pape, 1992), in that it activates rather slowly (activation time constants are between 200 and 500 ms at –140 to –100 mV) but is profoundly regulated by cAMP (~13 mV shift and significant acceleration of activation kinetics). $V_{1/2}$ is at –100 mV.
As for cardiac HCN channels, two genes are expressed in mouse and human heart, HCN2 and HCN4. Fig. 8 illustrates the electrophysiological properties of human HCN2 and HCN4 channels, heterologously expressed in human embryonal kidney cultured cells. *In situ* hybridization (Ludwig et al., 1998) and PCR analysis (Santoro et al., 1998) revealed that HCN2 is expressed throughout the heart including the sinoatrial node (Santoro et al., 1998). The exact distribution of HCN4 within the heart has not yet been investigated, however the relatively low abundance of HCN4 clones in human heart cDNA (see Biel et al., 1999b) indicates that this channel may exist in much lower concentrations in total heart than HCN2. The presence of HCN channels in a variety of heart cells is consistent with data from the literature describing I_h currents in both spontaneously firing pacemaker cells of

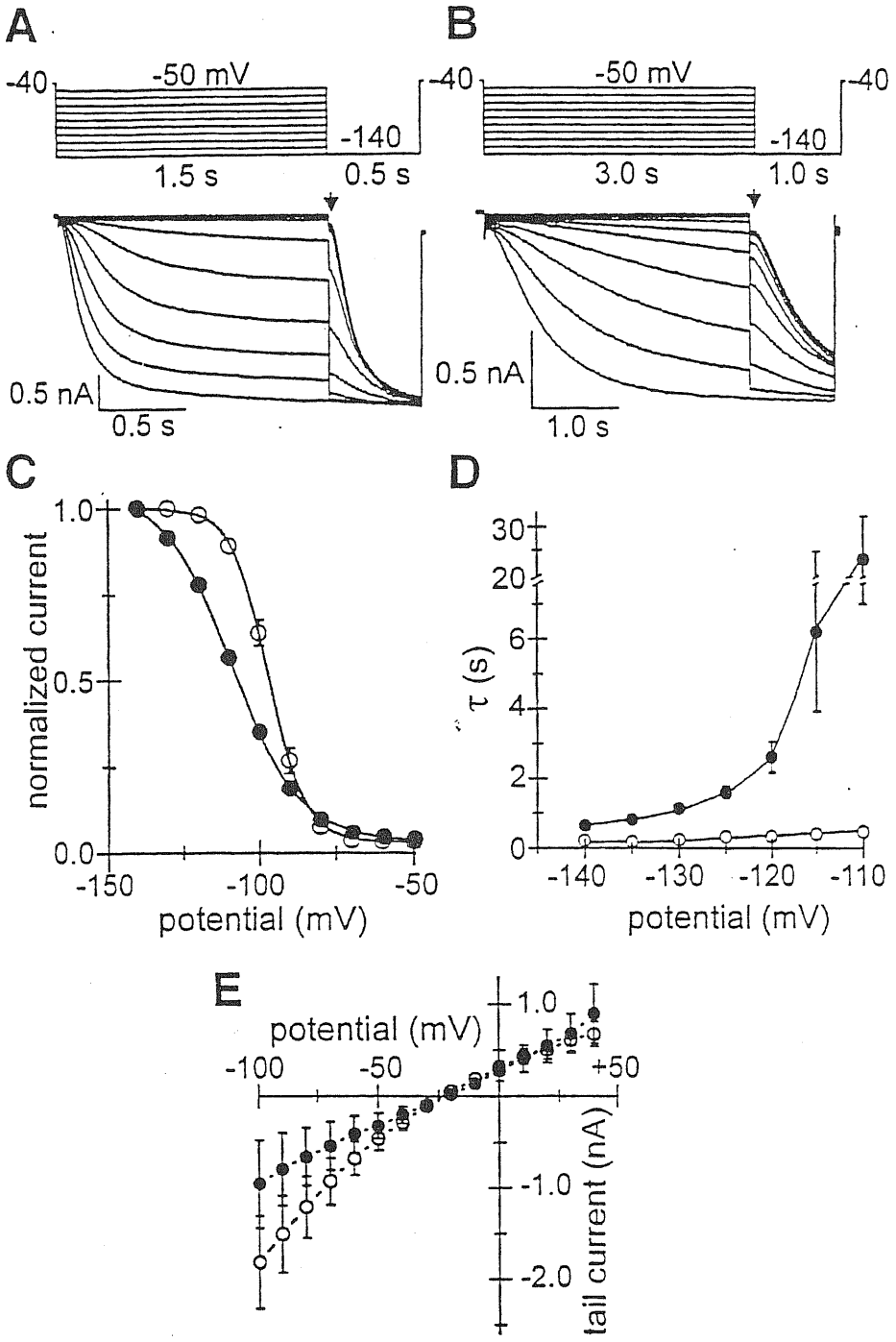

Fig. 8 A-E
See legend on the following page.

Fig. 8 A-E
Electrophysiological properties, measured in whole-cell voltage clamp, of the human HCN2 and HCN4 (hHCN2 and hHCN4) channels heterologously expressed in human embryonal kidney cultured cells (Ludwig et al., 1999b).
A hHCN2 channel currents.
Upper: voltage protocol. Cells were clamped from a holding potential of –40 mV to various voltages (–140 to –50 mV in 10 mV increments) for 1.5 s followed by a step to –140 mV.
Lower: current traces of a cell expressing hHCN2.
B hHCN4 channel currents.
Upper: voltage protocol. As in **A** except for 3 s long prepulses.
Lower: hHCN4 current traces.
C Activation curves of hHCN2 (*open circles*) and hHCN4 (*filled circles*) currents. Tail currents measured immediately after the voltage step to –140 mV, arrow in **A** and **B**, were normalized and plotted as a function of the preceding membrane potential.
D Voltage dependence of activation kinetics. Current traces at voltages ranging from –140 to –110 mV from hHCN2- or hHCN4-expressing cells were fitted with a single exponential. The time constants for hHCN2 (*open circles*) and hHCN4 (*filled circles*) activation are plotted against the corresponding potentials.
E determination of the I/V relationship of the fully activated hHCN2 (*open circles*) and hHCN4 (*filled circles*) channels. Steps to test voltages (range –100 to +40 mV) were applied after a prepulse to –140 mV (1.5 s for hHCN2 or 3 s for hHCN4; protocol A) or after a prepulse to –20 mV (protocol B). Tail current amplitudes were measured immediately after the test pulse. The difference of tail currents between protocol A and protocol B was determined and plotted against the test potential.

sinoatrial node and ventricular myocites that are normally not involved in generating pacemaker potential (Yu et al., 1995; Baker et al., 1997; Hoppe et al., 1998). The major difference between I_h currents from ventricular myocites and sinoatrial node cells is referred to the voltage dependence of channel activation. Sinoatrial I_h channels activate at significantly more positive potentials than I_h channels in ventricular myocites. The expressed HCN2 channel (Ludwig et al., 1998) fits the general properties of sinoatrial channels in terms of activation kinetics, pharmacology and modulation by cyclic nucleotides. However, HCN2 activates at membrane potentials ($V_{1/2}$ ~-100 mV) which are more consistent with potentials reported for ventricular (range of $V_{1/2}$: -95 mV to -135 mV; Yu et al., 1995; Baker et al., 1997; Hoppe et al., 1998) than for sinoatrial node channels (range of $V_{1/2}$: -65 mV to -90 mV; Denyer and Brown, 1990; DiFrancesco and Tortora, 1991; DiFrancesco and Mangoni, 1994). The reason for this discrepancy is unknown at present. An intrinsic factor that is present in sinoatrial node cells but is missing in heterologous expression systems may be necessary to confer channel activation at more positive voltages. Alternatively, the sinoatrial node channel may be a heteromer consisting of HCN2 and another channel subunit. It is obvious that HCN4 would be a good candidate for this potential second subunit. Its activation kinetics are much slower than those of HCN1 or HCN2 (Ishii et al., 1999; Ludwig et al., 1999b; Seifert et al., 1999). Time constants are between a few hundred milliseconds (at –150 mV) up to many seconds (>20 seconds at –70 mV) (Ludwig et al., 1999b; Seifert et al., 1999). The steady-state open probability is half-maximal at –75 mV (Seifert et al., 1999). Different values for the shift of the activation curve to more positive potentials by cAMP were reported, from 11 mV (Seifert et al., 1999) to 15 mV (Ludwig et al., 1999b) to 23 mV (Ishii et al., 1999).

1.2.12 Properties of invertebrate HCN channels

The identification of the SpHCN channel (see sections 1.2.1 and 1.2.4), originally named SPIH (Gauss et al., 1998), from the sea urchin *Strongylocentrotus purpuratus* indicates that HCN channels have emerged early in evolution. The primary structure of SpHCN reveals all the hallmarks of mammalian channels. Especially the core region of the channels including the six transmembrane segments, the pore loop and the CNBD are highly conserved among vertebrate and invertebrate channels (see section 1.2.7). This structural similarity concurs well with the variety of functional properties that are shared by both vertebrate and invertebrate channels,

namely activation by hyperpolarization, permeation of both Na^+ and K^+, blockage by Cs^+ and sensitivity for cAMP. However, there are also clear differences between the channels. For example, SpHCN activates at much more positive potentials than mammalian HCN channels. In addition, in the absence of cAMP the SpHCN current is transient, whereas mammalian HCN currents reveal no inactivation during maintained hyperpolarization. The most striking difference refers to the mechanism that underlies cyclic nucleotide modulation. cAMP enhances both vertebrate and SpHCN channels. However, the augmentation of the current arises in the case of SpHCN from an up to 20fold increase in the maximum current, while in mammalian HCN channels cAMP does not increase maximum current but shifts the activation curve towards positive membrane potentials. In addition, SpHCN is not sensitive to cGMP, whereas mammalian channels are affected by both cAMP and cGMP. Given the high similarity in the CNBD of SpHCN and mammalian channels, these functional differences might be determined by a few amino acid residues (see section 1.2.10).

The HvHCN channel from the silkmoth Heliothis virescens (see section 1.2.1) was mainly studied on the single channel level (Krieger et al., 1999). A single channel conductance of about 30 pS (with 200 mM K^+ on both sides of the membrane) was reported, considerably higher than the conductance of native mammalian channels of the sinoatrial node (about 1 pS; DiFrancesco, 1986). The HvHCN channel is strongly dependent on the concentration of cAMP, but also on voltage. From the voltage dependence and the amount of cAMP regulation, the authors concluded that the properties of HvHCN most closely resembled those of the SpHCN channel (Krieger et al., 1999).

2) MATERIALS AND METHODS

For our study of the pore region structure in both cyclic nucleotide-gated and hyperpolarization-activated channels, we have used techniques of molecular biology and electrophysiology. The corresponding protocols are given in the next sections.

2.1 The pore of CNG channels

The structure of the pore region of the α-subunit of the bovine rod cyclic nucleotide-gated channel was analyzed by means of the substituted-cysteine accessibility method (SCAM) (Karlin and Akabas, 1998). This is based on mutating into cysteines the residues that make up the pore region, one by one. The mutant protein is then expressed in a heterologous system (*Xenopus laevis* oocytes in our case) and probed with sulfhydryl-specific reagents like MTS compounds or Cd^{2+}. The eventual block of the current, as resulting from patch-clamp experiments, is a measure of the accessibility of each residue, and thus of its position in the pore region.
In the channel of interest, the aminoacids R345-S371, here called R1-S27, constitute the pore region. For this study, the following mutations were performed and analyzed:
V4C, S6C, T16C, I17C, T20C, P22C and S27C.
When testing accessibility from the inside, mutants containing the supplementary mutation C505T were used. C505 is located within the cyclic-nucleotide binding domain, and its reaction with thiol-specific reagents produces partial channel inhibition, in the closed state, which may obscure the effect on the P-loop cysteine residues. The C505T substitution is otherwise neutral (Becchetti et al., 1999; Sun et al., 1996).
Also, I was interested in sketching a three-dimensional model of the pore region in the mutant channel that contains an alanine in place of the glutamate 19: this acidic residue is known to interact with extracellular divalent cations and to contribute to ion conduction, and its substitution with a neuter alanine introduces channel desensitization (Bucossi et al., 1996). For this purpose, the following mutations were prepared and analyzed:
E19A, K2C-E19A, V4C-E19A, S6C-E19A, L7C-E19A, T15C-E19A, T16C-E19A, I17C-E19A, T20C-E19A, P22C-E19A, V24C-E19A and S27C-E19A.

2.2 The pore of HCN channels

The structure of the pore region of the SpHCN channel from sea urchin sperm was studied by analyzing the position and role of two amino acid residues, cysteine 428 and lysine 433, that might be especially important in conferring to HCN channels their peculiar characteristics (see section 1.2.9). I performed the following mutations on the wild-type protein:
C428S, K433Q, C428S-K433Q.

2.3 Molecular biology

2.3.1 DNA material

The laboratory of Prof. U. B. Kaupp (Institut für Biologische Informationsverarbeitung, Forschungzentrum Julich, Julich, Germany) kindly provided the cDNAs encoding for the wild type forms of both the α-subunit of the bovine rod cyclic nucleotide-gated channel and the SpHCN channel. Both cDNAs were cloned into a pGEM-3Z (Pharmacia, Uppsala, Sweden) modified vector named pGEM-HE (fig. 9); the resulting plasmids were initially transformed into *E. coli* DH5αF' competent cells following a classical $CaCl_2$ method (Sambrook et al., 1989). Medium scale DNA preparations (midipreps) were obtained using the Plasmid Midi Kit (Qiagen GmbH, Hilden, Germany).

2.3.2 Site-directed mutagenesis: the classical method

The classical method of site-directed mutagenesis, described below, was only used in the case of the α-subunit of the bovine rod cyclic nucleotide-gated channel to perform the mutations T15C, T16C, I17C, T20C, the corresponding ones in the E19A background, and E19A itself. All the other mutations described in the cyclic nucleotide-gated channel and in the SpHCN channel were obtained by means of the QuickChange Site-Directed Mutagenesis method (Stratagene, La Jolla, CA), which is explained in section 2.3.3.
The cloning vector was obtained by digesting the pGEM-HE plasmid expressing the α-subunit of the bovine rod cyclic nucleotide-gated channel with *SnaB*I (Promega Corporation, Madison, WI) and *SgrA*I (Boehringer Mannheim, GmbH, Mannheim, Germany). The digestion sample was run on

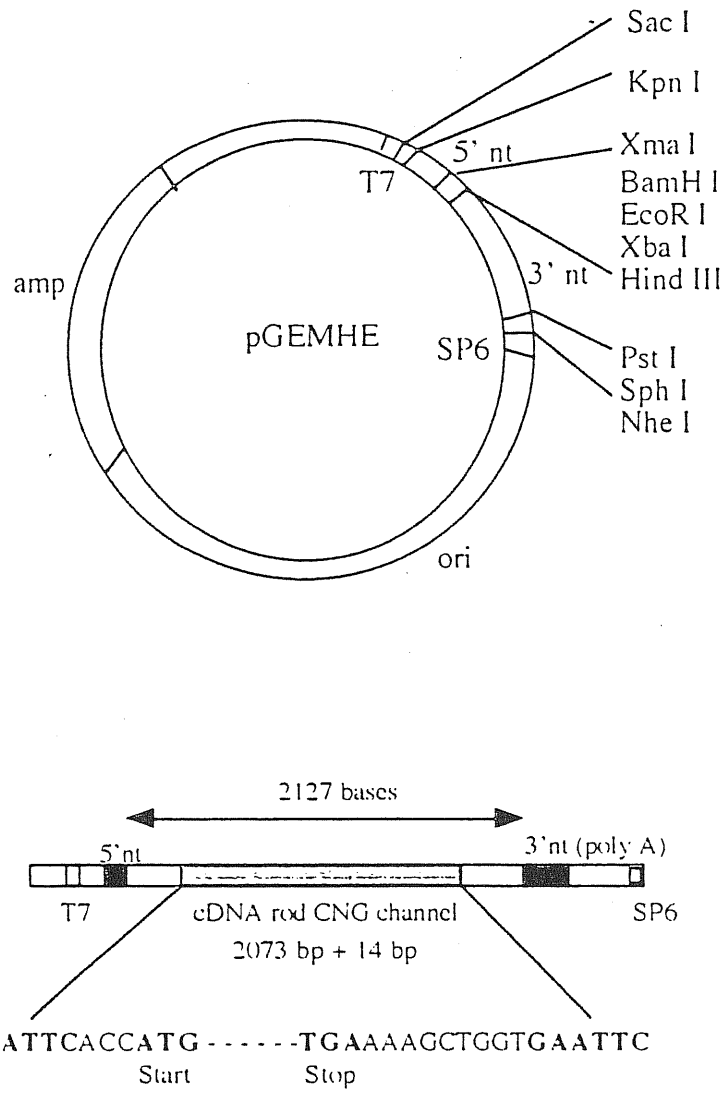

Fig. 9

Upper: plasmid map of pGEM-HE, the vector for heterologous expression in *Xenopus laevis* oocytes derived from the commercial vector pGEM-3Z (Pharmacia, Uppsala, Sweden).

Lower: in this plasmid, cDNA coding for the α-subunit of the bovine rod CNG channel was cloned EcoRI-EcoRI (instead, cDNA coding for the SpHCN channel from sea urchin sperm was cloned BamHI-XbaI).

a preparative 1% agarose gel (FMC BioProducts, Rockland, MF), and the 4.5 kb expected band was then purified by Geneclean (Bio101, Vista, CA).
The insert was prepared by first linearizing the pGEM-HE vector with *Hind*III (Promega); the linearized product was then extracted by phenol-chloroform, precipitated with 3 M sodium acetate, washed with 70% ethanol (see Sambrook et al., 1989) and resuspended in Tris-EDTA (TE) 10:1 at a final concentration of 100 ng/µl. To introduce the desired mutation, Polymerase Chain Reaction (PCR) was performed in a total volume of 100 µl, and the reaction mix contained: 100 ng of *Hind*III-linearized DNA, 100 ng of the primer forward (5' AGA ACC CCC ACG CAA GGG 3'), 250 ng of the primer back which contained both the mutation and the *SgrA*I site (needed as a checking point: 5' AGA ATC CCT CAC CGG TGG TGG TGT TTC GCC AAT AGT GGT C 3'), plus 250 µM dNTPs, buffer and 2 units (U) of *Taq* Polymerase (these two from Perkin-Elmer Applied Biosystems, Forrest City, CA). The mix was overlaid with mineral oil (Sigma, St. Louis, MO) and the PCR was performed in a PTC-100 Programmable Thermal Controller (MJ Research Inc., Waltham, MA) using the following programme: a denaturation step of 2 minutes at 94 °C, then 30 cycles each of 50 seconds at 94 °C, 50 seconds at 50 °C, 30 seconds at 72 °C, and finally an extension step of 10 minutes at 72 °C. The PCR product was digested by both *SgrA*I and *SnaB*I, and the 0.6 kb expected band, containing the mutation, was purified by Geneclean. A ligation reaction was then performed, using 2 units (U) of T4 DNA ligase (New England Biolabs, Beverly, MA) and an overnight incubation at 16 °C, to link 50 ng of the mutated DNA insert with 100 ng of the cloning vector as of above.
The product of the ligation reaction was then transformed into *E. coli* DH5αF' competent cells using the $CaCl_2$ method, and small scale DNA preparation (miniprep) was obtained following the alkaline lysis protocol (Sambrook et al., 1989).

2.3.3 Site-directed mutagenesis: the Quickchange method

With this procedure (a kit from Stratagene), mutations can be obtained in a shorter time than with the classical method. Mutant clones can be prepared in 2-3 days with a minimal mutagenesis efficiency of 33% (with the positive control provided in the kit, the pWhitescript plasmid, the efficiency was of 62%).
The flowchart is shown in fig 10. The QuickChange site-directed mutagenesis method uses the *Pfu* DNA polymerase, which replicates both

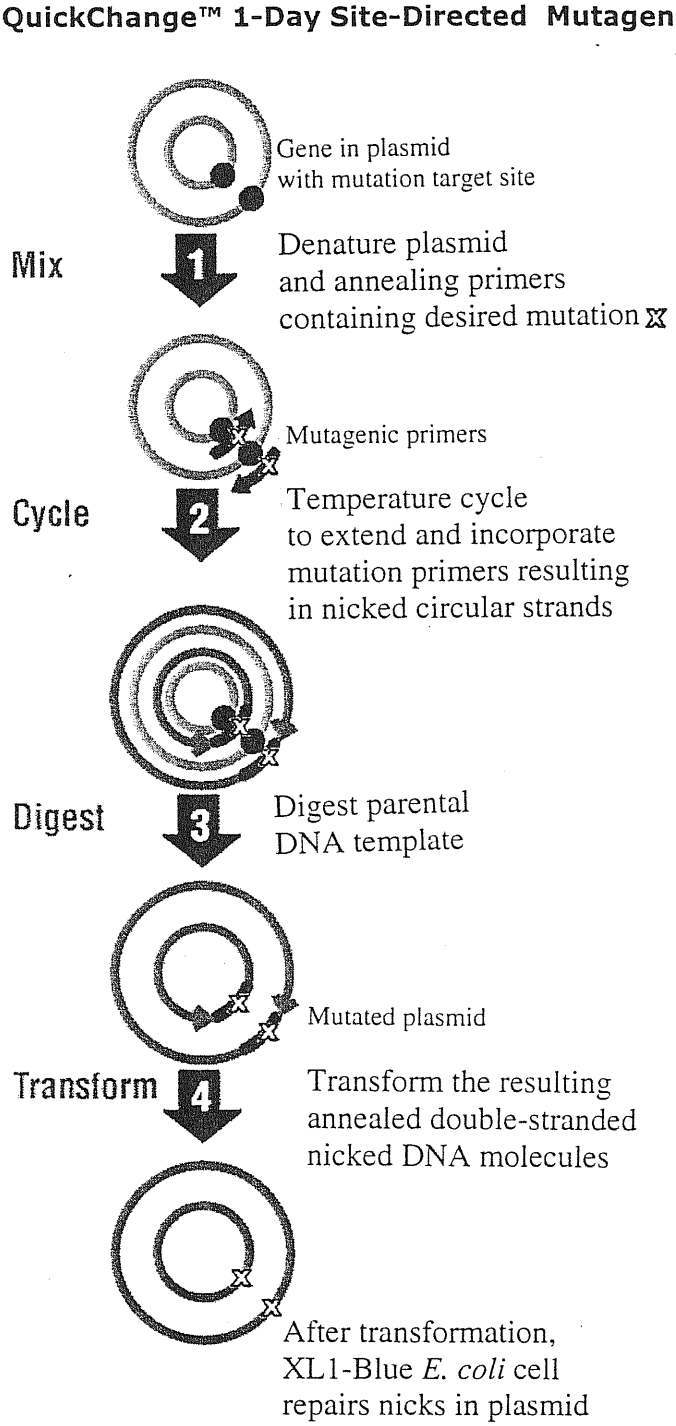

Fig. 10
Quickchange 1-day site-directed mutagenesis method (Stratagene, La Jolla, CA): overview of the experimental protocol.

strands of the supercoiled plasmid DNA template with a higher fidelity than the *Taq* polymerase (estimated error rates are 1.3 x 10^{-6} and 8 x 10^{-6}, respectively) and avoids the linearization step required with the classical method. The two primers are designed to be complementary to each strand of the vector (thus overlapping) and to both contain the desired mutation; they should have a length of 25-45 bp, a minimum GC content of 40% and a recommended melting temperature of 78 °C (although good results with T_m just above 73 °C have also been experienced). A PCR reaction is performed to extend the primers, and the result is a circular mutated plasmid containing nicks. The parental DNA template, which doesn't contain the mutation, is *dam* methylated, like most DNAs extracted from *E. coli* strains, and can be recognized and digested by *Dpn*I, contrarily to the newly synthesized DNA. (*Dpn*I is an endonuclease which targets the methylated or hemimethylated sequence 5'-G^{m6}ATC-3'). The nicked, mutated DNA vector is then transformed by heat-shock into Epicurean Coli XL1-Blue supercompetent cells, which repair the nicks.

The reaction mix for the Quickchange was prepared using 50 ng of the pGEM-HE plasmid containing the cDNA of either the CNG or the HCN channel of interest, and following the instructions of the manufacturer. All the pipetting steps were done using small 10 µl ART pipet tips with filter, which are guaranteed sterile and RNase/Dnase free by the manufacturer (Molecular Bio-Products Inc., San Diego, CA). Thin-Wall tubes (Stratagene) were used for each reaction sample. The cycling reactions were performed by a PTC-100 thermo-cycler (MJ Research) using the following parameters: 95 °C, 30 s (denaturation step) followed by either 12 cycles (for single point mutations) or 16 cycles (for 2-3 bases change) at 95 °C, 30 s; 55 °C, 1 min; 68 °C, 10 min (2 min/kb of plasmid length). After the cycling, the reactions were cooled down on ice and then treated with *Dpn*I to digest the parental DNA. *Dpn*I-treated samples were transformed into Stratagene XL1-Blue supercompetent cells using a classical $CaCl_2$ method with a 42 °C heat shock of 45 s. The transformation reactions were plated on LB+ampicillin Petri dishes.

For each putative mutant, 3 colonies were picked up from the plates and grown for making DNA minipreps, which were obtained using either the Qiagen Plasmid Mini Kit (Qiagen) or the Talent equivalent (Talent srl, Trieste, Italy).

2.3.4 Mutation analysis

The putative mutant DNAs obtained through the Classical Method were digested by *SgrA*I as a first control. The DNA of the clones which resulted positive was purified using the Microspin S-400 HR columns (Pharmacia). 1-2 μg of this DNA was then used to sequence the region of interest with the T7 sequencing kit (Pharmacia), and primers used were:

p69: 5' AGA AAG AGG AGA AAG GC 3'

p71: 5' CAT CAT CAT CAT CAT CC 3'

p72: 5' GCA GAG ATC GCC ATC AAT G 3'

The sequencing reactions were ran on the CastAway Precast sequencing System (Stratagene).
At the same time when the QuickChange site-directed procedure was adopted, we also moved to automated DNA sequencing (LI-COR, 4000L type; LI-COR, Lincoln, NE). In this way we sequenced completely all of the mutants produced with both methods, thus giving more relevance to our studies by gaining confidence in the real nature of the mutants and their electrophysiological characterization. 1 μg of each clone was sequenced using the *SequiTherm EXCEL* II *Long-Read* DNA Sequencing Kit-LC (Epicentre Technologies, Madison, WI) with 1 pmol of primer, as follows.
To sequence the α-subunit of the bovine rod cyclic nucleotide-gated channel, the primers needed were:

T7: 5' TAA TAC GAC TCA CTA TAG GG 3'

CNG-147: 5' GAG GAA GAG AAG AAG GAA GTC G 3'

CNG-313: 5' GCG TGT GTG TAC TTC TCT ATT TCC 3'

CNG-481: 5' TGT GAA GCT GGT CTG TTG GTG 3'

CNG-reverse: 5' ATT CGG GTG TTC TTG AGG C 3'

Four primers were often enough to cover the entire region, depending on the quality of the sequencing gel.
In the case of the SpHCN channel, five primers were needed:

T7: as above

SPIH-145: 5' GAC ACT GGT GCA CTA GGC TC 3'

SPIH-310: 5' ATC TTC CTC CTC GCT GGC GG 3'

SPIH-473: 5' TCC AGC AGG CAA TAC CGT GAG 3'

CNG-reverse: as above

For all mutants, the sequences were of good quality and reproducibility.

2.3.5 RNA synthesis

Complementary RNA (cRNA) of wild type and mutant channels was synthesized starting from 5-10 µg of DNA, and then injected in the cytoplasm of *Xenopus laevis* oocytes.
DNA coming from midipreps was linearized by *Nhe*I (New England Biolabs), extracted, precipitated, washed and finally resuspended in 5-10 µl DEPC-treated ddH_2O. All steps following this one were carried out in Rnase-free conditions.
The DNA was then transcribed *in vitro* using the T7 RNA polymerase and the mCAP RNA Capping Kit (Stratagene); the remaining untranscribed DNA was digested by *Dnase*I, and the RNA was extracted following a classical phenol/chloroform method. After resuspension in DEPC-treated ddH_2O, RNAs were precipitated with sodium acetate (2M) for 1 hour at –20 °C, and then centrifuged at high speed for about 1 hour at 4 °C. These precipitation/centrifugation steps were repeated again, to eliminate any residual debris that might cause problems during injection. RNAs were finally resuspended in DEPC-treated ddH_2O, and divided into aliquots suitable for microinjection (2 µl aliquots at about 1 µg/µl).

2.4 Electrophysiology

The electrophysiological experiments performed in this thesis consisted in measuring the currents activated by cGMP and cAMP in wild type and

mutant CNG and SpHCN channels, respectively. The channels were expressed heterologously in *Xenopus laevis* oocytes; recordings were done on excised patches, in inside-out or outside-out configuration.

2.4.1 Chemicals

The MTS compounds were purchased from Toronto Research Chemicals (Ontario, Canada). All the other chemicals were purchased either from Sigma (St. Louis, MO, USA) or from Merck (Darmstadt, Germany).

2.4.2 Isolation and preparation of *Xenopus laevis* oocytes

Xenopus laevis frogs were anaesthetized by immersion in a 0.2% aqueous solution of tricaine (methanesulphonate salt of 3-aminobenzoic acid ethyl esther) for about half an hour. The anaesthetized animal was put on its back on a bed of ice, and a small incision of about 1 cm was performed with a scalpel laterally on the abdomen. Once the skin and the underneath abdominal muscles were cut through, the ovarian lobes became visible. The follicles (oocytes and follicle cells) were surgically removed from the ovary, and placed in Barth's solution (in mM: 88 NaCl, 1 KCl, 0.82 $MgSO_4$, 0.33 $Ca(NO_3)_2$, 0.41 $CaCl_2$, 2.4 $NaHCO_3$, 5 TRIS-HCl, buffered to pH 7.4 with NaOH). Follicles were then separated in small groups containing about ten oocites and incubated for 1 hour at 19 °C in Barth's solution without calcium but supplemented with 1 mg/ml of collagenase. After the collagenase treatment, oocytes were washed extensively with Barth's solution and the residual follicle cells were removed manually with fine forceps. At this step the healthiest defolliculated oocytes presenting two clearly delineated hemispheres were selected, and incubated in Barth's solution supplemented with gentamycin (50 µg/ml), during injection and incubation, until patch-clamp experiments were performed.
Injection needles of about 10 µm of tip diameter were made from borosilicate glass capillaries (World Precision Instrument, Sarasota, FL, USA) by using a horizontal puller (BB-CH-PC, Mecanex S.A., Geneva, Switzerland). Oocytes were injected under a binocular microscope at low magnification (Olympus, Japan) using a manual microinjector (CellTram Air, Eppendorf, Germany). About 100-200 nl of capped cRNA (at approximately 1 µg/µl in DEPC-treated ddH_2O) were injected in each oocyte. Cells were then incubated at 19 °C for 2-6 days. Just prior to patch-clamping, the vitelline membrane was removed from the oocytes under

visual control in a hyperosmotic medium. During the experiments, oocytes were mantained in Ringer solution (in mM: 110 NaCl, 2.5 KCl, 1 $CaCl_2$, 1.6 $MgCl_2$, 10 HEPES-NaOH, buffered to pH 7.4 with NaOH).

2.4.3 Recording apparatus

CNG and HCN currents from excised patches (Hamill et al., 1981) were recorded with a patch-clamp amplifier (Axopatch 200B, Axon Instruments Inc., Foster City, CA, USA), 2-6 days after RNA injection, at room temperature (20-22 °C). Borosilicate glass pipettes had resistances of 3-5 MΩ in symmetrical standard solution. Currents were low-pass filtered at 1 kHz and acquired on-line (at 5 kHz). Current traces from long (5-20 min) experiments at constant membrane potential were low-pass filtered at 5 kHz and stored on either PCM/VCR or DAT tape (Sony PCM-601ES and Panasonic NV-F70 HQ, respectively). The patch currents were subsequently digitized offline. For data acquisition, digitization and analysis, we used pClamp hardware and software (Axon Instruments) and Origin (Microcal Software, Inc.) software. Data are usually given as mean values ± standard error of the mean. When necessary, the Student t-test was used to test for significance.
The Cd^{2+} effect on w.t. CNG channels (section 3.1.1) was quantitated from current-voltage relations. The steady-state current amplitude at a given potential and $[Cd^{2+}]$ (I_{Cd}) was normalized to the current in the absence of Cd^{2+} (I_0), at the same potential. In the case of T16C mutant (section 3.1.2), the K_d for the steady-state channel inhibition by Cd^{2+} was estimated by fitting a Hill-Langmuir theoretical curve to the experimental data:

$$I_{Cd}/I_{max} = \{ 1 + ([Cd^{2+}]/K_d)^n \}^{-1} \qquad (1)$$

where I_{max} = maximal CNG current, measured immediately after Cd^{2+} application, i.e. before inhibition had occurred, I_{Cd} = CNG current in the presence of a certain $[Cd^{2+}]$, at the steady state, K_d = $[Cd^{2+}]$ which yielded 50% of the maximal current, n = Hill coefficient. This simple model assumes that the CNG current measured immediately after patch exposure to cGMP plus Cd^{2+} is essentially equal to the maximal current, irrespective of the $[Cd^{2+}]$. This assumption is justified by the slow time course of the Cd^{2+} effect. The theoretical curves best fitting the experimental data were obtained by a nonlinear least squares procedure (Levenberg-Marquardt algorithm, Origin software). Data points are usually given as mean values ± standard error of the mean.

2.4.4 Solutions and experimental protocols

For all the experiments carried out in this thesis, the perfusion system used was as described in Sesti et al., 1995, and allowed complete solution changing within 1 s.

2.4.4.1 Accessibility of Cd^{2+} from the cytoplasmic side of the plasma membrane, in the w.t. CNG background

The pipette solution contained (in mM): 110 NaCl, 10 HEPES, 0.2 EDTA ("standard solution" buffered at pH 7.6 with tetramethylammonium hydroxide). The cytoplasmic face of the excised patches was perfused with the same solution, supplemented or not with 1 mM cGMP. Soon after patch excision, cGMP was applied several times to verify the presence and the stability of the CNG current. After this control, the inner side of the patch was perfused with a standard solution without EDTA. The difference in CNG current amplitude in the presence and in the absence of EDTA was negligible for w.t. and mutant channels. We then tested the Cd^{2+} effect in the closed and in the open state applying a standard solution without EDTA, containing $CdCl_2$ (from 0.01 to 1 mM, as appropriate) and supplemented or not with 1 mM cGMP. After Cd^{2+} washout, the residual current was measured by applying the initial procedure again.

2.4.4.2 Accessibility of Cd^{2+} from the external side of the plasma membrane, in the w.t. CNG background

At negative membrane potentials, millimolar concentrations of Mg^{2+} completely block CNG currents when applied to the outer side of the plasma membrane (Root and MacKinnon, 1993; Eismann et al., 1994). Thus, we measured CNG currents from outside-out patches as the difference between the current in the absence and in the presence of 5 mM $MgCl_2$ in the bath (extracellular side), using pipettes containing our standard solution plus 1 mM cGMP (internal side). After checking that the CNG current was stable, we applied Cd^{2+} in the absence of $MgCl_2$, usually for 60-120 s, at –40/-60 mV. After washout, we measured the residual CNG current by repeating the initial procedure. In this way, we checked the current remaining immediately after Cd^{2+} removal and followed if any recovery occurred.

2.4.4.3 Application of the sulfhydryl-specific reagents, in the E19A CNG background

Patch pipette contained (in mM): 110 NaCl, 10 HEPES, 0.2 EDTA ("standard solution" buffered at pH 7.6 with tetramethylammonium hydroxide). Soon after patch excision, the cytoplasmic face of the plasma membrane was perfused with the same solution supplemented or not with 0.5 mM cGMP. About 90 s were always left between consecutive cGMP applications to allow full channel recovery from desensitization (Bucossi et al., 1996). The Cd^{2+} effect was tested by perfusing the inner side of the patch with a standard solution without EDTA (to avoid partial Cd^{2+} chelation; Gordon and Zagotta, 1995) supplemented with 0.5 mM cGMP and/or $CdCl_2$ (from 0.01 to 1 mM). The only effect of the EDTA withdrawal was the activation of a background offset current due to the well-known presence of Ca^{2+}-dependent Cl^- channels in *Xenopus* oocytes (Miledi and Parker, 1984). This current reached the steady state soon after the solution changing. Therefore, we never added any Cl^- channel blockers, during these experiments. The effect of MTS compounds was tested at a concentration of 2.5 mM, in standard solution with EDTA, as previously described (Becchetti et al., 1999). To study the effect of the probe in the closed state, patches were exposed to the appropriate reagent for 2 min in the absence of cGMP. After washout, cGMP was applied to measure the residual current. To study the effect in the open state, the probe was applied in the presence of cGMP and the CNG current was thus followed for about 2 min. In this case, also, cGMP was applied again after washout to measure the residual current.

2.4.4.4 Application of the sulfhydryl-specific reagents to w.t. SpHCN channel and its mutant C428S

To measure I_h current, patches of membrane where excised from *Xenopus laevis* oocytes heterologously expressing the SpHCN channel. Currents were measured in both inside- and outside-out patch-clamp configurations. In inside-out experiments, the patch pipette contained (in mM): 150 KCl, 10 HEPES, 0.2 EDTA ("standard solution" buffered at pH 7.6 with tetramethylammonium hydroxide). The external solution was symmetrical and supplemented or not with 1 mM cAMP. I_h currents were elicited applying hyperpolarizing steps to the membrane voltage (in most experiments, -100 mV), and were taken as the difference between the current recorded in the presence of cAMP and in its absence. In outside-out

experiments, the patch pipette contained (in mM): 150 KCl, 10 HEPES, 0.2 EDTA, 1 cAMP ("standard solution" buffered at pH 7.6 with tetramethylammonium hydroxide). The external solution contained (in mM): 150 KCl, 10 HEPES, 0.2 EDTA. The I_h current activated by stepping the membrane voltage from 0 to –X mV was taken as the sum of the current recordings when the voltage was stepped from 0 to –X mv and from 0 to +X mV.

To test the effect of sulfhydryl-specific reagents on SpHCN current, Cd^{2+} or MTSET were applied from the intra- or extracellular side of the membrane. In the inside-out patch-clamp configuration, soon after patch excision, the cytoplasmic face of the plasma membrane was perfused with the same pipette-filling solution supplemented or not with 1 mM cAMP. The Cd^{2+} effect was tested by perfusing the inner side of the patch with a standard solution without EDTA (to avoid partial Cd^{2+} chelation; Gordon and Zagotta, 1995) supplemented with 1 mM cAMP and/or 50 µM $CdCl_2$. Also in this case, the only effect of the EDTA withdrawal was the activation of a background offset current due to the well-known presence of Ca^{2+}-dependent Cl^- channels in *Xenopus* oocytes (Miledi and Parker, 1984), and since this current reached the steady state soon after the solution changing, we never added any Cl^- channel blockers during these experiments. The effect of MTS compounds was tested at a concentration of 2.5 mM, in standard solution with EDTA, as previously described (Becchetti et al., 1999). To study the effect of the probe in the closed state, patches were exposed to the appropriate reagent for about 2 min in the absence of cAMP. After washout, cAMP was applied to measure the residual current. To study the effect in the open state, the probe was applied in the presence of cAMP and the HCN current was thus followed for about 2 min. In this case, also, cAMP was applied again after washout to measure the residual current.

In outside-out experiments, soon after patch excision, the extracellular face of the plasma membrane was perfused with the same pipette-filling solution deprived of cAMP and supplemented or not with 50 µM $CdCl_2$.

2.4.4.5 Determination of ionic selectivity in w.t. SpHCN channel and its mutant K433Q

Ionic selectivity was determined in inside-out patches by stepping V_m, from a holding potential of 0 mV, from –120 mV to test values between +50 and –60 mV in 10 mV increments. For mutant K433Q, the pre-pulse at –120 mV lasted 50 ms, in order to fully activate the I_h current and measure the tail

currents before development of inactivation. The patch pipette contained (in mM): 150 KCl, 10 HEPES, 0.2 EDTA ("standard solution" buffered at pH 7.6 with tetramethylammonium hydroxide). Soon after patch excision, the cytoplasmic face of the plasma membrane was perfused with a solution containing (in mM): 50 KCl, 100 XCl, 10 HEPES, 0.2 EDTA and supplemented or not with 1 mM cAMP, where X is either K, Na or Li.
Since mutant K433Q I_h current also exhibits run-down, we tested the different ions on separate membrane patches, immediately after patch excision. The current recordings shown for each ion are representative of 3 to 5 different experiments.

2.4.4.6 Application of chloride-substituting anions to w.t. SpHCN channel and its mutant K433Q

To determine the effect of the substitution of external chloride with larger anions on SpHCN current, current recordings were performed in both inside- and outside-out patch-clamp configuration. In inside-out experiments, the patch pipette contained (in mM): 150 KCl, 10 HEPES, 0.2 EDTA ("standard solution" buffered at pH 7.6 with tetramethylammonium hydroxide). Soon after patch excision, the cytoplasmic face of the plasma membrane was perfused with a solution containing (in mM): 150 KX, 10 HEPES, 0.2 EDTA and supplemented or not with 1 mM cAMP (buffered as above), where X is either acetate, glutamate or sulphate. In outside-out experiments, the patch pipette contained (in mM): 150 KCl, 10 HEPES, 0.2 EDTA, 1 cAMP (buffered as above). Soon after patch excision, the extracellular face of the plasma membrane was perfused with a solution containing (in mM): 150 KX, 10 HEPES, 0.2 EDTA (buffered as above).

3) RESULTS

3.1 Structure-function relationship in the brCNGCα pore in the wild-type background

The cyclic nucleotide-gated (CNG) channels belong to the molecular family of the voltage-dependent ion channels and share considerable homology with the voltage-dependent K^+ channels (Kaupp et al., 1989; Jan and Jan, 1990). They are thought to be formed by 4 independent subunits, surrounding a single pore (Zagotta and Siegelbaum, 1996). In voltage-gated channels, a fundamental component of the pore is the "P-loop", i.e. the stretch of amino acids connecting the S5 and S6 transmembrane domains. Four identical P-loops line part of the conduction pathway, comprising the selectivity filter (Doyle et al., 1998). To explain the structure-function relation of ion channels, it is important to understand the location of the different P-loop residues and whether or how they move during gating. Accordingly, the pore structure of the voltage-gated K^+ channels has been extensively studied. The results of such studies have been used for developing molecular models of the 3D location of the pore residues (Durell et al., 1998). These models can be now compared with the X-ray resolved structure of the K^+ channel from *Streptomyces lividans* (KcsA; Doyle et al., 1998).

On the other hand, our knowledge of the CNG channel pore is lagging behind: no specific toxin is presently available to target the ion conduction pathway, nor have high-resolution structures been determined for any channel portion. However, in spite of overall sequence homology, the details of the pore structure of CNG channels may be quite different from that of voltage-gated K^+ channels. CNG channels do not possess the GYG (or GFG) triplet typically present in the K^+ channel P-loop (Heginbotham et al., 1992) and poorly select monovalent alkali cations. Their gating is independent of membrane potential, but requires the presence of cyclic nucleotides (Zagotta and Siegelbaum, 1996). Moreover, increasing evidence points to a direct contribution of the P-loop to the CNG channel gating (Bucossi et al., 1996; Fodor et al., 1997; Becchetti et al., 1999; Becchetti and Gamel, 1999).

In the rod CNG channel, the glutamate E19, corresponding to an aspartate residue immediately following the GYG triplet in K^+ channels, is accessible to monovalent and divalent cations from both sides of the plasma membrane (Root and MacKinnon, 1993; Eismann et al., 1994; Sesti et al., 1995). The location of the other P-loop residues has been recently analyzed with the

substituted-cysteine accessibility method (SCAM; Karlin and Akabas, 1998). Most of the residues between R345 and S371 (here named R1-S27, following common usage) were substituted in turn with a cysteine residue. The accessibility of the substituted cysteines was then tested with two methanethiosulfonate (MTS) sulfhydryl-specific reagents which covalently bind the added sulphur (Karlin and Akabas, 1998), namely MTS-ethylammonium (MTSEA; Sun et al., 1996) and MTS-ethyltrimethyl-ammonium (MTSET; Becchetti et al., 1999). When an MTS compound irreversibly blocks a cysteine mutant's current, the effect is usually ascribed to reaction with the added thiol (Karlin and Akabas, 1998). In this way, it is possible to identify which residues are more sensitive to chemical modification among those facing the aqueous milieu. Furthermore, MTSET, at variance with MTSEA, does not permeate the lipid bilayer (Holmgren et al., 1996). Therefore, a cysteine reaction with MTSET applied either from the external or from the internal side of the membrane is diagnostic of the location of the mutated residue. The residues V4, T20 and P22 were only accessible to MTSET from the outside, suggesting that the stretch T20C-S27C and the first portion of the P-loop (up to V4, at least) face the external portion of the pore (Becchetti et al., 1999). Less clear is the location of the residues immediately preceding E19, along the sequence. G18C channels are not functional, when expressed in oocytes (Becchetti and Gamel, 1999). T16C and I17C channels yield measurable currents and respond to MTSET applied from the inside, but the effect is difficult to interpret. High concentrations of MTSET (2-3 mM) only produce a partial steady-state T16C channel inhibition, when MTSET is applied in the presence of cGMP, with a very slow time course. On the other hand, MTSET produces some acceleration of the typical I17C channel rundown, independently of the presence of cGMP (Becchetti et al., 1999). Clear-cut results for residues around E19 are important because these residues are thought to form the selectivity filter and appear to rearrange during gating (Bucossi et al., 1996; Fodor et al., 1997; Becchetti and Gamel, 1999; Becchetti et al., 1999).

To understand whether the poor block of MTSET on T16C and I17C is due to restricted access to the substituted cysteine, accessibility tests with alternative probes are advisable. Cd^{2+} avidly binds to thiols and has been used to study the K^+ channel pore (Yellen et al., 1994; Kurz et al., 1995; Krovetz et al., 1997). Its ionic diameter is about 0.1 nm (Dart et al., 1998), smaller than the 0.6 nm length of the shorter side of the asymmetrical MTS compounds (Karlin and Akabas, 1998). Furthermore, it does not permeate through the lipid bilayer. Thus, Cd^{2+} is potentially useful to control the results obtained with MTSET. In analogy with other divalent cations,

however, Cd^{2+} inhibits CNG channels from the inside in a voltage-dependent way (Ildefonse and Bennett, 1991; Karpen et al., 1993). We show that, at negative membrane potentials, [Cd^{2+}] lower than 100 μM produced negligible steady state CNG channel block. Hence, to study the internal cysteine accessibility, we have applied 10-100 μM Cd^{2+} to the inner face of membrane patches, at negative membrane potentials, to minimize the non-specific effect. Divalent cations also block CNG channels from the outside (34Root and MacKinnon, 1993; Eismann et al., 1994). However, the external Cd^{2+} effect was quickly reversible in w.t. channels. A persistent inhibition was only observed in some mutant channels, an effect we attributed to specific interaction with the substituted cysteines.
We have studied the following cysteine mutants (the common nomenclature is adopted, and the indication in brackets refers to the amino acid position in the cloned sequence; see also fig. 7): V4C (V348), S6C (S350C), T16C (T360C), I17C (I361C), T20C (T364C), P22C (P366C) and S27C (S371C). This ensemble contains the residues most sensitive to MTS compounds (i.e. V4C, T16C, I17C, T20C and P22C) and two residues scarcely affected by MTS compounds (S6C and S27C; Sun et al., 1996; Becchetti et al., 1999). Residues T16-P22 are particularly interesting since they bracket the channel selectivity filter and some of them are thought to participate in gating. In these mutant channels, the selectivity to monovalent alkali cations and the dose-response to cGMP were similar to w.t. (Becchetti and Gamel, 1999). In particular, 1 mM cGMP was saturating. Some peculiar features of T16C and I17C mutants will be commented upon below.

3.1.1 Effect of Cd^{2+} applied to the inner side of w.t. channels

Cd^{2+} (10-20 μM) applied to the inner face of inside-out patches potentiated w.t. CNG channels at the steady state (fig. 11B, 12A). This is a well-known effect of transition metal divalent cations (Ildefonse and Bennett, 1991; Karpen et al., 1993), which maximize the CNG channel open probability (P_o) through interaction with the histidine residue H420, on the cytoplasmic face of the channel (Gordon and Zagotta, 1995). At –100 mV, 10-20 μM Cd^{2+} produced a 70% steady state potentiation. At this membrane potential, the w.t. single-channel P_o is around 0.6 (Bucossi et al., 1997), so that the observed potentiation is maximal. We conclude that, at negative potentials, no significant steady state channel inhibition is produced by 10-20 μM Cd^{2+}. Higher [Cd^{2+}] progressively inhibited the w.t. channels in a voltage-

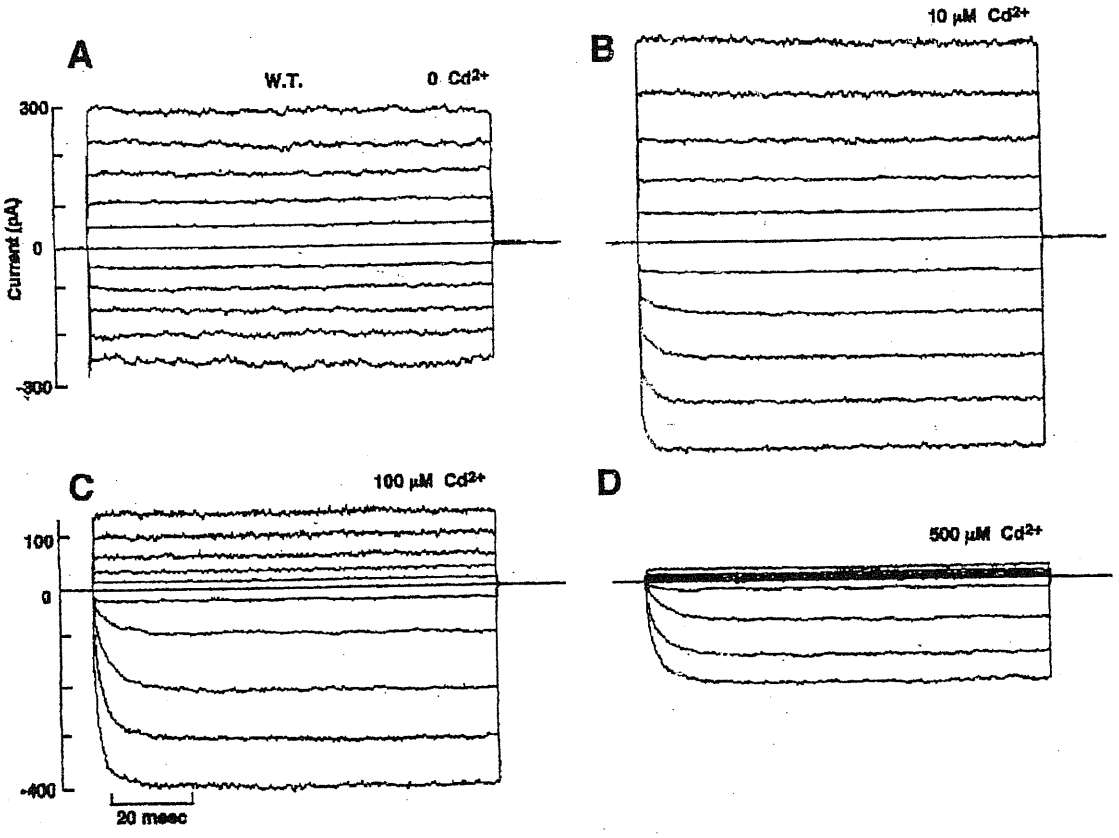

Fig. 11A-D

Typical w.t. CNG current traces, in the absence (**A**) and in the presence of Cd^{2+} (**B**, **C** and **D**, respectively 10, 20 and 100 µM). Currents were elicited from inside-out patches by applying different membrane potentials for 200 ms (from -100 to +100 mV, step 20 mV, holding potential was 0 mV), in the presence of 1 mM cGMP, at the indicated [Cd^{2+}]. The CNG currents were isolated by subtracting the current in the absence of cGMP from the current in the presence of cGMP. Cd^{2+} was applied to the cytoplasmic side of the patch. Cd^{2+} (10-20 µM) potentiated w.t. currents. Higher [Cd^{2+}] inhibited the CNG current, in a voltage dependent way.

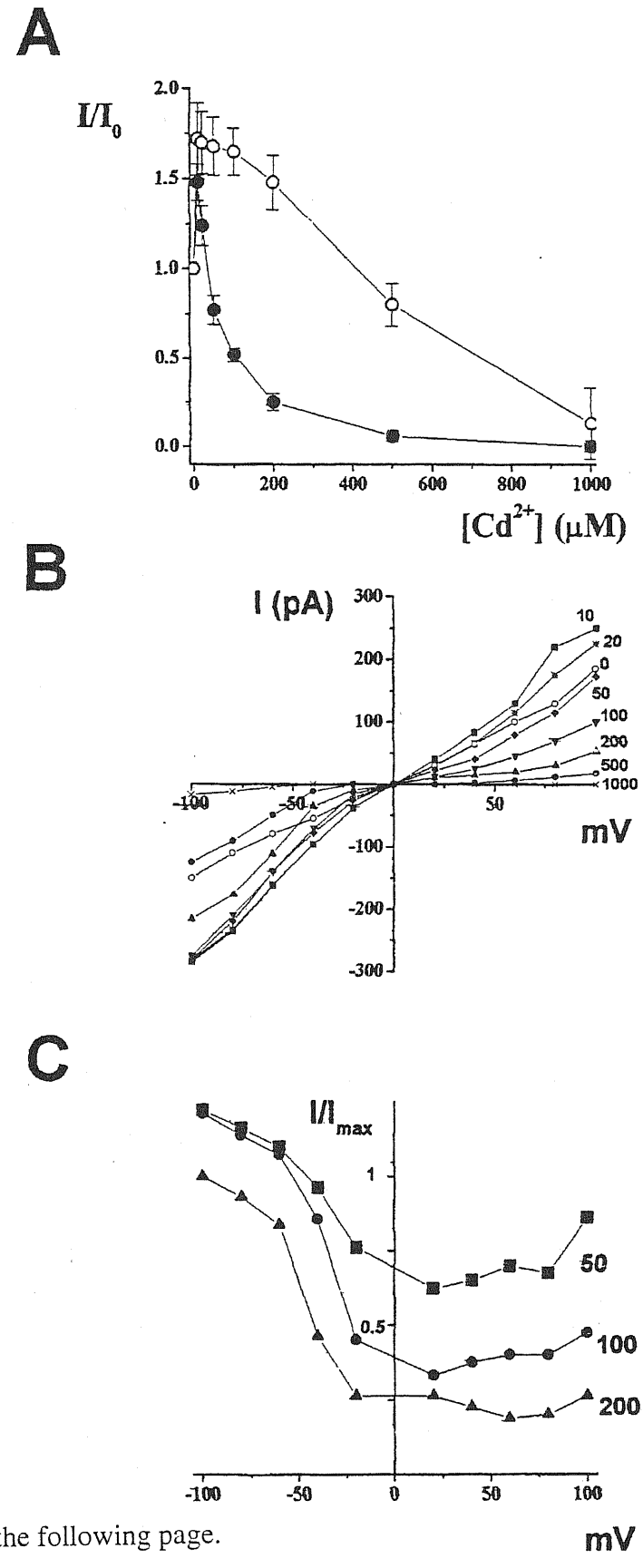

Fig. 12A-C
See legend on the following page.

Fig. 12A-C
Effect of Cd^{2+} applied to w.t. CNG channels from the cytoplasmic side of the plasma membrane.
A Steady state dose-response curves to Cd^{2+} of CNG currents, at +100 mV (*closed circles*) and –100 mV (*open circles*). Data points are average (n=5) steady state current values, normalized to the current in the absence of Cd^{2+}. The experimental procedure was as illustrated in Fig. 11.
B Typical steady state current-voltage (I-V) curves, in the presence of different $[Cd^{2+}]$. Data points are current values from traces obtained as illustrated in Fig. 11. (*Open circles* 0 Cd^{2+}, *squares* 10 μM Cd^{2+}, *stars* 20 μM Cd^{2+}, *diamonds* 50 μM Cd^{2+}, *downward triangles* 100 μM Cd^{2+}, *upward triangles* 200 μM Cd^{2+}, *closed circles* 500 μM Cd^{2+}, *crosses* 1000 μM Cd^{2+}.) At negative membrane potentials, the I-V curves obtained at $[Cd^{2+}]$ between 10 and 100 μM are clustered, showing that the Cd^{2+} effect is weak, under these conditions.
C Normalized steady state I-V relationships, obtained in the presence of 50 (*squares*), 100 (*circles*) and 200 (*triangles*) μM Cd^{2+}.
Data points for **B** and **C** are representative of 5 experiments.

dependent way. At negative membrane potentials, the instantaneous block produced by [Cd^{2+}] up to 100-200 μM was mostly relieved, at the steady state, as is apparent from the progressive increase of the current amplitude in the presence of Cd^{2+} (Fig. 11). At –100 mV, the [Cd^{2+}] producing steady state half-block was about 400 μM (Fig. 12A). At [Cd^{2+}] greater than 400-500 μM, the effect was poorly reversible. Fig. 12B shows typical steady state w.t. I/V curves at different [Cd^{2+}]. The current values at negative membrane potentials in the presence of Cd^{2+} up to 100 μM were clustered, and a clear current block appeared only at higher [Cd^{2+}] than 200 μM. The I-V curves at the indicated [Cd^{2+}] and normalized to the maximal current are plotted in Fig. 12C, showing that [Cd^{2+}] up to about 100 μM produced negligible effects on CNG w.t. currents at membrane potentials more negative than –60 mV.

3.1.2 Effect of Cd^{2+} applied to the inner side of the mutant channels

A cysteine introduced within the channel P-loop provides an additional binding site for Cd^{2+}. In this case, however, we expect that the "quasi-covalent" (Glusker, 1991) nature of the S-Cd bond makes the reaction slowly reversible (and slowly developing) and scarcely dependent on membrane potential at the steady state. Therefore, to distinguish the Cd^{2+} effects on the substituted cysteine residues from the background effect, we applied 1-100 μM Cd^{2+} to the inner face of excised patches maintained at negative membrane potentials. After measuring the CNG current at -60 mV in our standard solution, we applied 100 μM Cd^{2+} (in the absence of EDTA, to avoid partial Cd^{2+} chelation) to the inner side of the patch (Fig. 13).
In these conditions, the CNG current in the presence of Cd^{2+} was the difference between the current in the presence of cGMP plus Cd^{2+} (without EDTA) and the current in the same solution without cGMP. In the absence of divalent ion chelators, the stray calcium present in the perfusing medium activated a background current due to the well-known presence of Ca^{2+}-dependent Cl^- channels in *Xenopus* oocytes (Miledi and Parker, 1984; Gordon and Zagotta, 1995). The amplitude of this background current was always moderate and reached the steady-state within about 30 sec from solution changing (Fig. 13). Therefore, we never added any Cl^- channel blockers during our experiments. The CNG current amplitude in the absence of EDTA, before Cd^{2+} addition, was always scarcely different from that measured in the presence of EDTA (Fig. 13B); therefore, we often compared the CNG current after Cd^{2+} addition to the initial control in the presence of

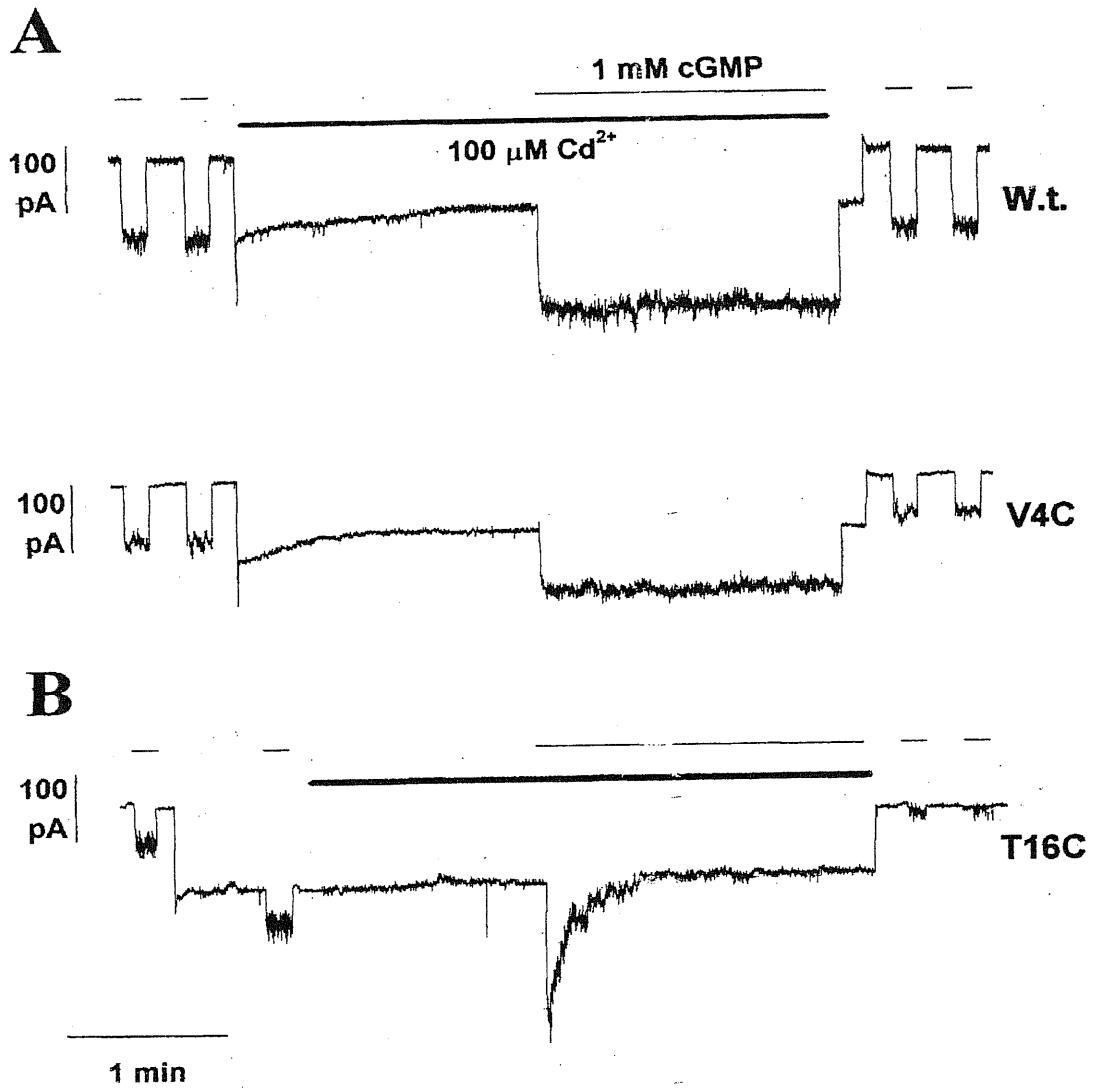

Fig. 13A-B

Effect of Cd^{2+} applied from the inner side of the plasma membrane. CNG currents were recorded at -60 mV from inside-out patches expressing the indicated mutants. The thick line indicates Cd^{2+} application, the thin line indicates cGMP application.

A After checking the CNG current stability by several brief applications of 1 mM cGMP, the patch was perfused with a solution containing 100 μM Cd^{2+}, in the absence of EDTA. The offset current after EDTA withdrawal is due to the activation of the calcium-activated Cl^- currents normally present in *Xenopus* oocytes (Miledi and Parker, 1984). cGMP was applied two min after Cd^{2+} application. Cd^{2+} produced no major effect on w.t. and V4C channels, either in the closed or in the open state.

B Effect of Cd^{2+} applied to the inner side of T16C channels. Same procedure as in **A**, except that, in this case, cGMP was also applied soon after EDTA withdrawal (before Cd^{2+} addition), to show that the CNG mutant currents in the presence and in the absence of EDTA are not different. T16C currents were completely inhibited by 100 μM Cd^{2+}.

EDTA to reduce the duration of the experiment (Fig. 13A). Cd^{2+} slightly potentiated w.t., S6C, P22C and S27C channels, while V4C and T20C channels were scarcely affected. Moreover, after returning to the standard solution, the CNG current amplitude was the same as it was before treatment. Fig. 13A illustrates typical experiments for w.t. and V4C channels. The effect of Cd^{2+} applied from the inside is summarized in Fig. 16A. We conclude that the above cysteine residues were not accessible to Cd^{2+} from the inner side of the plasma membrane.

The effect on T16C channels, on the other hand, was biphasic. T16C current was quickly and strongly potentiated by Cd^{2+}, irrespective of whether Cd^{2+} was applied at the same time with cGMP (not shown) or for 30-120 s before cGMP addition (Fig. 13B). Thus, the potentiation was much stronger in T16C channels compared to w.t. and the other mutant channels. This was not unexpected, because the T16C channel P_o is distinctly lower at both polarities compared with both w.t. and the other mutant channels studied in this work. At saturating cGMP concentrations, $P_o \leq 0.2$-0.3 in T16C channels, compared to 0.7-0.9 in the other cases (Bucossi et al., 1997; Becchetti and Gamel, 1999). Cd^{2+} can thus produce a three- to fourfold increase in T16C currents (see section 4.1.3). In fact, in all cysteine mutants with P_o lower than normal a similar potentiation is also produced by metal cations unable to react with thiol groups, such as Ni^{2+} (Becchetti et al., 1999).

However, when Cd^{2+} was applied to T16C channels in the presence of cGMP (i.e. in the open channel state), the current amplitude progressively decayed, after the initial potentiation, and total inhibition occurred after about 30 s (Fig. 13B). The K_d for Cd^{2+} block on T16C channels was about 15 μM (Fig. 16C). The effect was thus well distinguishable from the non-specific block produced by higher $[Cd^{2+}]$. These results show that the cysteine in position 16 is inwardly accessible to Cd^{2+}, and it is likely to rearrange during gating.

3.1.3 Mutant I17C has a different behavior

Current from I17C channels spontaneously decays in excised patches (Becchetti and Gamel, 1999; Becchetti et al., 1999). This decay is probably due to the formation of disulphide bridges between the cysteine residues inserted into the different channel subunits, because it is considerably slowed down by the reducing compound dithiothreitol (Becchetti and Gamel, 1999). When 100 μM Cd^{2+} was applied to the inner surface of

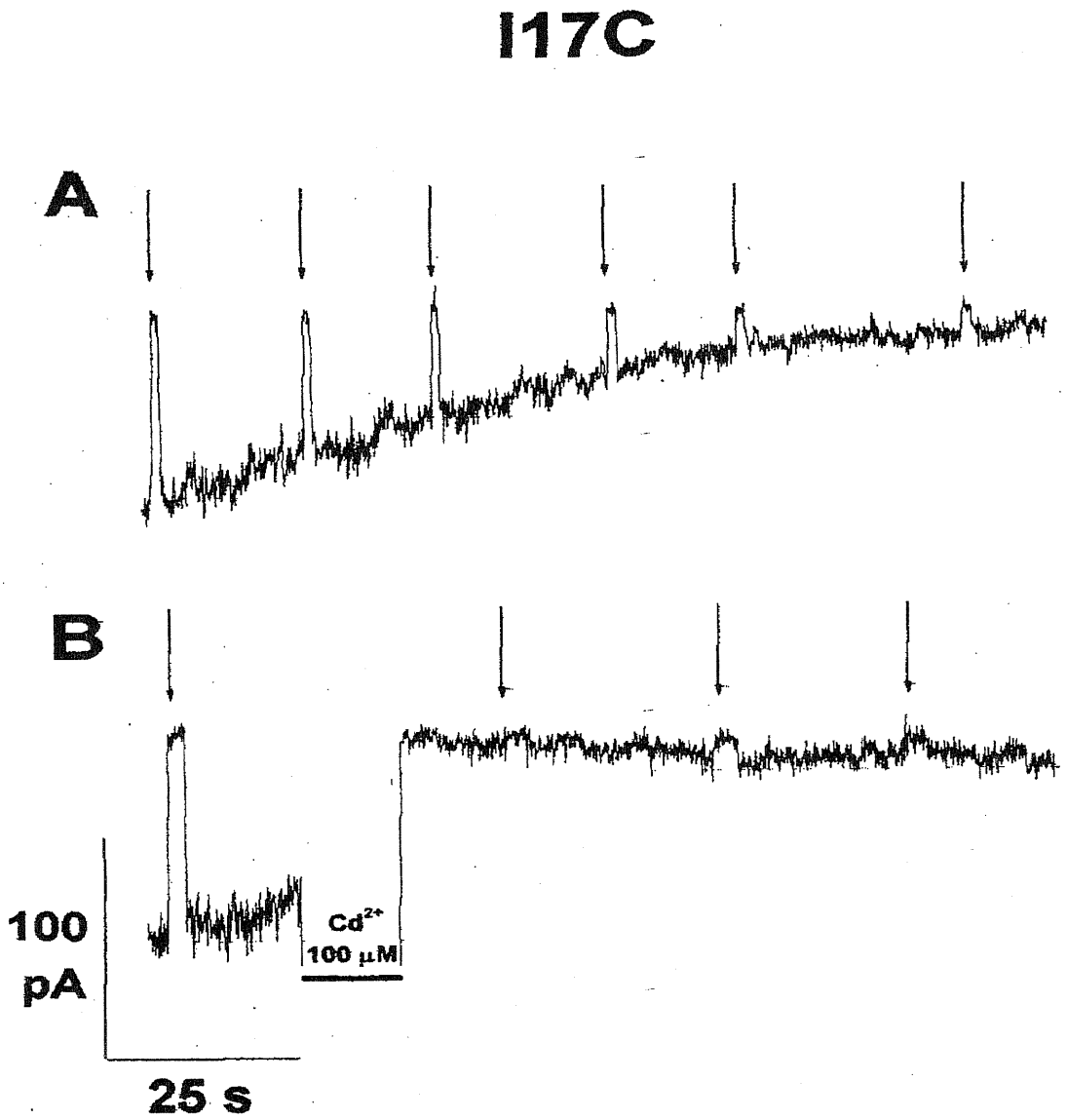

Fig. 14A-B
Effect of Cd^{2+} applied to the inner face of I17C channels.
A I17C currents decayed to 5-10 % of the initial value, about 2 min after patch excision. Current was elicited by 1 mM cGMP, at -40 mV. Every 10-15 s, the baseline stability was checked by brief applications of a standard solution without cGMP (arrows).
B After recording the I17C current for about 20 s, we applied 100 µM Cd^{2+} (without EDTA). The absence of EDTA led to activation of Ca^{2+}-dependent chloride channels, the ensuing current is off scale. After returning to the standard solution, cGMP application was almost ineffective, at a time when control I17C currents were usually still about 0.6 of the starting value (compare with **A**).

patches containing I17C channels soon after excision, the channel decay was strongly accelerated. In six experiments, 10 s of Cd^{2+} application was sufficient to produce 95 ± 2 % current inhibition, whereas a comparable decay occurred in about 2 min in the absence of Cd^{2+} (Figs. 14, 16A).

3.1.4 Effect of Cd^{2+} applied to the outer side of the mutant channels

The effect of Cd^{2+} on the external surface of the mutant channels was tested on outside-out membrane patches. Many divalent cations, included Cd^{2+}, inhibit w.t. CNG channels when applied externally, since they bind to the E19 residue (Root and MacKinnon, 1993; Eismann et al., 1994). This effect is always quickly reversible, even when high concentrations are used. In particular, the channel block produced by 5 mM Mg^{2+}, at –40 mV, was reversed by washout within a few seconds.
Even long treatment (3-4 min) never produced any persistent inhibition in either w.t. or mutant channels. A typical example is illustrated in Fig. 15A, showing that the full T20C current amplitude was soon recovered at wash-out, even after a prolonged exposure to 5 mM Mg^{2+}. In addition Cd^{2+} produced no long-lasting effect on w.t. channels. In this case also, the channel block produced by 100 μM Cd^{2+} was promptly reversible by wash-out (Fig. 15A). On the other hand, when Cd^{2+} was applied for 60-90 s to some of the mutant channels, the CNG current remained inhibited after washout and did not recover its initial amplitude within 4-5 min. We assume that the long-lasting channel inhibition produced by Cd^{2+} on mutant channels is due to the reaction between the ion and the cysteine residues introduced into the P-loop. Thus, we interpret a persistent Cd^{2+} effect, when present, as indicating outward accessibility of the tested residues. Mutants V4C, T20C, and P22C were inhibited by 100 μM Cd^{2+}, while S6C and S27C mutant channels were not. These results are summarized in Fig. 16B. The outward accessibility of I17C residues could not be tested because, in outside-out patches, the I17C current was always too small to allow reliable measurements. We believe this is because channels are constantly exposed to cGMP from the time of patch excision in the outside-out mode, and, as we have previously reported, I17C channel rundown is quicker in the presence of cGMP (Becchetti et al., 1999). Finally, T16C mutants were also partly inhibited by outwardly applied Cd^{2+} (Fig. 16B). However, in this case the $[Cd^{2+}]$ producing half-maximal blockade was about an order of magnitude higher than it was for internal block (Fig. 16C). This result is commented on in section 4.1.3.

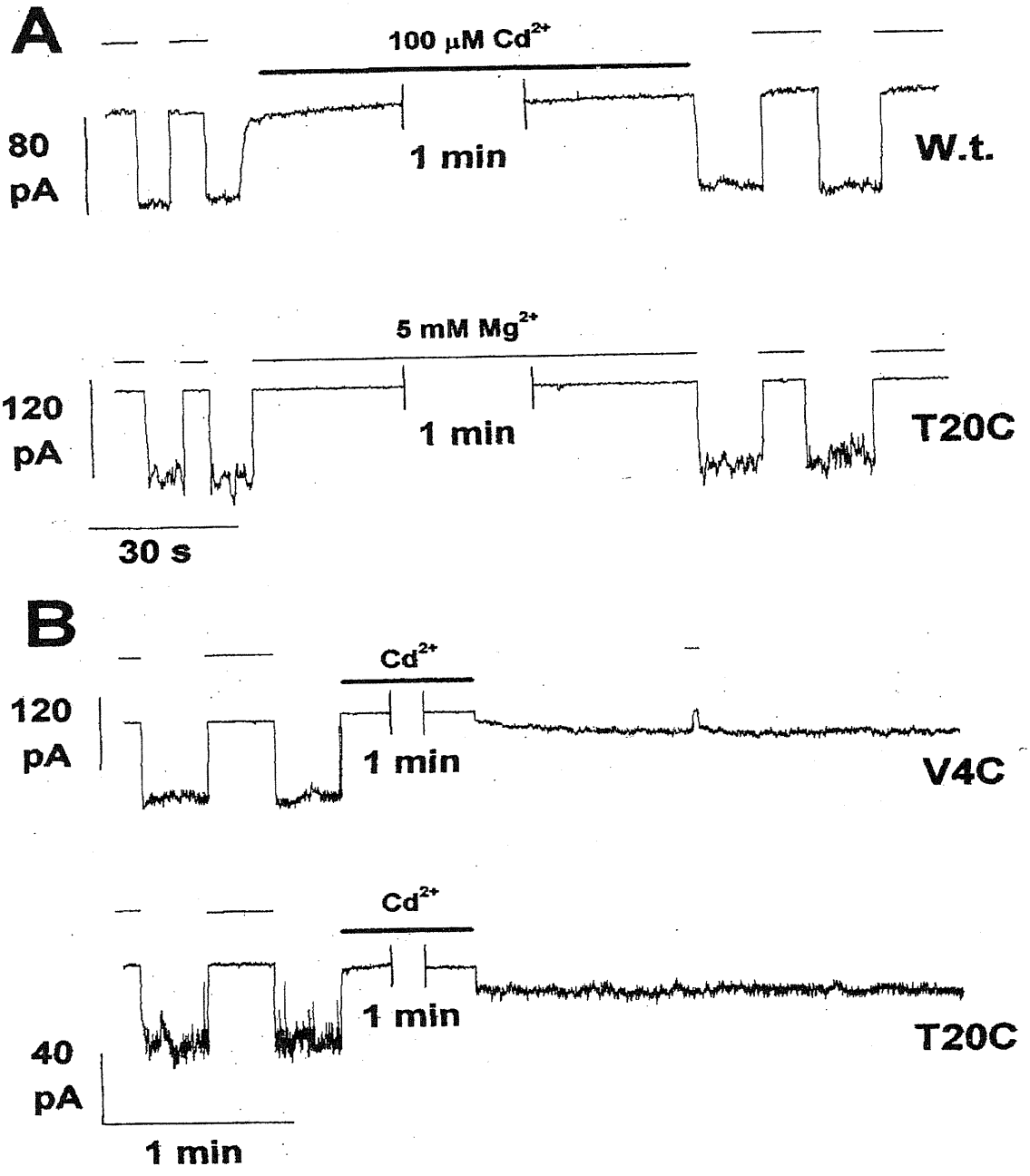

Fig. 15A-B

Effect of Cd^{2+} applied to the external side of the plasma membrane. CNG channels in outside-out patches were constantly exposed to 1 mM cGMP, present within the patch pipette. The baseline was checked by 5 mM Mg^{2+} application. Membrane potential was -40 mV. *Thick bars* indicate Cd^{2+} application, *thin bars* indicate Mg^{2+} application.

A A 2 min application of 100 μM Cd^{2+} had no effect on w.t. currents (*upper panel*) and 5 mM Mg^{2+} had no effect on T20C channels (*lower panel*).

B 100 μM Cd^{2+} inhibited V4C and T20C channels. Cd^{2+} was applied for about 90 s.

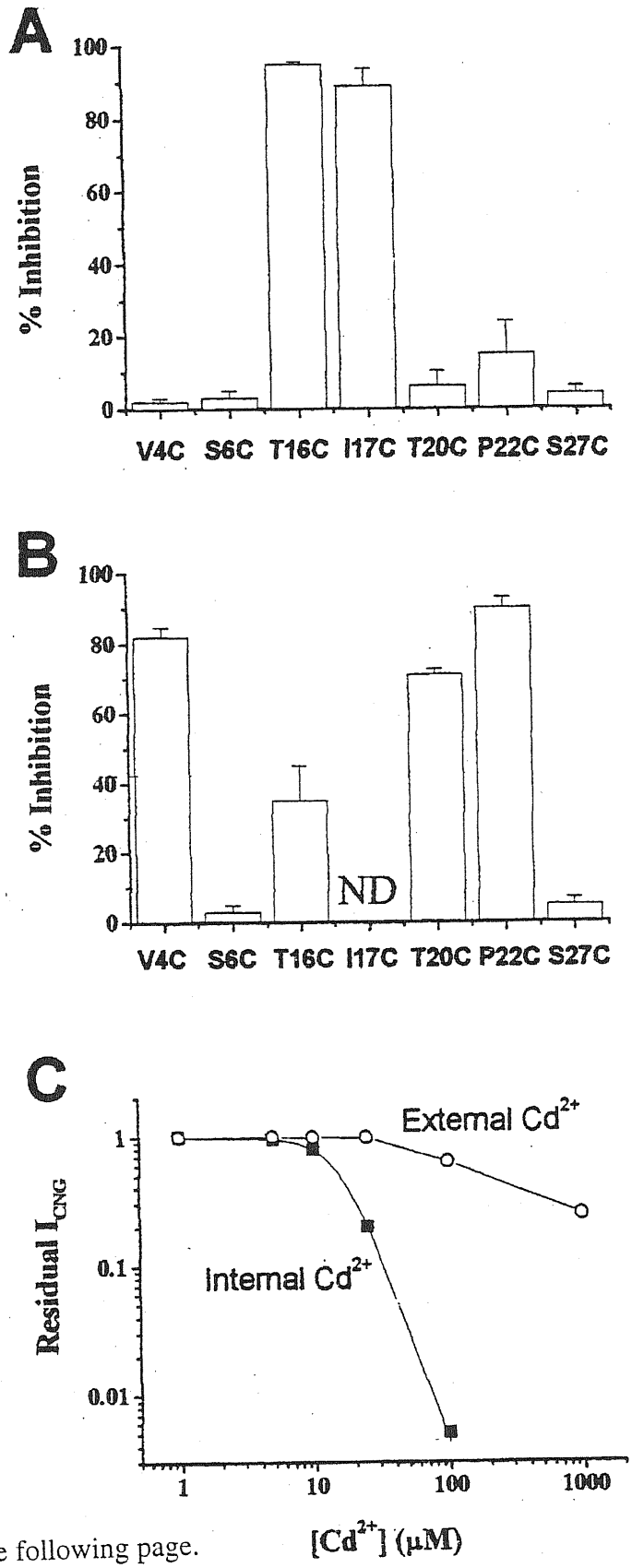

Fig. 16A-C
See legend on the following page.

Fig. 16A-C
Summary of the effects of Cd^{2+} on mutant channels, expressed as percentage inhibition with respect to the CNG current measured before treatment. Data were obtained as explained in Figs. 13, 14, 15 and are averages of 5-10 experiments.
A Cd^{2+} effect on the internal side of the indicated mutant channels.
B Effect of external Cd^{2+} measured after Cd^{2+} washout. The external Cd^{2+} effect on I17C mutant was not determined (ND, see text).
C Dose-response to external and internal Cd^{2+} for T16C channels, at –40 mV. Data points are average steady-state current values at the indicated $[Cd^{2+}]$, normalized to the initial current. The *continuous line* interpolating the data points for internal Cd^{2+} effect is fit to equation 1, with n = 2,97, and K_d = 16 μM. The errors of the data points at 100 μM Cd^{2+} are given in **A** and **B**.

3.2 Structure-function relationship in the brCNGCα pore in desensitizing E19A mutants

CNG channels share sequence homology with voltage-gated K^+ channels, especially within the pore-loop, or "P-loop", and the voltage-sensor (Kaupp et al., 1989; Jan and Jan, 1990). The transmembrane topology is also well conserved in both channel families (Henn et al., 1995). Function, however, is considerably different. CNG channels are not voltage dependent, but require the presence of cyclic nucleotides to open. In addition, their ion selectivity and channel interaction with divalent cations resemble those observed in Ca^{2+} channels (for a review, see Zagotta and Siegelbaum, 1996). No voltage-dependent inactivation or time-dependent desensitization is present in wild type CNG channels.

The P-loop of the a subunit of the bovine rod CNG channel (Kaupp et al., 1989) is formed by the residues R345 to S371 (here named R1-S27; see section 3.1). It contributes crucially to the above channel properties. In particular, glutamate E19 is the major binding site for extracellular divalent cations (Root and MacKinnon, 1993; Eismann et al., 1984) and determines some of the conduction features, since neutralization of this residue removes anomalous mole fraction behaviour (Sesti et al., 1995). Interestingly, when E19 is neutralized by substitution with a number of different residues, the channels desensitize in the presence of a steady ligand concentration (Bucossi et al., 1996). Single channel recording showed that the CNG channel desensitization after E19 substitution is mostly due to a progressive decrease in the channel open probability "P_o" (Bucossi et al., 1996), suggesting that the P-loop portion around E19 plays a part in the mechanism of CNG channel gating. Further evidences support this idea. In particular, cysteine substitution of most residues between Y8 and G18 decreases the channel P_o (Becchetti and Gamel, 1999), with limited effect on selectivity and the affinity to cyclic nucleotides. Moreover, E19 is more accessible to tetracaine block from the internal side of the membrane when the channels are closed (Fodor et al., 1997), showing that it moves during gating and suggesting that there may be no bulky gate obstructing the internal access to this residue.

The precise molecular mechanism of channel gating, in general, is not known. *A priori*, local interactions between amino acid residues and global channel rearrangements may both occur. The artificial CNG channel desensitization introduced by substituting E19 offers useful general clues to study the energetic interactions occurring between residues involved in

channel gating, in ligand-gated channels. Accordingly, we studied whether major rearrangements in the P-loop topology occur in desensitizing channels, by using the substituted cysteine accessibility method (SCAM; Karlin and Akabas, 1998). Most residues within the E19A channel P-loop were substituted in turn with a cysteine residue, whose accessibility was subsequently tested with sulfhydryl specific reagents. To this purpose, we have used probes previously employed to study the w.t. CNG channel P-loop (Sun et al., 1996; Becchetti et al., 1999; see section 3.1), i.e. Cd^{2+}, 2-trimethylammonioethylmethane thiosulfonate (MTSET) and 2-aminoethylmethane thiosulfonate (MTSEA; for a review, see Karlin and Akabas, 1998). These compounds bind covalently (MTS's) or "quasi-covalently" (Cd^{2+}) to the thiol group (Karlin and Akabas, 1998; Glusker, 1991). Thus, irreversible (or slowly reversible) effects after channel treatment from the outer or the inner side of excised patches indicate whether each substituted cysteine is exposed to the internal or the external side of the membrane. In addition, a strong current inhibition is often considered a suggestion that the residue may line the channel pore. In this way, it is possible to obtain a preliminary 3D picture of the side chains within a channel pore, useful as "initial conditions" for more quantitative approaches to the study of channel function.

We have studied: a) whether cysteine substitutions altered the E19A channel desensitization; b) whether the pore topology was modified in desensitizing channels.

We have studied the following cysteine mutants, in E19A background: K2C, V4C, S6C, L7C, T15C, T16C, I17C, T20C, P22C, V24C and S27C (see section 3.1). This set contains most of the residues previously studied in w.t. background, including the residues surrounding E19 (except G18 and P21, whose expression in oocytes is poor; Sun et al., 1996; Becchetti and Gamel, 1999; Becchetti et al., 1999; see sections 3.1 to 3.1.4). As it was the case for SCAM in w.t. background, we have used both Cd^{2+} and MTS compounds to test for accessibility, because their different chemical nature permits to obtain complementary information. The smaller Cd^{2+} is potentially more effective at reaching channel regions less accessible to the larger MTSET. However, Cd^{2+}, as other metal cations, also produces aspecific effects on CNG channels which might partly obscure the effect on target cysteines. The use of MTSEA is explained in section 3.2.6.

3.2.1 The cysteine mutant desensitization in E19A background

We describe CNG currents elicited by 0.5 mM (saturating) cGMP applied to the cytoplasmic surface of excised membrane patches, mantained for 30-60 s at -40/-60 mV. The channel desensitization in mutants K2C-E19A, V4C-E19A, S6C-E19A, L7C-E19A, P22C-E19A, V24C-E19A and S27C-E19A had time course similar to the one observed in E19A channels (Bucossi et al., 1996). The time for the current to reach 0.5 of the initial value ($t_{1/2}$) was usually around 3 s, at –40 mV, consistent with published values (Bucossi et al., 1996). Representative examples are shown in fig. 17 and Fig. 18 (left panels).
Between consecutive tests, a 90 s perfusion with a standard solution without cGMP allowed full recovery. Interestingly, the desensitization kinetics was altered in cysteine mutants around the position 19. In fact, the channel desensitization was slowed down in T16C-E19A (fig. 17, $t_{1/2}$ was 15.3 ± 3 s, n=6), T20C-E19A (fig. 17 and ig. 18, $t_{1/2}$ was 64.3 ± 7 s, n=4), and T15C-E19A, in which no significant desensitization occurred within 2 min recording in the presence of cGMP. The differences between mutant $t_{1/2}$ and the corresponding control value (3.6 ± 0.3 s, n=5) are highly significant ($p < 0.01$). These data are summarized in tab. 3. The peculiar properties of I17C-E19A channels are described in section 3.2.4.

3.2.2 Steady state effect of thiol-specific reagents applied to the intracellular side of control (E19A) channels

We have applied our probes in the absence and in the presence of cGMP, to test the cysteine accessibility in the closed and in the open channel state, respectively. However, the effect of both MTSET and Cd^{2+} in the open state was the same irrespective of whether the chemical was applied at the same time as cGMP, or was applied for some time before cGMP. Thus, for brevity, in figs. 17 and 18 we only show experiments in which the effect of the probes in the two channel states was tested consecutively. As a preliminary control, we have studied the effect produced by MTSET and Cd^{2+} on E19A channels. MTSET was ineffective when applied to the inner side of the plasma membrane either before (closed state) or during (open state) cGMP application. Fig. 18 shows that a 90 s MTSET perfusion in the closed state did not affect the CNG current peak measured at cGMP application. Subsequently, the patch was exposed to MTSET also during cGMP addition. No appreciable difference was found in the time course of

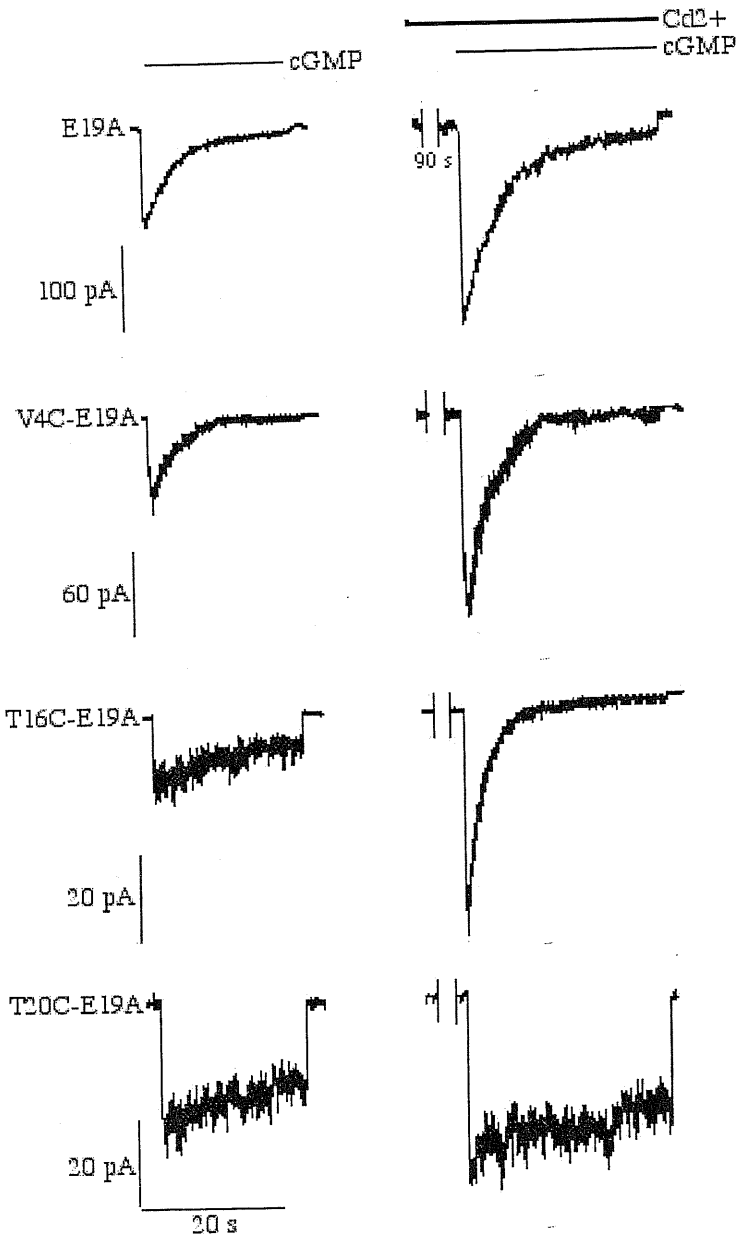

Fig. 17
See legend on the following page.

Fig. 17
The effect of Cd^{2+} applied to E19A and the indicated cysteine mutant channels from the internal side of the membrane. CNG currents from inside-out patches were elicited by 0.5 mM cGMP, at -40 mV, in the absence of EDTA.
Left panels: control current before treatment.
Right panels: current traces in the presence of Cd^{2+} (50 μM).
Cd^{2+} was applied about 90 s before cGMP and was also present during cGMP application. The gap in the baseline before cGMP application (*right panels*) indicates about 90 s of continuous recording. The *thin line* indicates cGMP application, the *thick line* indicates Cd^{2+} application. In E19A, V4C-E19A and T20C-E19A mutants, Cd^{2+} potentiated both the peak and the steady state current, with no effect on the time course of the channel desensitization. In T16C-E19A mutant, Cd^{2+} potentiated the peak current, but completely inhibited the steady state current. In T16C-E19A and T20C-E19A mutants, the channel desensitization was considerably slower than it was in E19A channels. Data are representative of at least 4 experiments.

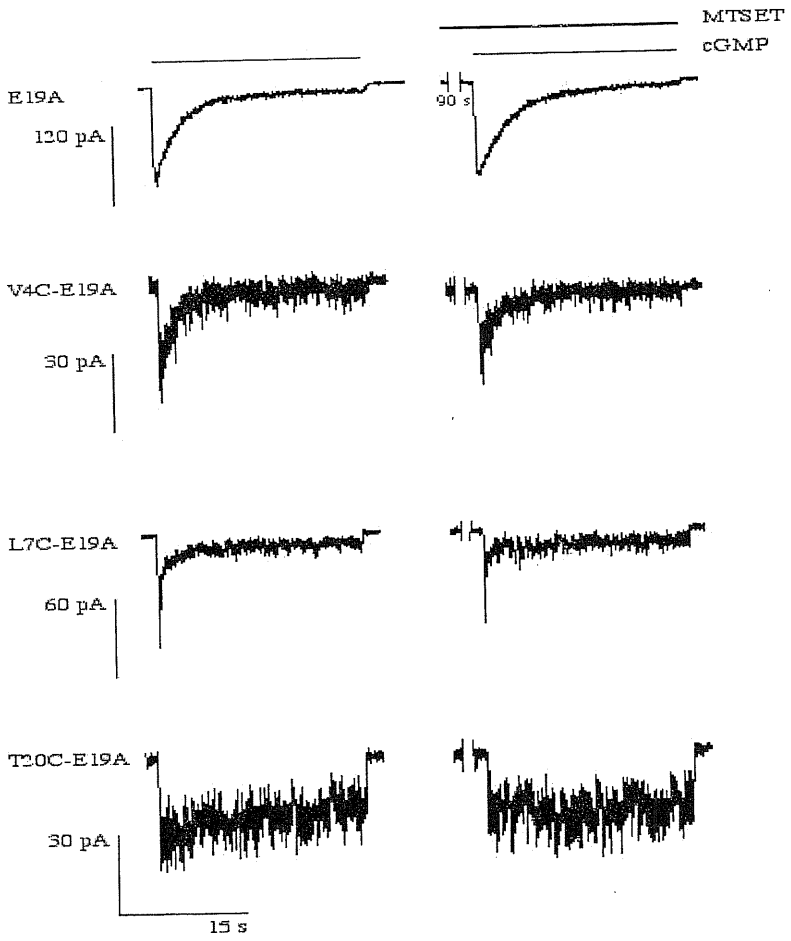

Fig. 18
The effect of MTSET applied to E19A and the indicated cysteine mutant channels from the internal side of the membrane. CNG currents from inside-out patches were elicited by 0.5 mM cGMP, at -40 mV.
Left panels: control currents before treatment.
Right panels: current traces in the presence of cGMP plus MTSET (2.5 mM).
MTSET was applied about 90 s before cGMP and was also present during cGMP application. The gap in the baseline before cGMP application (*right panels*) indicates about 90 s of continuous recording. The *thin line* indicates cGMP application, the *thick line* indicates MTSET application. MTSET did not produce any major persistent effect on E19A, V4C-E19A, L7C-E19A and T20C-E19A channels. Data are representative of at least 4 experiments.

Mutant	Desensitization ($t_{1/2}$, s)
E19A	3.6 ± 0.3
K2C-E19A	2.1 ± 0.2
V4C-E19A	2.5 ± 0.5
S6C-E19A	2.0 ± 0.6
L7C-E19A	0.5 ± 0.1
T15C-E19A	*
T16C-E19A	15.3 ± 3
I17C-E19A	**
T20C-E19A	64.3 ± 7
P22C-E19A	3.3 ± 1
V24C-E19A	2.6 ± 0.3
S27C-E19A	2.2 ± 0.4

Tab. 3
The influence of cysteine substitutions on the desensitization of E19A channels. The half-time ($t_{1/2}$) of the cGMP-activated current is given for each indicated mutant. Data were obtained from inside-out membrane patches as illustrated in fig. 17 and fig. 18, in saturating cGMP. Values are averages of at least 4 experiments.
*No appreciable desensitization was observed in mutant T15C-E19A within 2 min after cGMP application.
**After the initial partial rundown (see Fig. 19), no desensitization was observed in I17C-E19A.

channel desensitization or in the steady state current amplitude, in the presence of MTSET. The effect of Cd^{2+} in the same experimental conditions was somewhat more complex. [Cd^{2+}] smaller than 100 μM quickly potentiated the E19A channels, in analogy with the effect observed on w.t. channels (see section 3.1.1). The potentiation was quickly reversible, and no persistent steady state inhibition was observed. The time course of desensitization was also unchanged (Fig. 17).
Greater [Cd^{2+}] progressively inhibited control channels, with a half-blocking concentration around 1 mM, and were thus not suitable for testing accessibility. Fig. 17 illustrates the effect of 50 μM Cd^{2+}, the concentration we have used to test for cysteine accessibility. For our purposes, the essential point is that, at negative membrane potentials, no significant channel block was produced by 50 μM Cd^{2+}. Our results are in agreement with previous work on the internal effect of divalent cations on CNG channels in which E19 had been neutralized (Root and MacKinnon, 1993; Eismann et al., 1994). Thus, the Cd^{2+} effect on E19A mutants is not further illustrated here. The quick channel potentiation was similar to the CNG channel potentiation produced by many metal cations, caused by interaction between the ion and the H420 residue (Gordon and Zagotta, 1995). Since Cd^{2+} potentiated control and cysteine mutant channels in similar ways, the potentiation was very quick and was not observed during MTSET treatment, we conclude that this early Cd^{2+} effect was an aspecific effect, not due to the interaction between Cd^{2+} and the substituted cysteines. To stay as close as possible to the structure and function of w.t. CNG channels, we have not substituted the H420 residue.

3.2.3 Cysteine residue accessibility from the internal side

In T16C-E19A channels, Cd^{2+} applied for 30-90 s in the absence of cGMP increased the peak current amplitude (fig. 17), in analogy with what was observed in control channels. However, after cGMP application, Cd^{2+} progressively inhibited the T16C-E19A channels (fig 17). The T16C-E19A current decay in the presence of Cd^{2+} was much faster than the current desensitization in the absence of the probe, and its time course was comparable to the one observed for the inhibition produced by Cd^{2+} on T16C channels in w.t. background (see section 3.1.2). At the steady state, the T16C-E19A current block was complete and slowly reversible, whereas in the absence of Cd^{2+}, a measurable CNG current always remained at the steady state, since the channel desensitization was not complete. On the

other hand, Cd^{2+} did not produce any persistent inhibition or alteration of the desensitization kinetics on mutants K2C-E19A, V4C-E19A, S6C-E19A, T15C-E19A, T20C-E19A, P22C-E19A, V24C-E19A and S27C-E19A, when applied either in the presence or in the absence of cGMP. The effects on V4C-E19A and T20C-E19A channels are shown in fig. 17. Cd^{2+} (50 μM) produced the usual current potentiation. However, the time course of channel desensitization and the steady state current were not significantly different from those observed in the controls.
Consistently, MTSET had no effect on K2C-E19A, V4C-E19A, S6C-E19A, L7C-E19A, T15C-E19A, T20C-E19A, P22C-E19A (representative examples are illustrated in Fig. 18). In this case, as it was the case for the controls, no potentiation was observed. The results of the experiments described in the present paper are summarized in tab. 4, along with the results of previous work on cysteine mutants in wt background, for comparison.

3.2.4 The behavior of I17C-E19A channels

We have previously reported that I17C channel activity spontaneously decays in inside-out patches. This effect is likely due to the formation of disulphide bridges between opposing cysteines present on different channel subunits, since it is considerably slowed down by the reducing compound dithiothreitol (Becchetti and Gamel, 1999; Becchetti et al., 1999). In I17C-E19A channels, the current rundown, although still present, was not complete.
Fig 19A (left panel) shows I17C-E19A currents elicited by 0.5 mM cGMP, at –40 mV, soon after patch excision. The current amplitude decreased to about 40% of the starting value, within 1 min of continuous recording, in the presence of the ligand. After cGMP was washed-out, current did not recover the initial amplitude, irrespective of the recovery time (fig 19A, right panel; in this case the patch was left in the absence of cGMP for 4 min). Thus, the current decay occurring during the first cGMP addition was a genuine rundown and not a channel desensitization. Subsequently, the current amplitude remained stable. The fact that the channel rundown is not complete suggests that the contact between the substituted cysteines located on opposite subunits is partially prevented, in I17C-E19A mutant (see section 4.2.2). When Cd^{2+} was applied for 90 s in the absence of cGMP, after the completion of the initial rundown, no significant block was observed on cGMP re-application (not shown). In the presence of cGMP, instead, Cd^{2+} produced a quick potentiation analogous to that observed in the

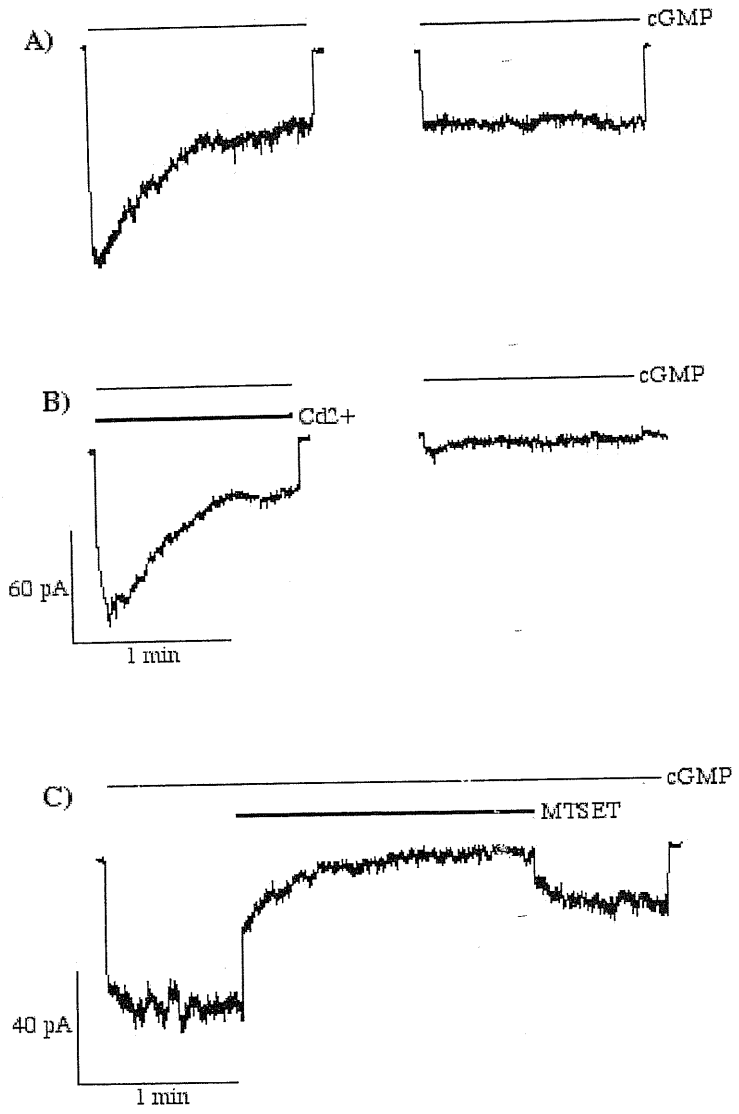

Fig. 19A-C
See legend on the following page.

Fig. 19A-C
The effect of Cd^{2+} and MTSET applied to the internal surface of I17C-E19A channels. CNG currents were elicited by 0.5 mM cGMP, at –40 mV. The *thin lines* indicate cGMP application, the *thick lines* indicate Cd^{2+} or MTSET application, as indicated.
A *Left panel*: time course of the partial spontaneous channel decay occurring in excised patches expressing I17C-E19A channels; *right panel*: steady state current after rundown. Consecutive cGMP applications did not show any further rundown, neither any sign of channel desensitization was apparent.
B *Left panel*: Cd^{2+} treatment, after rundown had reached the steady state. Cd^{2+} (50 μM) produced a quick channel potentiation, followed by a slower channel inhibition; *right panel*: after washout, subsequent cGMP applications revealed a further inhibition. The channel block was irreversible. Current traces shown in **A** and **B** were recorded from the same patch and are representative of 5 similar experiments. About 2 min were always left between consecutive cGMP applications. Longer intervals produced negligible differences.
C MTSET (2.5 mM) was applied in the open channel state after the current rundown had reached the steady state. It produced a strong channel inhibition, which was poorly reversible (data are representative of 3 experiments).

other cysteine mutants, followed by a slower, progressive channel inhibition (fig 19B, left panel). After washout, the current did not recover the initial amplitude (fig 19B, right panel). On the contrary, it was further decreased. This effect is discussed below. At the steady state, the residual current after Cd^{2+} treatment was 10.5 % ± 1.1 % (n = 5) of the initial value. MTSET, too, produced irreversible inhibition (but no potentiation), when applied to the cytoplasmic face of the plasma membrane, in the presence of cGMP (fig. 19C). The residual CNG current was 33% ± 10%, at the steady state (n=3). No further block was observed on cGMP application after MTSET was washed out. In addition, no effect was produced by MTSET, in the closed state. We conclude that the residue in position 17, in E19A background, was not accessible to our probes from the inside in the closed state, while it was accessible to both Cd^{2+} and MTSET, in the open state.

3.2.5 Cysteine residue accessibility from the internal side after desensitization

We have also tested whether the cysteine residue accessibility was changed after channel desensitization had reached the steady state. This control is particularly important in the case of T16C-E19A, which shows a slower desensitization. It was possible that the exogenous cysteine was accessible before desensitization, but not after. In this case, the probe might produce substantial block before desensitization, and the difference between the two channel states would not be appreciable. However, the pattern of accessibility was not different when the probes were added at the steady state (fig. 20A). Representative traces are shown for the two most relevant desensitizing mutants, i.e. T16C-E19A and P22C-E19A (fig. 20A,B). In both cases, Cd^{2+} addition at the steady state, in the presence of cGMP, yielded the usual rapid potentiation. This effect was followed by irreversible channel inhibition only in the case of T16C-E19A, suggesting that the cysteine accessibility was not different before and after desensitization.

3.2.6 Cysteine residue accessibility from the external side

A complete picture of the cysteine accessibility pattern around the glutamate E19, after its neutralization, requires a demonstration that the stretch of residues immediately following E19 remains externally accessible, as it is in w.t. background (Becchetti et al., 1999; see section 3.1.4). The accessibility from the external side of the plasma membrane, in CNG channels, is usually

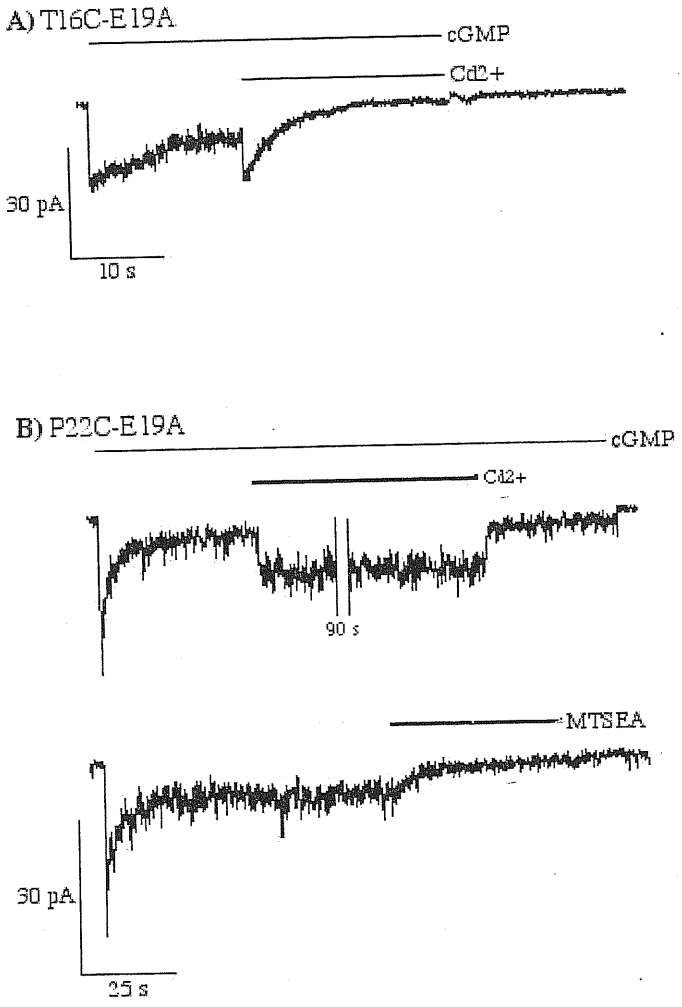

Fig. 20A-B
See legend on the following page.

Fig. 20A-B
Effect of Cd^{2+} and MTSEA on T16C-E19A and P22C-E19A channels, at the steady state. The CNG currents were elicited by 0.5 mM cGMP, at –40 mV. The *thin lines* indicate the cGMP application. The *thick lines* indicate the Cd^{2+} or MTSEA application, as indicated. **A** Cd^{2+} (50 μM) was applied to the inner side of inside-out patches expressing T16C-E19A channels, at the steady state. After a quick potentiation, Cd^{2+} inhibited the T16C-E19A channels irreversibly.
B *Upper panel*: application of Cd^{2+} (50 μM) to the internal surface of P22C-E19A channels, at the steady state. Cd^{2+} caused no irreversible block. *Lower panel*: application of MTSEA (2.5 mM) to inside-out patches, at the steady state. MTSEA produced a complete irreversible channel inhibition. As explained in the text, the comparison of the effects of Cd^{2+} and MTSEA was considered an evidence that the P22C residue is accessible from the external side of the membrane, in E19A background. Data are representative of at least 3 experiments.

tested by applying the thiol-specific reagents to outside-out patches expressing the different mutant channels, with cGMP contained within the patch pipette (Sun et al., 1996; Becchetti et al., 1999; see section 3.1.4). However, due to channel desensitization, this experimental approach is not feasible in E19A background. In fact, in the outside-out mode, the constant exposition to cGMP prevents the channel recovery from desensitization. On the other hand, in the inside-out mode, our reagents should be dissolved in the pipette solution, and could not be applied and washed out quickly. This would make it impossible to distinguish between persistency of channel inhibition (fundamental to diagnose accessibility) and slow washout of the probe. Hence, we tested the external cysteine accessibility indirectly, as follows. We compared the effect of MTSEA applied to the internal side of inside-out patches to the effects of Cd^{2+} and MTSET applied in the same way. MTSEA is known to permeate the plasma membrane as uncharged amine, while Cd^{2+} and MTSET do not permeate through the lipid bilayer (Holmgren et al., 1996; Karlin and Akabas, 1998). Therefore, we assumed that a channel block produced by MTSEA applied intracellularly, not paralleled by inhibition produced by Cd^{2+} and MTSET applied in the same way, was caused by MTSEA reaching the cysteine from the outside. Under this assumption, we concluded that P22C-E19A channels were only blocked from the external side (fig. 20), in agreement with the external accessibility of this residue in w.t. background (tab. 4). On the other hand, internally applied MTSEA produced no persistent effect on control channels. It also had no effect on S6C-E19A and T15C-E19A (tab. 4), i.e. cysteine residues not affected by the thiol-specific compounds from either side of the plasma membrane, in w.t. background.

3.3 Structure-function relationship in the SpHCN channel pore

If SpHCN is heterologously expressed in *Xenopus laevis* oocytes, recordings from excised patches clearly show an I_h current when cAMP is present at the intracellular side of the patch and the membrane voltage is stepped to hyperpolarizing potentials. If cAMP is removed, the current usually disappears within about one second; therefore, I_h currents can be clearly and easily identified and isolated. In inside-out patches, the I_h current was taken as the difference between the current recorded in the presence of cAMP and in its absence (fig. 21A); in outside-out patches, the I_h current activated by stepping the voltage from 0 to –x mV was taken as the sum of the currents

Cysteine mutant	wt background*		E19A background	
Effect from inside	MTSET	Cd^{2+}	MTSET	Cd^{2+}
WT	1.25	0.97	1.08 ± 0.02	1.20 ± 0.04
K2C	**	nd	1.10 ± 0.09	1.18 ± 0.05
V4C	0.95	0.98	1.18 ± 0.04	1.22 ± 0.07
S6C	0.94	0.97	0.93 ± 0.02	1.03 ± 0.02
L7C	0.75	nd	0.82 ± 0.07	0.86 ± 0.03
T15C	0.97	nd	1.15 ± 0.02	1.03 ± 0.04
T16C	0.45	0.05	nd	0.01 ± 0.02
I17C	***	0.10	0.37 ± 0.06	0.05 ± 0.04
T20C	1.20	0.94	0.94 ± 0.08	0.97 ± 0.02
P22C	0.90	0.85	0.96 ± 0.07	1.07 ± 0.03
V24C	1.09	nd	nd	1.03 ± 0.02
S27C	1.09	0.96	nd	1.04 ± 0.07

Effect from outside	MTSET	Cd^{2+}	MTSEA
WT	0.94	0.98	0.96 ± 0.03
V4C	0.13	0.19	nd
S6C	nd	0.97	0.92 ± 0.04
L7C	0.98	nd	nd
T15C	1.13	nd	1.08 ± 0.02
T16C	1.13	0.65	nd
T20C	0.07	0.30	nd
P22C	0.15	0.10	0.05 ± 0.02

Tab. 4

Summary of the effects of sulfhydryl-specific reagents on cysteines introduced into the P-loop of the α subunit of CNG channels from mammalian rod, in w.t. and in E19A background. All data refer to experiments executed at –40 mV. Wt background: the effect of the probe is expressed as residual current after treatment, i.e. as the ratio between the CNG current after washout of the probe and the current before treatment. E19A background: the effect of MTSET (or MTSEA) is expressed as the ratio of the peak CNG current after washout and the peak current before treatment. Persistent effects were only observed for I17C-E19A mutant (and, marginally, for L7C-E19A). The effect of Cd^{2+} is complicated by the concomitant channel potentiation. In this case, thus, the currents measured 20 s after cGMP application were normalized to the corresponding peak currents. The table reports the ratio of the values thus obtained after and before Cd^{2+} application. A significant current inhibition, persisting after washout, was only observed for T16C and I17C mutants. Data are averages of at least 3 determinations. For simplicity, we only report the standard errors relative to the experiments described in the present paper.

* The effects in wt background are from Becchetti et al., 1999 (for MTSET) and sections 3.1.1 to 3.1.3 (for Cd^{2+}).

** The residue K2C was found to be unmodified by MTSEA by Sun et al., 1996.

*** MTSET produced an acceleration of I17C channels rundown, in wt background (Becchetti et al., 1999).

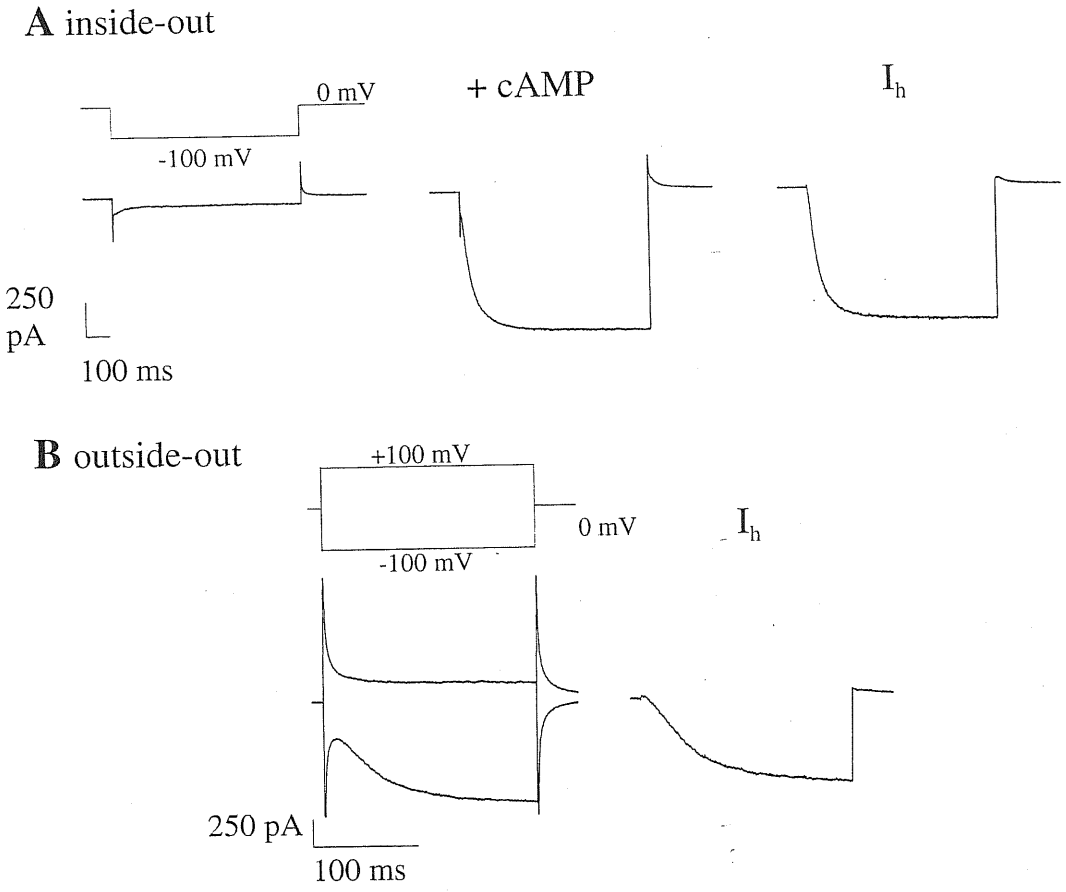

Fig. 21A-B
Identification of the I_h current.
A current recordings in an inside-out patch during voltage steps from 0 to –100 mV in the absence (*left*) and in the presence (*middle*) of 1 mM cAMP in the intracellular medium. Voltage steps lasting about 1 s. The I_h current (*right*) is taken as the difference of the two traces.
B current recordings in an outside-out patch during voltage steps from 0 to –100 mV and from 0 to +100 mV in the presence of 1 mM cAMP in the extracellular medium filling the patch pipette (*left*). Voltage steps lasting about 250 ms. The I_h current (*right*) is taken as the sum of the two traces.

recorded when the voltage was stepped from 0 to –x mV and from 0 to x mV (fig. 21B).
In most experiments, we have applied cAMP at a concentration of 1mM and we have stepped the membrane voltage from a holding potential of 0 mV to –100 mV, because these conditions elicit large Ih currents, with a sigmoidal waveform that is characteristic of the time course of vertebrate Ih currents (DiFrancesco, 1993; Pape, 1996; for the characterization of the SpHCN wild type channel heterologously expressed in a different cell system, see Gauss et al., 1998).

3.3.1 Effect of Cd^{2+} and MTSET applied to the inner side of w.t. channels

SpHCN, like all HCN channels cloned so far, has a cysteine residue in position 428 in the putative pore region that corresponds to larger residues in other K^+ channels, like threonine in KAT1, Shaker, KcsA and the α-subunit of the bovine rod CNG channel, and serine in DmEAG and HERG (see fig. 7). SpHCN also contains other cysteine residues, mainly located in the putative transmembrane segments, with the exception of one in the cytoplasmic N-terminal domain and three in the cytoplasmic cyclic nucleotide-binding domain (CNBD). We have investigated the role of cysteine 428 in the pore topology of the SpHCN channel by using sulfhydryl-specific reagents like Cd^{2+} and MTSET.
The SpHCN channel may be in three different states: unliganded (i.e. in the absence of cAMP), liganded and closed (i.e. in the presence of cAMP and at non-hyperpolarized potentials), and liganded and open (i.e. in the presence of cAMP and at hyperpolarized potentials). It is therefore necessary to analyze the blocking effect of Cd^{2+} and MTSET in different conditions. As shown in fig. 22A, when the I_h current was activated by the addition of 1 mM cAMP to the intracellular medium and by stepping the voltage to –100 mV, 50 μM Cd^{2+} powerfully – and almost irreversibly – abolished the I_h current within 30 seconds. However, if Cd^{2+} ions were added to the bathing medium for 2 minutes but keeping the membrane voltage at 0 mV and the channel in a liganded but closed state, the observed blockage was much less pronounced, being on average just 27% (fig. 22B). When MTSET was added to the intracellular medium in the presence of cAMP, the I_h current was only marginally affected (fig. 22C) and the observed blockage was on average 14%. If Cd^{2+} or MTSET were added in the absence of cAMP, and

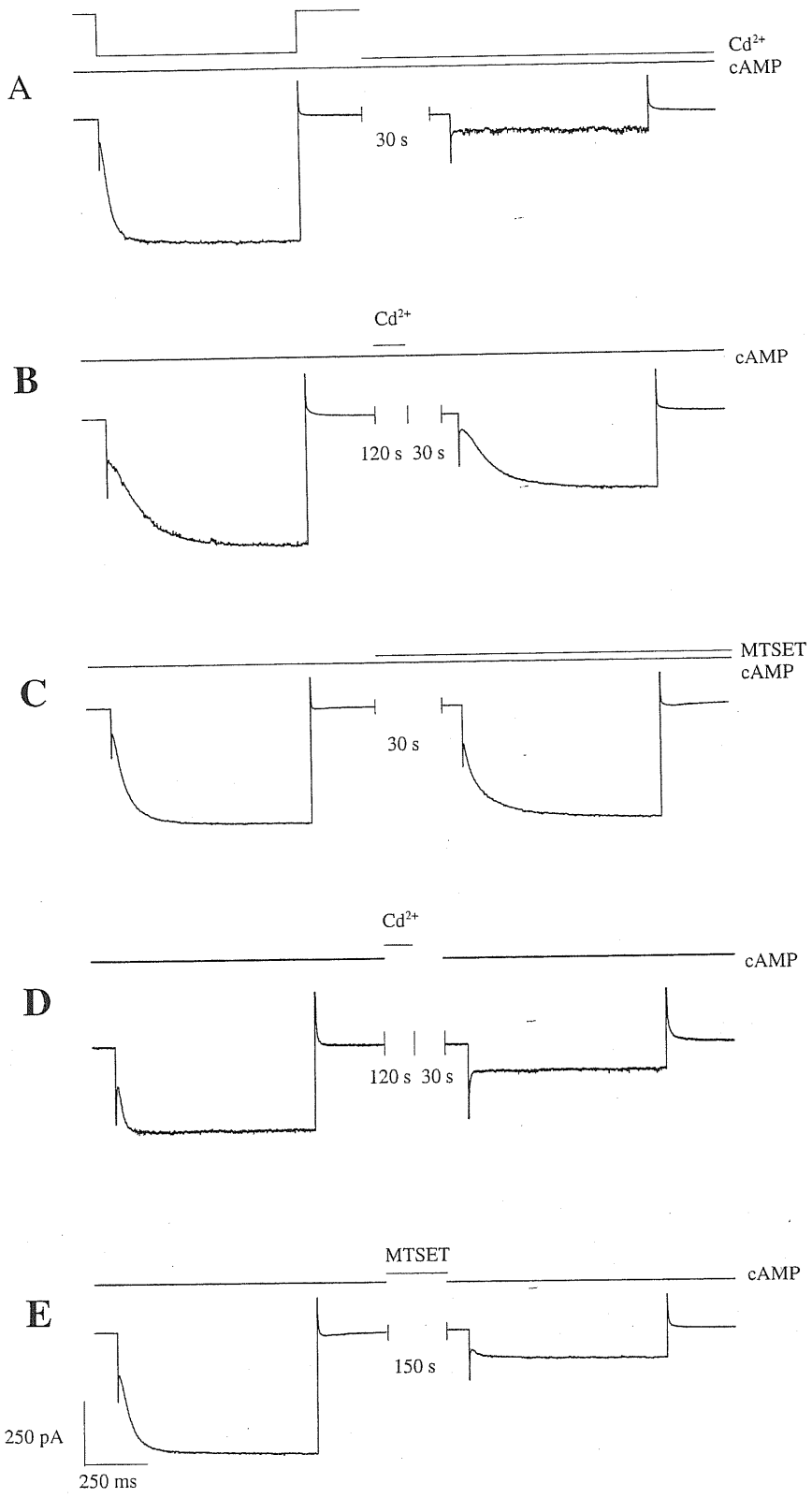

Fig. 22A-E
See legend on the following page.

Fig. 22A-E
Effect of intracellularly applied Cd^{2+} and MTSET on the I_h current of the SpHCN channel. The I_h current is elicited by stepping the membrane voltage from 0 to –100 mV, in the presence of 1 mM cAMP in the intracellular medium. *Solid bars* indicate when 1 mM cAMP was added to the bathing medium; *thin bars* indicate when 50 µM $CdCl_2$ or 2.5 mM MTSET were added to the bathing medium in different channel states.
A Complete Cd^{2+} blockage in the liganded and open channel state.
Cd^{2+} is applied, in the presence of cAMP, while the channel is kept open by constant repetitions of the hyperpolarizing voltage step. Traces shown are before (*left*) and after (*right*) 30 s application.
B Partial Cd^{2+} blockage in the liganded and closed channel state.
Cd^{2+} is applied, in the presence of cAMP, while the channel is kept closed by keeping the holding potential at 0 mV. Traces shown are before (*left*) and after (*right*) 2 min application followed by 30 s wash-out.
C No MTSET blockage in the liganded and open channel state.
MTSET is applied, in the presence of cAMP, while the channel is kept open by constant repetitions of the hyperpolarizing voltage step. Traces shown are before (*left*) and after (*right*) 30 s application.
D Almost complete Cd^{2+} blockage in the unliganded channel state. Cd^{2+} is applied, in the absence of cAMP, while the channel is kept closed by keeping the holding potential at 0 mV. Traces shown are before (*left*) and after (*right*) 2 min application followed by 30 s wash-out.
E Partial MTSET blockage in the unliganded channel state.
MTSET is applied, in the absence of cAMP, while the channel is kept closed by keeping the holding potential at 0 mV. Traces shown are before (*left*) and after (*right*) 2.5 min application.

therefore when the SpHCN channel was in unliganded state, the I_h current was significantly reduced and almost abolished, as shown in fig. 22D-E. These results will be commented upon in section 4.3.1.

3.3.2 Effect of Cd^{2+} applied to the inner side of mutant channels C428S

When cysteine 428 is mutated into a serine, intracellular Cd^{2+} does not block the SpHCN channel in its liganded and open state, in contrast to what happens in the w.t. channel. As shown in fig. 23A, in inside-out membrane patches intracellular Cd^{2+} does not reduce the I_h current activated at –100 mV in the C428S mutant, while the blockage of the w.t. channel is almost complete (fig. 22A).

3.3.3 Effect of Cd^{2+} applied to the outer side of w.t. channels

When the patch pipette contained 1 mM cAMP and outside-out patches were obtained, it was possible to analyze the blocking effect of Cd^{2+} applied on the extracellular side of the membrane of w.t. HCN channels. As shown in fig. 23B, extracellular Cd^{2+} does not block significantly the I_h current activated at –100 mV. Fig. 23C illustrates that the major effect of extracellular Cd^{2+} is to shift by some mV the activation of the I_h current.

3.3.4 The behavior of mutant channels K433Q

The great majority of K^+ and CNG channels have at the extracellular side of the pore a ring of negative charges (see fig. 7) controlling the inflow of permeating ions (for K^+ channels, see Doyle et al., 1998 on the KcsA channel; for CNG channels, see Root and MacKinnon, 1993, and Eismann et al., 1994, on the α-subunit of bovine rod channel). As shown in fig. 7, at the corresponding position the SpHCN, mHCN2 and hHCN4 channels have a positively charged residue, i.e. a lysine or an arginine, while mHCN1 and mHCN3 channels have neuter residues. It is interesting to verify whether lysine in position 433 in the SpHCN channel is an extracellular residue controlling the blockage by extracellular large anions, a phenomenon observed both in native (Frace et al., 1992) and in cloned (Santoro et al., 1998) channels.
As shown in fig. 24B, when lysine 433 is mutated into a glutamine the time course of the activation of the I_h current is significantly modified. Current recordings from the w.t. channel obtained when the voltage command is stepped from 0 mV to negative voltages exhibit the activation characteristic

A Intracellular Cd^{2+} effect on C428S

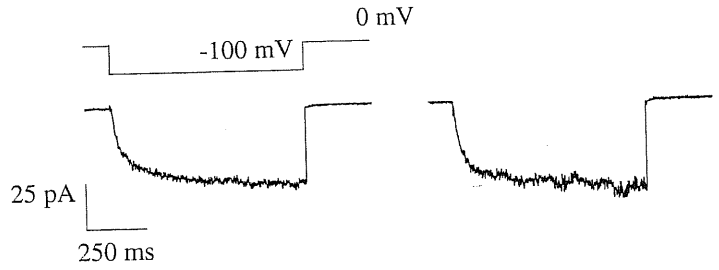

B Extracellular Cd^{2+} effect on w.t.

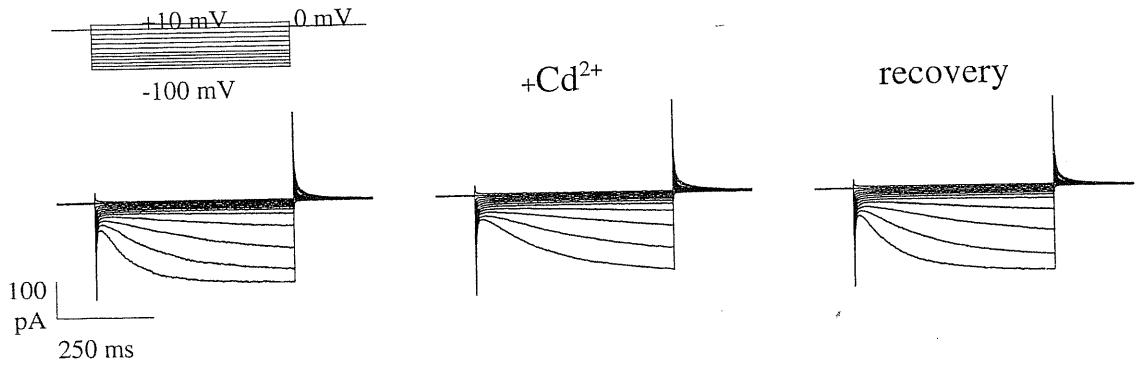

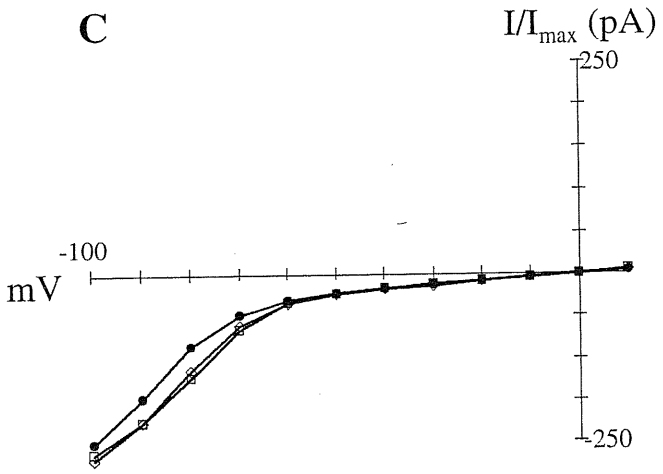

Fig. 23A-C
See legend on the following page.

Fig. 23A-C
Cysteine in position 428 is accessible only from the intracellular side.
A Intracellular Cd^{2+} effect in the open state in mutant C428S.
Current recordings from inside-out patches. Traces shown are before (*left*) and after (*right*) application of 50 μM $CdCl_2$, in the presence of cAMP in the intracellular medium. Voltage steps as in figs. 21B and 22.
B No extracellular Cd^{2+} blockage in the w.t. channel.
Current recordings obtained from outside-out patches. Traces shown are before (*left*), during (*middle*) and after (*right*) application of 50 μM $CdCl_2$, in the presence of cAMP in the extracellular medium filling the patch pipette. Voltage steps are from –100 to +10 mV in 10 mV steps.
C Extracellular Cd^{2+} shifts the I_h current activation curve by some mV.
Current-voltage (I/V) relationship taken from **B**. Current values are normalized to I_{max} (i.e., at –100 mV). Control (before Cd^{2+} application), *hollow diamonds*; Cd^{2+} application, *filled circles*; recovery (after Cd^{2+} application), *hollow squares*.

A w.t.

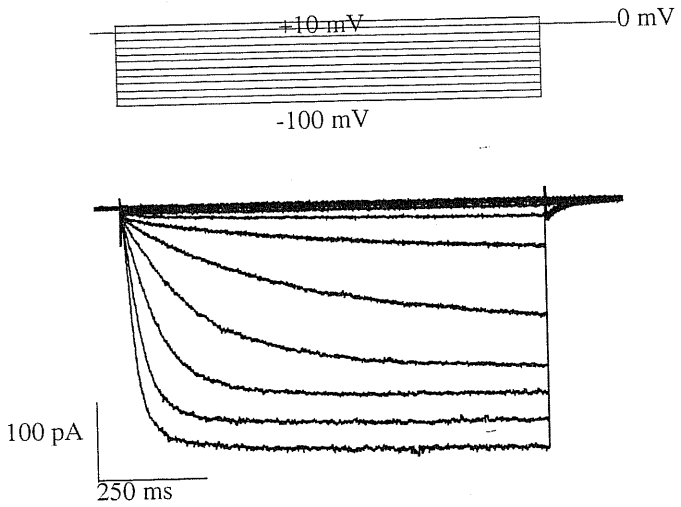

B K433Q

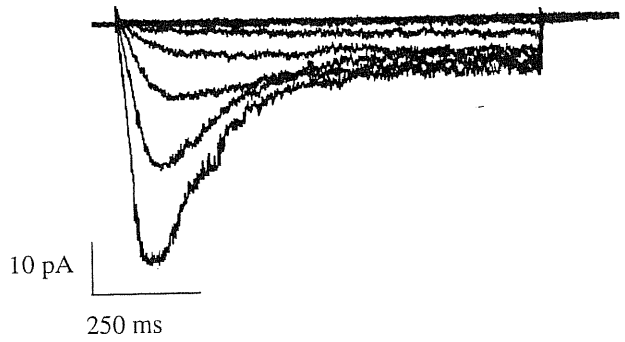

C g/g_{max}

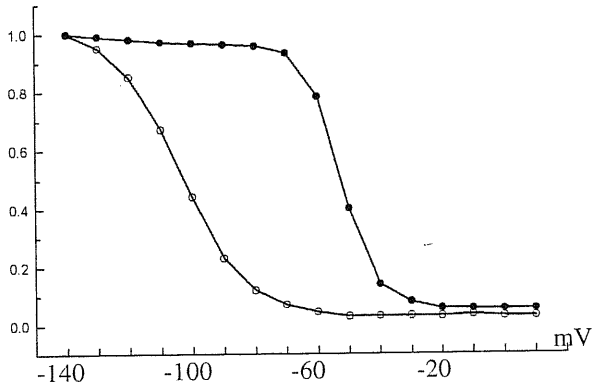

Fig. 24A-C
See legend on the following page.

Fig. 24A-C
Properties of the w.t. and K433Q mutant channels.
A Current recordings from inside-out patches for the w.t. channel. Voltage steps are from –100 to +10 mV in 10 mV steps, in the presence of 1 mM cAMP in the intracellular medium.
B Current recordings from inside-out patches for the K433Q mutant channel. Voltage steps as in A.
C Neutralization of lysine 433 shifts the half-activation by about 50 mV.
Conductances underlying I_h currents for the w.t. channel at the steady state (*filled symbols*) and for the K433Q mutant channel at the peak of its activation and before development of inactivation (*open symbols*). Conductances are relative to experiments in which voltage steps were applied from –140 to +10 mV in 10 mV steps, in the presence of 1 mM cAMP in the intracellular medium. Conductance values are normalized to g_{max} (i.e., at –140 mV).

of the native I_h current (fig. 24A). On the contrary, current recordings from mutant K433Q show an initial activation followed by inactivation, as seen in fig. 24B. The steady state activation of the conductance underlying the I_h current for the w.t. channel is shown in fig. 24C (filled symbols). The conductance was half activated at about –45 mV, in agreement with previous reports (Gauss et al., 1998). The activation of the conductance of the I_h current in the mutant K433Q at the peak of its activation and before development of inactivation is shown in fig. 24C as open symbols. In this case, the apparent half activation occurred at more negative voltages around –95 mV.

I_h current recordings for mutant K433Q in the inside-out patch-clamp configuration exhibit a significant rundown. As shown in fig. 25A, the I_h current activated at –100 mV declined by about 50% within 60 s after patch excision and perfusion with 1 mM cAMP of the intracellular side of the membrane. Instead, no significant current rundown was observed in the double mutant C428S+K433Q, as illustrated in fig. 25B.

Ionic selectivity of mutant K433Q can be reliably studied in inside-out membrane patches, provided that the tail currents are elicited and measured before development of inactivation (see section 2.4.4.5), and that the measurements are performed on separate patches for each different ion, due to the progressive rundown of K433Q current. Figs. 26A, B and C, respectively, show current recordings from the K433Q mutant channel, when intracellular K^+ only was present (A) and when it was partly replaced with Na^+ (B) or Li^+ (C) (the SpHCN channel conducts little, if any, Na^+ in the absence of K^+ ions; Gauss et al., 1998). The relationship between the amplitude of tail currents and the membrane voltage for the K433Q mutant channel are shown in fig. 26D. Values for V_{rev} were: 14.5 mV (Na^+), 27.8 mV (Li^+). Analogous measurements of ion selectivity performed on the w.t. SpHCN channels (not shown) yielded results in agreement with those previously obtained when the channel was expressed in a different system (HEK293 cells; Gauss et al., 1998), i.e. V_{rev} values of 16.9 mV for Na^+ and 20.6 mV for Li^+.

3.3.5 Substitution of chloride with larger anions in w.t. and mutant SpHCN channels

Large extracellular anions are known to reduce or block the I_h current in both native I_h channels (Frace et al., 1992) and heterologously expressed HCN channels (Santoro et al., 1998). It has been suggested that chloride might interact with extracellular positive charges present in the pore region

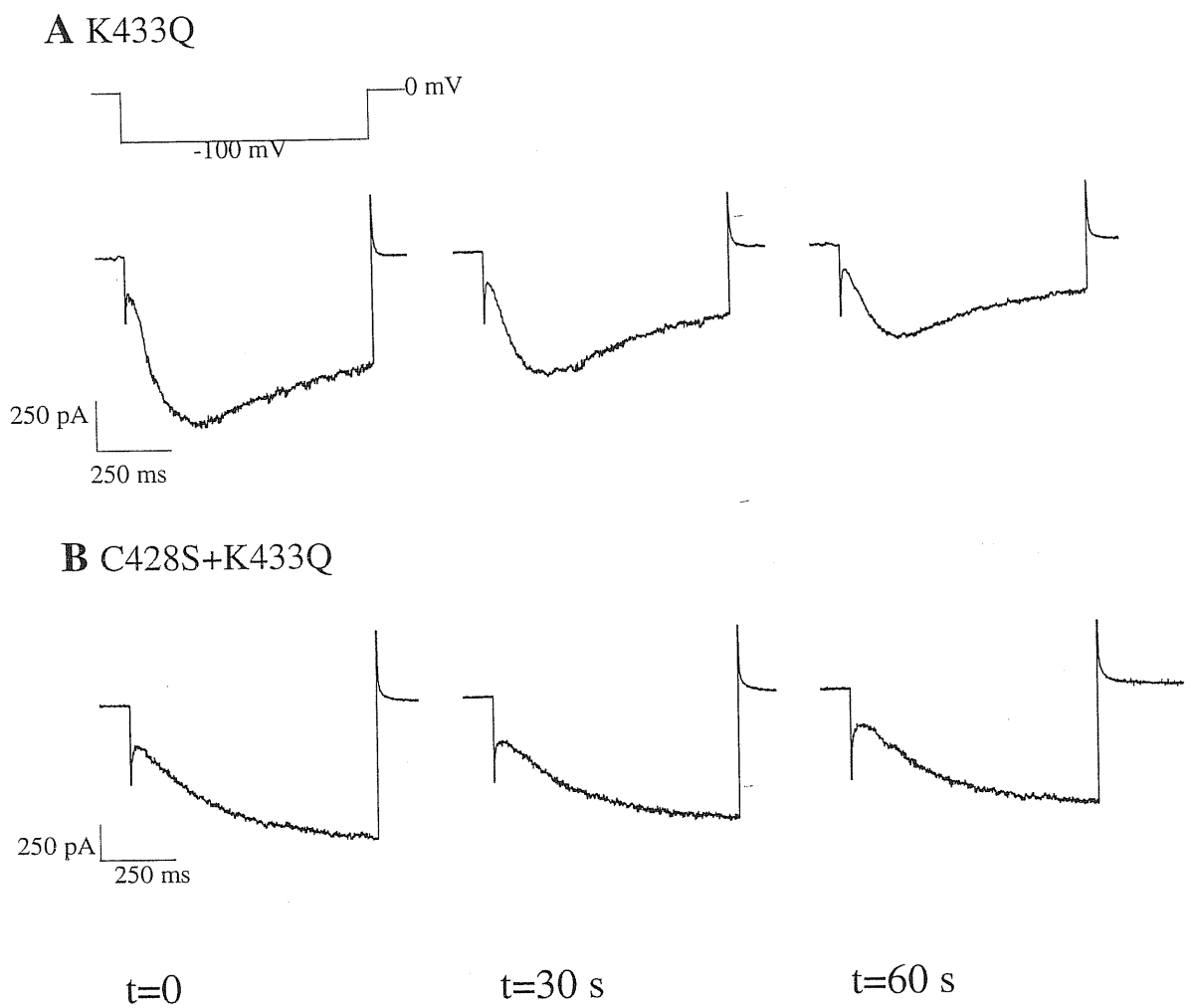

Fig. 25A-B
Current recordings to test current rundown in mutant channels K433Q and C428S+K433Q. I_h currents were elicited by applying a hyperpolarizing step of –100 mV to inside-out patches of membrane, in the presence of 1 mM cAMP on the cytoplasmic side of the patch. The protocol was applied continuously, and the traces shown were recorded immediately after patch excision (*left*) and after 30 (*middle*) or 60 s (*right*).
A About 60 s after patch excision, K433Q mutant current is reduced to about half its initial value.
B After the same time, C428S+K433Q mutant current does not exhibit a significant rundown.

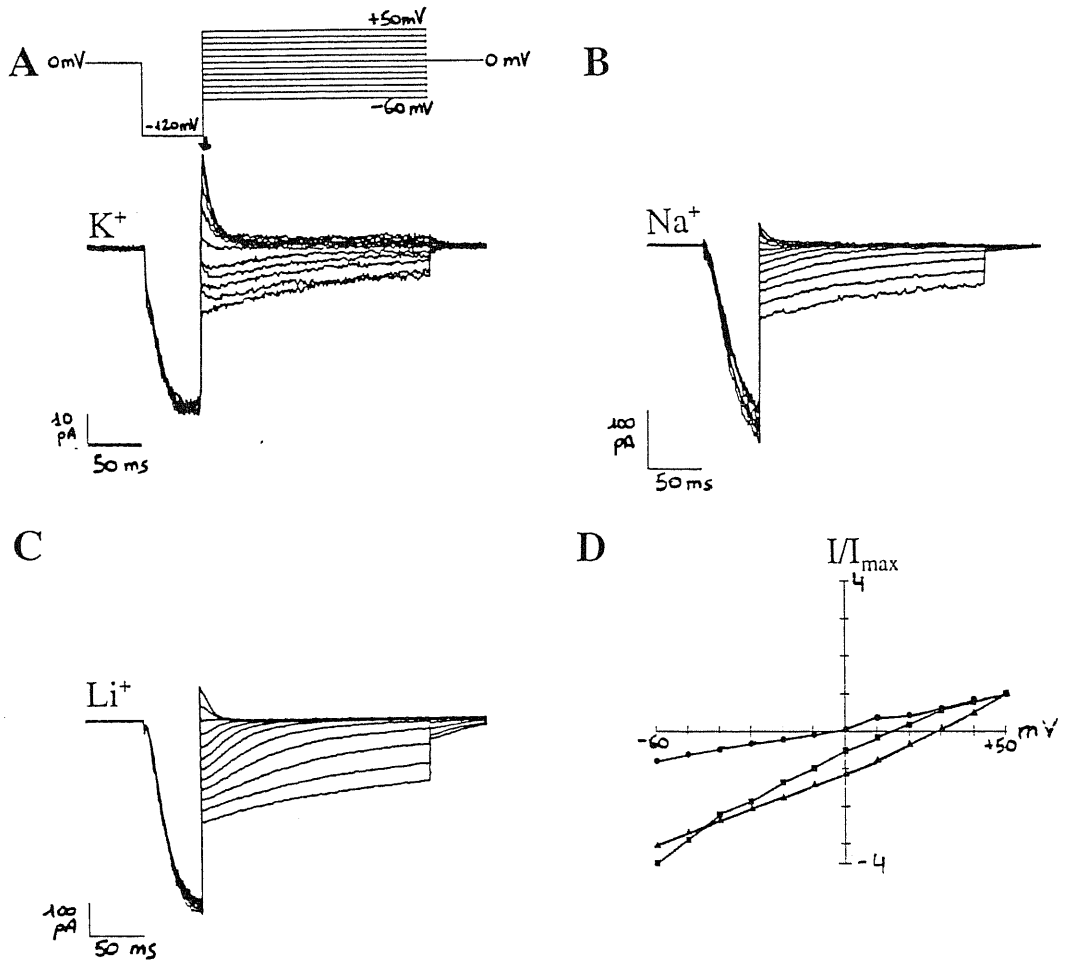

Fig. 26A-D
Ion selectivity of mutant channel K433Q.
Current recordings in inside-out patch clamp configuration. Solutions on the intracellular side of the membrane contained:
A 150 mM KCl;
B 50 mM KCl + 100 mM NaCl;
C 50 mM KCl + 100 mM LiCl.
The protocol , from a holding potential of 0 mV, consisted in a hyperpolarizing step to –120 mV, lasting 50 ms, followed by tests of voltage from +50 to –60 mV, in 10 mV steps. The *arrow* in **A** indicates the time when instantaneous current-voltage relationship was taken.
D Instantaneous current-voltage relationship from experiments as in **A-C**. Currents were normalized to the maximum tail current (i.e., at +50 mV). KCl: *circles*; NaCl, *squares*; LiCl: *triangles*.

of these channels (see Ludwig et al., 1999a). It is interesting to test whether extracellular chloride-substitutes have a similar effect on SpHCN channel, and whether lysine in position 433 has a role in the interaction with these anions. Therefore, we tested chloride-replacement in the w.t. channel, in both the intra- and extracellular side of the membrane, and in the K433Q mutant channel, in the extracellular medium. The results are shown in fig. 27A-C. In the w.t. channel, when the I_h current was activated by adding cAMP to the intracellular medium during inside-out recordings, the substitution of intracellular chloride with acetate, glutamate or sulphate only slightly modified the current amplitude (fig. 27A). On the contrary, when in the same w.t. channel the external chloride was replaced with larger anions as above during outside-out recordings, the I_h current was significantly reduced (fig. 27B). K-aspartate was also tested in this case (data not shown), and its effect was comparable to the other tested anions. The I_h current block was usually reversible (data not shown). In K433Q mutant channels, substitutions of external chloride had a very similar blocking effect (fig. 27C).

A w.t., intracellular side

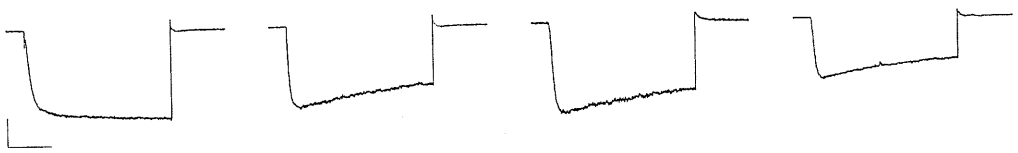

B w.t., extracellular side

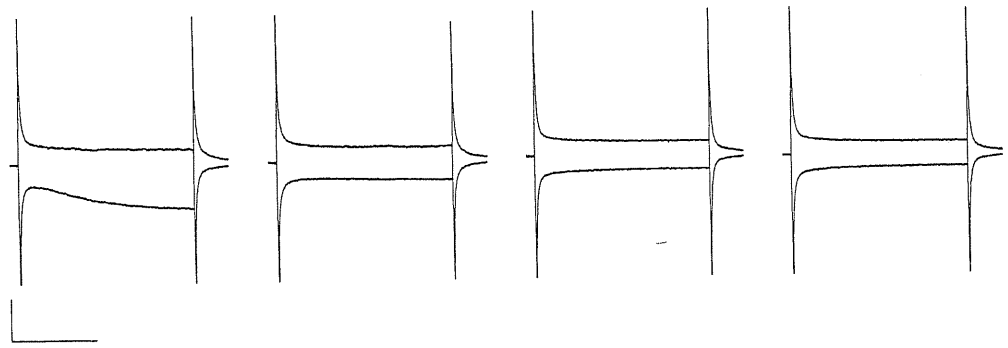

C K433Q, extracellular side

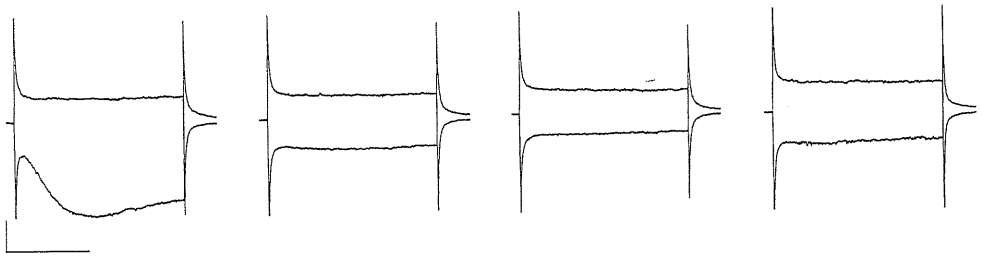

KCl K-acetate K-glutamate K-sulphate

Fig. 27A-C

The effect of substituting external chloride with larger anions in SpHCN channel. KCl (*left*) was substituted with either K-acetate (*center-left*), K-glutamate (*center-right*) or K-sulphate (*right*).
A Replacement of intracellular chloride with larger anions in w.t. SpHCN channel. Current recordings obtained with inside-out patch-clamp. Voltage step as in fig. 21A.
B Replacement of extracellular chloride with larger anions in w.t. SpHCN channel. Current recordings obtained with outside-out patch-clamp. Voltage steps as in fig. 21B.
C Replacement of extracellular chloride with larger anions in K433Q mutant channel. Current recordings obtained with outside-out patch-clamp. Voltage steps as in fig. 21B.

4) DISCUSSION

4.1 Structure-function relationship in the brCNGCα pore in the wild-type background

4.1.1 Using Cd^{2+} to test cysteine accessibility in CNG channels

For studying inward cysteine accessibility, we assumed that a robust CNG current inhibition produced by low [Cd^{2+}] at negative membrane potentials was due to Cd^{2+} interaction with the added cysteine residue. We also assumed that 100 μM Cd^{2+} was a concentration sufficient to test the accessibility of the substituted cysteine residues. In fact, the Cd^{2+} affinity for thiol groups varies depending on the chemical surroundings of the -SH group (Martell and Smith, 1974; Krizek et al., 1993). However, in ion channels tested to date, the affinity for Cd^{2+} of the substituted cysteine residues in the pore region is rarely larger than 100 μM, and often much lower (Yellen et al., 1994; Kurz et al., 1995; Krovetz et al., 1997; Liu et al., 1997; Kubo et al., 1998). Other metal cations react with thiol groups, but none of the other possible candidates offers particular advantages for testing cysteine accessibility in CNG channels, compared to Cd^{2+}. For example, Ag^{+}, often used to test cysteine accessibility (Lu and Miller, 1995; Dart et al., 1998), blocks CNG channels at concentrations around 1 μM (Ildefonse and Bennett, 1991).

4.1.2 Accessibility of V4C, S6C, T20C, P22C and S27C residues

No effect was found on any of the above mutants when Cd^{2+} was applied to the cytoplasmic face of the patch. Instead, V4C, T20C and P22C channels were inhibited when Cd^{2+} was applied from the outside, in agreement with the results obtained by using MTSET (Becchetti et al., 1999). These data suggest that V4, T20 and P22 are located in the external channel vestibule, in analogy with the corresponding residues in *Shaker*-type voltage-dependent K^{+} channels (Pascual et al., 1995; Kurz et al., 1995; Gross and MacKinnon, 1996). The structural significance of our data is reinforced by the fact that cysteine mutation in these positions has a minor effect on channel function. Hence, in these cases, the CNG channel structure is unlikely to be altered considerably. In particular, the selectivity to monovalent alkali cations, the dose-response to cGMP, the voltage dependency and the single-channel P_o were scarcely different from the

w.t.'s, although some alterations were observed in the single-channel conductance of T20C and P22C mutants (Becchetti and Gamel, 1999).

4.1.3 Accessibility of residue T16C

T16C channels were potently blocked by internal Cd^{2+}, with a K_d around 15 μM at the steady state. The inhibition was preceded by a quick potentiation which was also observed in w.t. and in the other mutant channels. Several transition metal divalent cations, such as Ni^{2+}, Zn^{2+}, Cd^{2+} Co^{2+} and Mn^{2+} have been reported to potentiate the rod CNG channels (Ildefonse and Bennett, 1991; Karpen et al., 1993). Ni^{2+} was shown to potentiate the rod channels through interaction with the histidine residue in position 420 (Gordon and Zagotta, 1995). Thus, although we have not investigated the mechanism of channel potentiation, the simpler hypothesis to explain our data is that Cd^{2+} potentiates w.t. and mutant channels by the same mechanism, and that the potentiation is larger in T16C channels simply because their basal P_o is lower (Bucossi et al., 1997; Becchetti and Gamel, 1999). On the other hand, the time course of the T16C channel block was considerably slower and paralleled the time course of the Cd^{2+} effect on substituted cysteine residues that others have measured (Yellen et al., 1994; Krovetz et al., 1997). The slowness of the Cd^{2+} effect on substituted cysteine residues is usually attributed to the progress of the reaction forming the S-Cd covalent bond. Therefore, we consider the inhibition of T16C channels to be due to the specific binding of Cd^{2+} to the introduced thiol group. However, even if part of the quick channel potentiation were due to Cd^{2+} interaction with the added cysteine, this would not modify our conclusions about T16C accessibility.

The cysteine T16C was also partially accessible to Cd^{2+} from the external side of the plasma membrane, but with a much lower affinity (fig. 16C). Since divalent cations are known to be "permeant blockers" of CNG channels (Colamartino et al., 1991; Zagotta and Siegelbaum, 1996), it is likely that, at high concentrations, some Cd^{2+} ions can reach the T16C residues permeating the conduction pathway. Considering the large difference in affinity between the external and the internal effects, our data support the idea that T16 residues face the inner side of the membrane, in agreement with the ineffectiveness of extracellular MTSET (Becchetti et al., 1999).

4.1.4 Accessibility of residue I17C

As remarked above, I17C mutant currents decay in inside-out patches with a $t_{1/2}$ around 45 s (Becchetti and Gamel, 1999; Becchetti et al., 1999). We ascribe this decay to the formation of disulphide bridges between corresponding cysteine residues on different channel subunits, because it is significantly slowed down by the reducing compound dithiothreitol (Becchetti and Gamel, 1999). In contrast, Cd^{2+} quickly blocked I17C channels when applied to the cytoplasmic side of the patch (fig. 14). A 10-s perfusion was sufficient to produce complete irreversible inhibition. This result suggests that I17C is a very sensitive residue and is accessible from the inner side of the membrane. However, the external accessibility could not be tested for the technical reasons explained in section 3.1.4. Further information may come from coexpression of mutant and w.t. channels (or concatemeric structures), to obtain channels containing only one to two cysteine residues per tetramer.

4.1.5 Comparison with previous work and structural implications

Our results extend and complete the data previously obtained with MTSET (Becchetti et al., 1999). In fact, MTSET only partially inhibited T16C channels when applied to the inner surface, and the effect took several minutes to reach steady state. This left some doubts about the structural significance of those results. Instead, the block produced by Cd^{2+} was complete, slowly reversible and much quicker. The same applies to I17C channels, also more strongly inhibited by Cd^{2+} than by MTSET. Importantly, T16C was not accessible when the channels were closed. Thus, either the gate is located towards the inside, with respect to T16, or these residues rearrange considerably during gating, being thus themselves part of the gate. Considering the available evidence, we prefer the second option. In the closed channel state, the E19 residue is more accessible to tetracaine applied from the inner surface than it is in the open state (Fodor et al., 1997). Furthermore, the I17C residue is partially accessible to MTSET applied from the inside in the closed state (Becchetti and Gamel, 1999). Thus the access from the cytoplasmic face of the channel to the residues near to the selectivity filter does not seem to be occluded in the closed state. Our data support the idea that the residues adjacent to E19 towards the inner side rearrange considerably during gating. These residues may be part of the channel gate.

4.2 Structure-function relationship in the brCNGCα pore in desensitizing E19A mutants

4.2.1 The accessibility of the P-loop residues in E19A background

The pattern of residue accessibility within the P-loop presented here is similar to the one previously obtained in w.t. background, using the same probes (tab. 4). Our results suggest that, after E19 neutralization, T16 and I17 remain the only residues accessible from the inside, while the external accessibility of P22C suggests that the residues immediately following E19 remain accessible from the external side. The results we have obtained with MTSET and Cd^{2+} overlap, and thus support each other.
Our interpretation is that the alterations in the pore structure are not massive, in E19A channels, suggesting that desensitization arises mostly through modification of the local interactions between the P-loop residues, especially around E19. The structural rearrangement occurring during channel desensitization appears to be sensitive to the chemical environment surrounding the selectivity filter, since only cysteine mutations between the position 15 and the position 20 had major effects on the time course of channel desensitization.
Thus, we suggest that the E19A channel desensitization is mostly determined by local pore remodeling in the area comprising the residues T15-T20.

4.2.2 The accessibility of I17C

The accessibility of I17C from the cytoplasmic side, in E19A background, was more clear-cut than the I17C accessibility in w.t. background, because in the latter the progressive channel rundown overlaps with the inhibition exerted by the thiol-sensitive reagents (Becchetti et al., 1999; see also section 3.1.3). In I17C-E19A channels, the effect produced by Cd^{2+} (but not MTSET) in the presence of cGMP was somewhat increased after the ligand was washed out and then re-applied. We attribute the supplementary channel block after cGMP removal to the fact that the Cd^{2+} ions which had reacted with the substituted cysteines in the open state remained bound after channel closing. This may either facilitate a chelation of the unbound cysteines still present within the P-loop, thus producing a further block revealed on cGMP reapplication, or somehow impede the subsequent opening. The chelating effect cannot be exerted by MTSET, which covalently binds one cysteine

only. Finally, since in the double mutant the current rundown was much weaker than it is in w.t. background, we suggest that, after E19 neutralization, the I17 residues become either more distant from (or less exposed to) the pore axis, or they are more constrained in their thermal motion. This would partially prevent contact between residues on different subunits, thereby decreasing the progressive formation of disulphide bridges between nearby cysteines.

4.2.3 Analogies between C-type inactivation in K^+ channels and CNG channel desensitization

The E19A channel desensitization presents some analogies with C-type inactivation observed in voltage-dependent K^+ channels (Hoshi et al., 1991). We mostly limit our discussion to the C-type inactivation described in Shaker-type channels, whose sequence homology with CNG channels is highest and whose P-loop conformational changes are best known (for a review, see Yellen, 1998). Both processes are relatively slow events and are weakly voltage-dependent, suggesting that they do not require extensive charge movements across the membrane electric field (Hoshi et al., 1991; Bucossi et al., 1996). The time required to recover from inactivation or desensitization, at negative membrane potentials, is also comparable (15-30 s; Bucossi et al., 1996; Liu et al., 1996). Interestingly, C-type inactivation in Shaker involves local residue remodeling in the outer side of the P-loop (Liu et al., 1996). Substituted cysteines in positions 448, 449 and 450, homologous to T20, P21 and P23 in CNG channels, show some alteration in the inactivation kinetics and become more accessible to the MTS probes after inactivation, but can still bind agitoxin with the same affinity, suggesting that the conformational changes involved are small. The comparison between Shaker and CNG channels can only be qualitative, at the present stage. This is due to the lack of specific toxins for CNG channels and to the difficulty of measuring the time-course of the effects of thiol-specific probes, because of the impossibility of applying the probe directly on the external side of the plasma membrane (a point discussed in section 3.2.6). However, from a structural point of view, the results obtained in voltage-dependent K^+ channels have some resemblance to ours. In fact, we show that no extensive P-loop rearrangement occurred during desensitization, but local effects appeared to be produced by mutations around E19, reflected by the alterations observed in the desensitization kinetics after cysteine substitution of the residues around E19.

The most striking difference between the C-type inactivation and the CNG channel desensitization concerns the alterations of channel selectivity. In CNG channels, the effect of substituting E19 with different amino acid residues has been extensively studied (Root and MacKinnon, 1993; Eismann et al., 1994; Bucossi et al., 1996; Bucossi et al., 1997; Sesti et al., 1996; Fodor et al., 1997). A number of substitutions on this position make the channel more permeable to the larger alkali cations (K^+, Rb^+ and Cs^+). This effect, however, is modest. The E19A channels remain poorly selective to monovalent alkali cations, with $P_K/P_{Na} \cong 1.3\text{-}1.4$ (Sesti et al., 1996), suggesting that the interaction between the permeant ions and the residues lining the pore is not disrupted, although the substitution of glutamate 19 makes the channel a single-ion pore (Sesti et al., 1995), the pore lumen diameter appears to be slightly increased (Sesti et al., 1996), and the channel conductance is lower (Bucossi et al., 1996). The apparent affinity of mutant channels for cGMP is also scarcely affected (Bucossi et al., 1996; Fodor et al., 1997). Moreover, single channel experiments show that the desensitization process is due to a progressive decrease in the single-channel open probability and not to a time-dependent modification of the conductive properties (Bucossi et al., 1996). On the other hand, in voltage-gated K^+ channels, a change in monovalent cation selectivity accompanies the slow inactivation, and the inactivated state appears to be a non-conducting state (Starkus et al., 1997; Kiss et al., 1999), although no single-channel data are available to date. A further comparison of the structural changes occurring during C-type inactivation and CNG channel desensitization may point to general properties of the ion channel structural rearrangements producing inactivation/desensitization.

4.3 Structure-function relationship in the SpHCN channel pore

4.3.1 Using sulfhydryl-specific reagents to study the role of cysteine 428

The results presented in fig. 22 indicate that Cd^{2+} and MTSET block the SpHCN current differently, and that their blocking effect depends on whether the channel is unliganded, liganded and closed, or liganded and open. Both Cd^{2+} and MTSET block the SpHCN channel in the absence of cAMP, i.e. in the unliganded state. MTSET does not block appreciably the liganded SpHCN channel neither in the open nor in the closed state. On the contrary, Cd^{2+} blocks rather powerfully the liganded SpHCN channel in the open state, but much less in the closed state. These results suggest the

presence of two distinct sites responsible for the effects of intracellular Cd^{2+} and MTSET: the first located in the cyclic nucleotide-binding domain (CNBD) of the channel, presumably corresponding to the cisteine residues in position 613, 626 and 630, and the second in the pore region. When cAMP is bound to the CNBD, neither Cd^{2+} nor MTSET can bind to the first site, and Cd^{2+} does not block the liganded and closed channel. The second site, presumably in the pore region, is accessible to intracellular Cd^{2+} only in the open state. On the contrary, intracellularly applied MTSET does not reach the second binding site neither in the closed nor in the open channel. The most likely candidate for the blocking site for intracellular Cd^{2+} is cysteine 428 (see fig. 7). In the liganded and open state, the drastic current inhibition observed when Cd^{2+} is applied, as opposed to the non-significant effect in the case of MTSET, indicates a different accessibility of the site to the two reagents which can be explained with their different sterical hindrance. In fact, cadmium ionic diameter is about 0.1 nm (Dart et al., 1998), smaller than the 0.6 nm length of the shorter side of the asymmetrical MTS compounds (Karlin and Akabas, 1998).
Fig. 23 illustrates how the substitution of cysteine 428 with a serine eliminates the blocking effect of Cd^{2+} on the intracellular side of membrane patches. Also, if Cd^{2+} is applied on the extracellular face of membrane patches in the w.t. SpHCN channel, the I_h current is not significantly modified, with the exception of a very slight shift in its activation curve. Together, the results shown in figs. 22 and 23 show that the cysteine in position 428 of the SpHCN channel is accessible only to intracellular Cd^{2+} in the open state, similarly to the threonine in position 360 in the α-subunit of bovine rod CNG channel (see section 3.1.2). Thus, cysteine 428 faces the intracellular mouth of the channel pore and is accessible to intracellular Cd^{2+} only when the channel opens.

4.3.2 Role of cysteine 428 and lysine 433 in the SpHCN channel pore

Substitution of the basic lysine in position 433 with a neuter glutamine introduces two features that are not characteristic of the w.t. channel. As shown in fig. 24B, the I_h current activated in mutant K433Q by hyperpolarizing steps and addition of cAMP exhibits an initial activation, reaching a peak in about 50 ms, and then inactivates. Analysis of the conductances for the w.t. channel and for mutant K433Q (fig. 24C) reveals that, while for the former the conductance is half-activated at about –50 mV (in agreement with data obtained for the same channel expressed in a different system; Gauss et al., 1998), neutralization of lysine 433 shifts the

half-activation point by approximately 50 mV, to about –105 mV. The kinetic of the conductance for mutant K433Q suggests that full activation might be reached at more hyperpolarized potentials, but the difficulty of obtaining good measurements on membrane patches at voltages more negative than –140 mV prevented us from further testing. The mutation of lysine 433 in glutamine relieves the negative electrostatic interactions between positive charges in the presumably tetrameric channel, while introducing neutral residues that can interact non-covalently, by the formation of polar bonds. In the mutant channel, it is possible that, following the initial activation of the I_h current and the opening of the channel pore, a rearrangement occurs in the position of glutamines 433 that brings these residues closer and enhances the formation of positive electrostatic interactions which trigger a modification in the pore structure, leading to inactivation of the current.

A second feature introduced in the I_h current by the mutation K433Q is current rundown (fig. 25A). In inside-out membrane patches, when the current is activated by continuous repetition of hyperpolarizing steps in the presence of cAMP, the amplitude of the current declines with time, and is reduced to about half its initial value within 1 minute after patch excision. An analogous, more pronounced current rundown is observed in the α-subunit of the bovine rod CNG channel when isoleucine in position 17 in the channel pore is mutated into cysteine, and has been shown to be due to the formation of disulfide bonds between the introduces cysteines (Becchetti and Gamel, 1999; Becchetti et al., 1999). We suggest that in mutant K433Q of the SpHCN channel the structural rearrangement of the pore due to the presence of neutral glutamines (see above) brings the cysteines natively present in position 428 in the channel pore closer to each other, and triggers the formation of disulfide bonds among them, which provokes current rundown. To test this hypothesis, we repeated the experiment after substituting cysteine residues in position 428 with serine. The double mutant C428S+K433Q current, activated with the same protocol, does not exhibit a significant decrease in its amplitude (fig. 25B). Also, the double mutant current does not inactivate. This could be explained with the non-formation of polar interactions among glutamines in position 433, due to the channel structure rearrangement introduced by substituting cysteine residues in position 428 with serine, which relieves from the possible formation of disulfide bonds and subsequent narrowing of the channel pore.

The observation that basic (or neutral) residues are present in the pore of HCN channels at a position where acidic residues are mostly found in the closely related voltage-gated K^+ channels suggests that these amino acids

might play a role in the different ionic selectivity observed in these channels, with a selectivity towards potassium that in HCN channels is half-way between that of CNG and voltage-gated K^+ channels. The analysis of ion selectivity in mutant K433Q of the SpHCN channel (fig. 26) indicates that this is not very different from the one observed in w.t. channels. Thus, lysine residues in position 433 are likely not to be the only candidates for the altered ion selectivity typical of HCN channels.

Ion permeation in HCN channel is under the control of various factors, one of which is the presence of extracellular chloride. In native mammalian I_h channels, substitution of external chloride with larger anions such as isethionate, glutamate, acetate or aspartate reduced the amplitude of the current without changing the reversal potential, whereas small anions such as iodide or nitrate supported an intact current (Frace et al., 1992). We tested whether replacement of external chloride had the same effect on the current of the SpHCN channel, and whether lysine 433 has any role in the control by external anions by being accessible to them. Our results indicate that in the SpHCN channel the current is indeed under the control of external anions (fig. 27B). Extracellular solutions containing acetate, aspartate, glutamate or sulphate in place of chloride reversibly blocked the I_h current. If chloride is substituted in the intracellular side of the membrane (fig. 27A), the amplitude of the current is not drastically altered, suggesting that the positive charges present in the w.t. channel pore, namely the lysines in position 421 and 433, are not accessible from the intracellular side of the pore. When extracellular chloride replacement was tested in the mutant K433Q (fig. 27C), a current inhibition was observed that was comparable to the one in the w.t. channel. Thus, lysine in position 433 is likely not to be the main candidate for interaction with extracellular anions. We propose that this tesidue is positioned within the SpHCN channel pore as the homologous aspartate in position 80 in the KcsA potassium channel (Doyle et al., 1998): on the extracellular side of the pore, but with its side chain pointing towards the lipid phase. This would imply that the three-dimensional structure of the pore of this HCN channel is homologous to that of K^+ channels (Doyle et al., 1998).

5) CONCLUSIONS AND PERSPECTIVES

In this thesis, the structural features of the pores of ion channels and their implication in the functional properties of these proteins have been analyzed, by performing electrophysiology experiments aimed at characterizing cyclic nucleotide-gated (CNG) channels and hyperpolarization-activated, cyclic nucleotide-gated (HCN) channels. In particular, this work focuses on the α-subunit of the CNG channel from bovine retinal rods, that has an important role in the mechanism of phototransduction, and on the HCN channel called SpHCN cloned from sea urchin sperm, which is likely to be involved in the control of flagellar beating and thus in the process of fertilization. This study took advantage of molecular biology techniques (site-directed mutagenesis) and of electrophysiological tools (patch-clamp current measurements); the ion channels were heterologously expressed in *Xenopus laevis* oocytes. The conclusions drawn from performed experiments, and the perspectives offered by the present study, are summarized below.

1) In my study of the pore region topology of the α-subunit of the CNG channel from bovine retinal rods, I have extended and completed a previous investigation (Becchetti et al., 1999) by testing the accessibility to Cd^{2+} of serially substituted cysteine residues. The results obtained provided a clearer understanding of the position of important residues close to the selectivity filter possibly involved in gating, and whose localization within the pore loop was not precisely defined yet, and allowed to sketch a three-dimensional model of the pore region of this channel which is different from a previously proposed one (Sun et al., 1996).
2) I have investigated eventual major rearrangements in the pore region topology of the α-subunit of the CNG channel from bovine retinal rods when glutamate residue in position 363 is substituted with a neuter alanine. This mutation is known to induce desensitization of the channel in presence of a steady ligand concentration (Bucossi et al., 1996). In view of understanding whether channel gating in ligand-gated channels occurs through both local interactions between amino acid residues and global channel rearrangement, this artificial CNG channel desensitization offers useful general clues to study the energetic interactions occurring between residues involved in channel gating. Experiments performed by means of the substituted cysteine accessibility method (SCAM) indicated that the pore region topology

was not disrupted by the mutation, and that the nature of the residues immediately close to position 363 influences the structural rearrangements leading to desensitization.

3) In investigating the pore channel topology of the SpHCN channel, I have focused on some residues in key positions that are different from the homologous ones in most of the closely related K^+ and CNG channels, namely cysteine in position 428 and lysine in position 433. My results indicate that cysteine 428 faces the intracellular side of the membrane and is responsible for the I_h current block induced by intracellular Cd^{2+}, and that residue K433 is located extracellularly, but with its side chain pointing towards the lipid phase, and is alone not responsible for the altered ion selectivity observed in HCN channels when compared to voltage-gated K^+-selective channels, and for the regulation of I_h current by external chloride which is a typical feature of HCN channels. Taken together, these findings indicate that the three-dimensional structure of the pore of HCN channels is homologous to that of K^+ channels (Doyle et al., 1998), and suggest that it would be justified to build a molecular model of the SpHCN channel pore by means of homology modeling based on the structural data obtained for crystals of the KcsA K^+ channel (Doyle et al., 1998).

6) REFERENCES

Ache BW, Zhainazarov A (1995) Dual second-messenger pathways in olfactory transduction. Curr Opin Neurobiol 5:461-466

Aggarwal SK, MacKinnon R (1996) Contribution of the S4 segment to the gating charge in the Shaker K^+ channel. Neuron 16:1169-1177

Almers W, McCleskey EW (1984) Nonselective conductance in calcium channels of frog muscle: calcium selectivity in a single-file pore. J Physiol 353:585-608

Altenhofen W, Ludwig J, Eismann E, Kraus W, Bönigk W, Kaupp UB (1991) Control of ligand specificity in cyclic nucleotide-gated channels from rod photoreceptors and olfactory epithelium. Proc Natl Acad Sci USA 88:9868-9872

Anderson JA, Huprikar SS, Kochian LV, Lucas WJ, Gaber RF (1992) Functional expression of a probable *Arabidopsis thaliana* potassium channel in *Saccharomyces cerevisiae*. Proc Natl Acad Sci USA 89:3736-3740

Armstrong CM, Neyton J (1992) Ion permeation through calcium channels. Ann NY Acad Sci 635:18-25

Arnoult C, Zeng Y, Florman HM (1996) ZP3-dependent activation of sperm cation channels regulates acrosomal secretion during mammalian fertilization. J Cell Biol 134:637-645

Attwell D, Wilson M (1980) Behavior of the rod network in the tiger salamander retina mediated by membrane properties of individual rods. J Physiol 309:287-315

Babcock DF, Bosma MM, Battaglia DE, Darszon A (1992) Early persistent activation of sperm K^+ channels by the egg peptide speract. Proc Natl Acad Sci USA 86:6001-6005

Bader CR, Bertrand D, Schwartz EA (1982) Voltage-activated and calcium-activated currents studied in solitary rod inner segments from the salamander retina. J Physiol 331:253-284

Bader CR, MacLeish PR, Schwartz EA (1979) A voltage-clamp study of the light response in solitary rods of the tiger salamander. J Physiol 296:1-26

Baker K, Warren KS, Yellen G, Fishman MC (1997) Defective "pacemaker" current (I_h) in a zebrafish mutant with a slow heart rate. Proc Natl Acad Sci USA 94:4554-4559

Bal T, McCormick DA (1996) What stops synchronized thalamocortical oscillations? Neuron 17:297-308

Bal T, von Krosigk M, McCormick DA (1995a) Synaptic and membrane mechanisms underlying synchronized oscillations in the ferret lateral geniculate nucleus in vitro. J Physiol 483:641-663

Bal T, von Krosigk M, McCormick DA (1995b) Role of the ferret perigeniculate nucleus in the generation of synchronized oscillations in vitro. J Physiol 483:665-685

Balasubramanian S, Lynch JW, Barry PH (1996) Calcium-dependent modulation of the agonist affinity of the mammalian olfactory cyclic nucleotide-gated channel by calmodulin and a novel endogenous factor. J Membr Biol 152:13-23

Banks MI, Pearce RA, Smith PH (1993) Hyperpolarization-activated cation current (I_h) in neurons of the medial nucleus of the trapezoid body: voltage-clamp analysis and enhancement by norepinephrine and cAMP suggest a modulatory mechanisms in the auditory brain stem. J Neurophysiol 70:1420-1432

Barnard EA (1992) Subunits of $GABA_A$, glycine and glutamate receptors. In "Receptor subunits and complexes" (Burgen ASV, Barnard EA), Cambridge University Press, 163-187

Barnstable CJ, Wei J-Y (1995) Isolation and characterization of the alpha-subunit of rod photoreceptor cGMP gated cation channel. J Molec Neurosci 6:289-302

Bauer PJ (1996) Cyclic GMP-gated channels of bovine rod photoreceptors: affinity, density and stoichiometry of Ca^{2+}-calmodulin binding sites. J Physiol 494:674-685

Baumann A, Frings S, Godde M, Seifert R, Kaupp UB (1994) Primary structure and functional expression of a *Drosophila* cyclic nucleotide-gated channel present in eyes and antennae. EMBO J 13:5040-5050

Baylor (1996) How photons start vision. Proc Natl Acad Sci USA 93:560-565

Baylor D, Lamb TD, Yau K-W (1979) The membrane current of single rod outer segments. J Physiol (Lond) 288:589-611

Becchetti A, Gamel K (1999) The properties of cysteine mutants in the pore region of cyclic nucleotide-gated channels. Pflügers Arch 438:587-596

Becchetti A, Gamel K, Torre V (1999) Cyclic nucleotide-gated channels: pore topology studied through the accessibility of reporter cysteines. J Gen Physiol 114:377-392

Belluscio L, Gold GH, Nemes A, Axel R (1998) Mice deficient in G_{olf} are anosmic. Neuron 20:69-81

Biel M, Altenhofen W, Hullin R, Ludwig J, Freichel M, Flockerzi V, Dascal N, Kaupp UB, Hofmann F (1993) Primary structure and functional expression of a cyclic nucleotide-gated channel from rabbit aorta. FEBS Lett 329:134-138

Biel M, Ludwig A, Zong H, Hofmann F (1999b) Hyperpolarization-activated cation channels: a multi-gene family. Rev Physiol Biochem Pharmacol 136:165-182

Biel M, Zong X, Distler M, Bosse E, Klugbauer N, Murakami M, Flockerzi V, Hofmann F (1994) Another member of the cyclic nucleotide-gated channels family expressed in testis, kidney and heart. Proc Natl Acad Sci USA 91:3505-3509

Biel M, Zong X, Ludwig A, Sautter A, Hofmann F (1999a) Structure and function of cyclic nucleotide-gated channels. Rev Physiol Biochem Pharmacol 135:151-171

Boekhoff I, Breer H (1992) Termination of second messenger signaling in olfaction. Proc Natl Acad Sci USA 89:471-474

Boekhoff I, Schleicher S, Strotmann J, Breer H (1992) Odor-induced phosphorylation of olfactory cilia proteins. Proc Natl Acad Sci USA 89:11983-11987

Boekhoff I, Tareilus E, Strotmann J, Breer H (1990) Rapid activation of alternative second messenger pathways in olfactory cilia by different odorants. EMBO J 9:2453-2458

Bönigk W, Altenhofen W, Müller F, Dose A, Illing M, Molday RS, Kaupp UB (1993) Rod and cone photoreceptor cells express distinct genes for cGMP-gated channels. Neuron 10:865-877

Bönigk W, Bradley J, Müller F, Sesti F, Boekhoff I, Ronnett GV, Kaupp UB, Frings S (1999) The native rat olfactory cyclic nucleotide-gated channel is composed of three distinct subunits. J Neurosci 19:5332-5347

Borisy FF, Ronnett GV, Cunningham AM, Juifs D, Beavo J, Snyder SH (1992) Calcium/calmodulin-activated phosphodiesterase expressed in olfactory receptor neurons. J Neurosci 12:915-923

Bradley J, Li J, Davidson N, Lester HA, Zinn K (1994) Heteromeric olfactory cyclic nucleotide-gated channels: a subunit that confers increased sensitivity to cAMP. Proc Natl Acad Sci USA 91:8890-8894

Breer H, Boekhoff I (1991) Odorants of the same class activate different second messenger pathways. Chem Senses 16:19-29

Broillet M-C, Firestein S (1996) Direct activation of the olfactory cyclic nucleotide-gated channel through modification of sulfhydryl groups by NO compounds. Neuron 16:377-385

Broillet M-C, Firestein S (1997) β-subunits of the olfactory cyclic nucleotide-gated channel form a nitric oxide activated Ca^{2+} channel. Neuron 18:951-958

Brown HF, DiFrancesco D (1980) Voltage clamp investigations of currents underlying pacemaker activity in rabbit sino-atrial node. J Physiol 308:331-351

Brown HF, DiFrancesco D, Noble SJ (1979a) Adrenaline action on rabbit sino-atrial node. J Physiol 290:31P-32P

Brown HF, DiFrancesco D, Noble SJ (1979b) How does adrenaline accelerate the heart? Nature 280:235-236

Brown HF, Giles W, Noble SJ (1977) Membrane currents underlying activity in frog sinus venosus. J Physiol 271:783-816

Brown LR, Gramling R, Bert RJ, Karpen JW (1995) Cyclic GMP contact points within the 63 kDa subunit and the 240 kDa associated protein of retinal rod cGMP-activated channels. Biochemistry 34:8365-8370

Brown HF, Ho WK (1996) The hyperpolarization-activated inward channel and cardiac pacemaker activity; in Morad M, Ebashi S, Trautwein W, Kurachi Y (eds): Molecular physiology and pharmacology of cardiac ion channels and transporters. Dordrecht, Kluwer Academic Publishers, pp 17-30

Brown RL, Snow SD, Haley TL (1998) Movement of gating machinery during the activation of rod cyclic nucleotide-gated channels. Biophys J 75:825-833

Brunet LJ, Gold GH, Ngai J (1996) General anosmia caused by a targeted disruption of the mouse olfactory cyclic nucleotide-gated cation channel. Neuron 17:681-693

Buck L, Axel R (1991) A novel multigene family may encode odorant receptors: a molecular basis for odor recognition. Cell 65:175-187

Bucossi G, Eismann E, Sesti F, Nizzari M, Seri M, Kaupp UB, Torre V (1996) Time-dependent current decline in cyclic GMP-gated bovine channels caused by point mutations in the pore region expressed in *Xenopus* oocytes. J Physiol (Lond) 493:409-418

Bucossi G, Nizzari M, Torre V (1997) Single-channel properties of ionic channels gated by cyclic nucleotides. Biophys J 72:1165-1181

Capovilla M, Caretta A, Cervetto L, Torre V (1983) Ionic movements through light-sensitive channels of toad rods. J Physiol 343:295-310

Catterall WA (1986) Voltage-dependent gating of sodium channels: correlating structure and function. Trends Neurosci 9:7-10

Chen TY, Illing M, Molday LL, Hsu YT, Yau K-W, Molday RS (1994) Subunit 2 (or β) of retinal rod cGMP-gated cation channel is a component of the 240-kDa channel-associated protein and mediates Ca^{++}-calmodulin modulation. Proc Natl Acad Sci USA 91:11757-11761

Chen TY, Peng YW, Dhallan RS, Ahamed B, Reed RR, Yau K-W (1993) A new subunit of the cyclic nucleotide-gated cation channel in retinal rods. Nature 362:764-767

Chen TY, Ukhanova M, Thomas D, Afshar G, Tanda S, Battelle BA, Payne R (1999) Molecular cloning of a putative cyclic nucleotide-gated ion channel cDNA from *Limulus poliphemus*. J Neurochem 72:461-471

Chen TY, Yau K-W (1994) Direct modulation by Ca^{++}-calmodulin of cyclic nucleotide-activated channel of rat olfactory receptor neurons. Nature 368:545-548

Choe S, Robinson R (1998) An ingenious filter: the structural basis for ion channel selectivity. Neuron 20:821-823

Clapham DE (1998) Not so funny anymore: pacing channels are cloned. Neuron 21:5-7

Cobbs WH, Barkdoll AE III, Pugh EN Jr (1985) Cyclic GMP increases photocurrent and light sensitivity of retinal cones. Nature 317:64-66

Coburn CM, Bargmann CI (1996) A putative cyclic nucleotide-gated channel is required for sensory development and function in *C. elegans*. Neuron 17:695-706

Colamartino G, Menini A, Torre V (1991) Blockage and permeation of divalent cations through the cyclic GMP-activated channel from tiger salamander retinal rods. J Physiol (Lond) 440:189-206

Conley EC (1996) The ion channel factsbook, vol.II ("Intracellular ligand-gated channels"), Academic Press , p. 382

Cook NJ, Hanke W, Kaupp UB (1987) Identification, purification, and functional reconstitution of the cyclic GMP-dependent channel from rod photoreceptors. Proc Natl Acad Sci USA 84:585-589

Cook NJ, Zeilinger C, Koch K-W, Kaupp UB (1986) Solubilization and functional reconstitution of the cGMP-dependent cation channel from bovine rod outer segments. J Biol Chem 261:17033-17039

Cotton FA, Wilkinson G (1980) Advanced Inorganic Chemistry. John Wiley and Sons, New York

Crunelli V, Kelly JS, Leresche N, Pirchio M (1987) The ventral and dorsal lateral geniculate nucleus of the rat: intracellular recordings in vitro. J Physiol 384:587-601

Dart C, Leyland ML, Spencer PJ, Stanfield PR, Sutcliffe MJ (1998) The selectivity filter of a potassium channel, murine Kir2.1, investigated using scanning cysteine mutagenesis. J Physiol (Lond) 511:25-32

del Castillo J, Katz B (1955) Production of membrane potential changes in the frog's heart by inhibitory nerve impulses. Nature 175:1035

Denyer JC, Brown HF (1990) Rabbit sino-atrial node cells: isolation and electro-physiological properties. J Physiol 428:405-424

de Rooij J, Zwartkruis FJ, Verheijen MH, Cool RH, Nijman SM, Wittinghofer A, Bos JL (1998) Epac is a Rap1 guanine-nucleotide-exchange factor directly activated by cAMP. Nature 396: 474-477

Dhallan RS, Macke JP, Eddy RL, Shows TB, Reed RR (1992) Human rod photoreceptor cGMP-gated channel: amino acid sequence, gene structure, and functional expression. J Neurosci 12:3248-3256

Dhallan RS, Yau K-W, Schrader KA, Reed RR (1990) Primary structure and functional expression of a cyclic nucleotide-activated channel from olfactory neurons. Nature 347:184-187

DiFrancesco D (1981a) A new interpretation of the pace-maker current in calf Purkinje fibers. J Physiol 314:359-376

DiFrancesco D (1981b) A study of the ionic nature of the pace-maker current in calf Purkinje fibers. J Physiol 314:377-393

DiFrancesco D (1993) Pacemaker mechanisms in cardiac tissues. Annu Rev Physiol 55:455-472

DiFrancesco D, Ducouret P, Robinson RB (1998) Muscarinic modulation of cardiac rate at low acetylcholine concentrations. Science 243:669-671

DiFrancesco D, Mangoni M (1994) Modulation of single hyperpolarization-activated channels (i_f) by cAMP in the rabbit sino-atrial node. J Physiol 474:473-482

DiFrancesco D, Noble D (1979) The influence of voltage non-uniformity on the determination of Erev for iK2. J Physiol 297:158-162

DiFrancesco D, Tortora P (1991) Direct activation of cardiac pacemaker channels by intracellular cyclic AMP. Nature 351:145-147

Dossi RC, Nunez A, Steriade M (1992) Electrophysiology of a slow (0.5-4 Hz) intrinsic oscillation of cat thalamocortical neurones in vivo. J Physiol 447:215-234

Doyle DA, Morais Cabral J, Pfuetzner RA, Kuo A, Gulbis JM, Cohen SL, Chait BT, MacKinnon R (1998) The structure of the potassium channel: molecular basis of K^+ conduction and selectivity. Science 280:69-77

Durell SR, Guy HR (1992) Atomic scale structure and functional models of voltage-gated potassium channels. Biophys J 62:238-250

Durell SR, Hao Y, Guy HR (1998) Structural models of the transmembrane region of voltage-gated and other K^+ channels in open, closed and inactivated conformations. J Struct Biol 121:263-284

Eismann E, Bönigk W, Kaupp UB (1993) Structural features of cyclic nucleotide-gated channels. Cell Physiol Biochem 3:332-351

Eismann E, Müller F, Heinemann S, Kaupp UB (1994) A single negative charge within the pore region of a cGMP-gated channel controls rectification, Ca^{2+} blockage, and ionic selectivity. Proc Natl Acad Sci USA 91:1109-1113

Emeis D, Kuhn H, Reichert J, Hofmann KP (1982) Complex formation between metarhodopsin II and GTP-binding protein in bovine photoreceptor membranes leads to a shift of the photoproduct equilibrium. FEBS Lett 143:29-34

Fain GL, Matthews HR, Cornwall WC (1996) Dark adaptation in vertebrate photoreceptors. Trends Neurosci 19:502-507

Fain GL, Quandt FN, Bastian BL, Gerschenfeld HM (1978) Contribution of a cesium-sensitive conductance increase to the rod photoresponse. Nature 272:466-469

Fesenko EE, Kolesnikov SS, Lyubarsky AL (1985) Induction by cyclic GMP of cationic conductance in plasma membrane of retinal rod outer segment. Nature 313:310-313

Filatov GN, Jainazarov AB, Kolesnikov SS, Lyubarsky AL, Fesenko EE (1989) The effect of ATP, GTP and cAMP on the cGMP-dependent conductance of the fragments from frog rod plasma membrane. FEBS Lett 245:185-188

Finn JT, Grunwald ME, Yau KW (1996) Cyclic nucleotide-gated ion channels: an extended family with diverse functions. Annu Rev Physiol 58:395-426

Finn JT, Solessio EC, Yau KW (1997) A cGMP-gated cation channel in depolarizing photoreceptors of the lizard parietal eye. Nature 385:815-819

Fodor AA, Black KD, Zagotta WA (1997) Tetracaine reports a conformational change in the pore of cyclic nucleotide-gated channels. J Gen Physiol 110:591-600

Frace AM, Maruoka F, Noma A (1992a) Control of the hyperpolarization-activated cation current by external anions in rabbit sino-atrial node cells. J Physiol 453:307-318

Frace AM, Maruoka F, Noma A (1992b) External K^+ increases Na^+ conductances of the hyperpolarization-activated current in rabbit cardiac pacemaker cells. Pflügers Arch 421:94-96

Frech GC, VanDongen AMJ, Schuster G, Brown AM, Joho RH (1989) A novel potassium channel with delayed rectifier properties isolated from rat brain by expression cloning. Nature 340:642-645

Frings S, Seifert R, Godde M, Kaupp UB (1995) Profoundly different calcium permeation and blockage determine the specific function of distinct cyclic nucleotide-gated channels. Neuron 15:169-179

Furman RE, Tanaka JC (1990) Monovalent selectivity of the cyclic guanosine monophosphatactivated ion channel. J Gen Physiol 96:57-82

Gargini C, Demontis GC, Bisti S, Cervetto L (1999) Effects of blocking the hyperpolarization-activated current (I_h) on the cat electroretinogram. Vision Res 39:1767-1774

Gauss R, Seifert R (2000) Pacemaker oscillations in heart and brain: a key role for hyperpolarization-activated cation channels. Chronobiol Int 17:453-469

Gauss R, Seifert R, Kaupp UB (1998) Molecular identification of a hyperpolarization-activated channel in sea urchin sperm. Nature 393:583-587

Glusker JP (1991) Structural aspects of metal liganding to functional groups in proteins. Adv Prot Chem 42:1-76

Gold GH (1999) Controversial issues in vertebrate olfactory transduction. Annu Rev Physiol 61:857-871

Gong L, Kraus N (1998) Molecular cloning of cDNA encoding the alpha subunit of CNGC gene from human fetal heart. Life Sci 63:1555-1562

Gorczyca WA, Gray-Keller MP, Detwiler PB, Palczewski K (1994) Purification and physiological identification of a guanylate cyclase activating protein from retinal rods. Proc Natl Acad Sci USA 91:4014-4018

Gordon SE, Oakley JC, Varnum MD, Zagotta WN (1996) Altered ligand specificity by protonation in the ligand binding domain of cyclic nucleotide-gated channels. Biochemistry 35:3994-4001

Gordon SE, Varnum MD, Zagotta WN (1997) Direct interaction between amino- and carboxyl-terminal domains of cyclic nucleotide-gated channels. Neuron 19:431-441

Gordon SE, Zagotta WN (1995a) A histidine residue associated with the gate of the cyclic nucleotide-activated channels in rod photoreceptors. Neuron 14:177-183

Gordon SE, Zagotta WN (1995b) Localization of regions affecting an allosteric transition in cyclic nucleotide-activated channels. Neuron 14:857-864

Gordon SE, Zagotta WN (1995c) Subunit interactions in coordination of Ni^{++} in cyclic nucleotide-gated channels. Proc Natl Acad Sci USA 92:10222-10226

Goulding EH, Ngai J, Kramer RH, Colicos S, Axel R, Siegelbaum SA, Chess A (1992) Molecular cloning and single-channel properties of the cyclic nucleotide-gated channel from catfish olfactory neurons. Neuron 8:45-58

Goulding EH, Tibbs GR, Liu D, Siegelbaum SA (1993) Role of H5 domain in determining pore diameter and ionic permeation through cyclic nucleotide-gated channels. Nature 364:61-64

Goulding EH, Tibbs GR, Siegelbaum SA (1994) Molecular mechanism of cyclic nucleotide-gated channel activation. Nature 372:369-374

Gray-Keller M, Detwiler P (1994) The calcium feedback signal in the phototransduction cascade of vertebrate rods. Neuron 13:849-861

Gray-Keller M, Polans A, Palczewski K, Detwiler P (1993) The effect of recoverin-like calcium-binding proteins on the photoresponse of retinal rods. Neuron 10:523-531

Gross A, MacKinnon R (1996) Agitoxin footprinting the Shaker potassium channel pore. Neuron 16:399-406

Guy HR, Conti F (1990) Pursuing the structure and function of voltage-gated channels. Trends Neurosci 13:201-206

Guy HR, Durell SR (1995) Structural models of Na^+, Ca^{2+}, and K^+ channels. In "Ion channels and genetic diseases", The Rockefeller University Press, 1-16

Guy HR, Seetharamulu P (1986) Molecular model of the action potential sodium channel. Proc Natl Acad Sci USA 83:508-512

Hageman GR, Urthaler F, James TN (1977) Differential sensitivity to neurotransmitters in denervated canine sinus node. Am J Physiol 233:H211-H216

Hagins WA, Penn RD, Yoshikami S (1970) Dark current and photocurrent in retinal rods. Biophys J 10:380-412

Halliwell JV, Adams PR (1982) Voltage-clamp analysis of muscarinic excitation in hippocampal neurons. Brain Res 250:71-92

Hamill OP, Marty A, Neher E, Sakmann B, Sigworth FJ (1981) Improved patch-clamp technique for high resolution current recording from cells and cell-free membrane patches. Pflügers Arch 391:85-100

Hanke W, Cook NJ, Kaupp UB (1988) cGMP-dependent channel protein from photoreceptor membranes: single channel activity of the purified and reconstituted protein. Proc Natl Acad Sci USA 85:94-98

Hansbrough JR, Garbers DL (1981) Speract - purification and characterization of a peptide associated with eggs that activates spermatozoa. J Biol Chem 256:1447-1452

Haynes LW (1992) Block of the cyclic GMP-gated channel of vertebrate rod and cone photoreceptors by *l-cis*-diltiazem. J Gen Physiol 100:783-801

Haynes LW, Kay AR, Yau K-W (1986) Single cyclic GMP-activated channel activity in excised patches of rod outer segment membrane. Nature 321:66-70

Haynes LW, Stotz SC (1997) Modulation of rod, but not cone, cGMP-gated photoreceptor channel by calcium-calmodulin. Vis Neurosci 14:233-239

Haynes LW, Yau K-W (1985) Cyclic GMP-sensitive conductance in outer segment membrane of catfish cones. Nature 317:61-64

Heginbotham L, Abramson T, MacKinnon R (1992) A functional connection between the pores of distantly related ion channels as revealed by mutant K^+ channels. Science 258: 1152-1155

Heginbotham L, Lu Z, Abramson T, MacKinnon R (1994) Mutations in the K^+ channel signature sequence. Biophys J 66:1061-1067

Heinemann SH, Terlau H, Stuhmer W, Imoto K, Numa S (1992) Calcium channel characteristics conferred on the sodium channel by single mutations. Nature 356:441-443

Henn DK, Baumann A, Kaupp UB (1995) Probing the transmembrane topology of cyclic nucleotide-gated ion channels with a gene fusion approach. Proc Natl Acad Sci USA 92:7425-7429

Hess P, Tsien RW (1984) Mechanism of ion permeation through calcium channels. Nature 309:453-456

Hille B (1992) Ionic channels of excitable membranes. Sunderland, MA: Sinauer. 607 pp. 2nd ed.

Ho WK, Brown HF, Noble D (1994) High selectivity of the i_f channels to Na^+ and K^+ in rabbit isolated sinoatrial node cells. Pflügers Arch 426:68-74

Holmgren M, Liu Y, Xu Y, Yellen G (1996) On the use of thiol-modifying agents to determine channel topology. Neuropharmacology 35:797-804

Hoppe UC, Jansen E, Südkamp M, Beuckelmann DJ (1998) Hyperpolarization-activated inward current in ventricular myocites from normal and failing human hearts. Circulation 97:55-65

Hoshi T, Zagotta WN, Aldrich RW (1991) Two types of inactivation in *Shaker* K^+ channels: effects of alterations in the carboxy-terminal region. Neuron 7:547-556

Hsu YT, Molday RS (1993) Modulation of the cGMP-gated channel of rod photoreceptor cells by calmodulin. Nature 361:76-79

Hsu YT, Molday RS (1994) Interaction of calmodulin with the cyclic GMP-gated channel of rod photoreceptors. Modulation of activity, affinity purification, and localization. J Biol Chem 269:29765-29770

Ildefonse M, Bennett N (1991) Single-channel study of the cGMP-dependent conductance of retinal rods from incorporation of native vescicles into planar lipid bilayers. J Membrane Biol 123:133-147

Ildefonse M, Crouzy S, Bennett N (1992) Gating of retinal rod cation channel by different nucleotides: comparative study of unitary currents. J Membrane Biol 130:91-104

Ishii TM, Takano M, Xie L-H, Noma A, Ohmori H (1999) Molecular characterization of the hyperpolarization-activated cation channel in rabbit heart sinoatrial node. J Biol Chem 274:12835-12839

Jan LY, Jan YN (1990) A superfamily of ion channels. Nature 345:672

Jan LY, Jan YN (1992) Tracing the roots of ion channels. Cell 69:715-718

Karlin A, Akabas MH (1998) Substituted-cysteine accessibility method. Methods Enzymol 293:123-145

Karpen JW, Lane Brown L, Stryer L, Baylor DA (1993) Interaction between divalent cations and the gating machinery of cyclic GMP-activated channels in salamander retinal rods. J Gen Physiol 101:1-25

Karpen JW, Loney DA, Baylor DA (1992) Cyclic GMP-activated channels of salamander retinal rods: spatial distribution and variation of responsiveness. J Physiol 448:257-274

Karpen JW, Zimmermann AL, Stryer L, Baylor DA (1988) Gating kinetics of the cyclic GMP-activated channel of retinal rods: flash photolysis and voltage-jump studies. Proc Natl Acad Sci USA85:1287-1291

Kaupp UB (1991) The cyclic nucleotide-gated channels of vertebrate photoreceptors and olfactory epithelium. Trends Neurosci 14:150-157

Kaupp UB (1995) Family of cyclic nucleotide-gated ion channels. Curr Opin Neurobiol 5:434-442

Kaupp UB, Niidome T, Tanabe T, Terada S, Bönigk W, Stuhmer W, Cook NJ, Kangawa K, Matsuo H, Hirose T (1989) Primary structure and functional expression from complementary DNA of the rod photoreceptor cyclic GMP-gated channel. Nature 342:762-766

Kawasaki H, Springett GM, Mochizuki N, Toki S, Nakaya M, Matsuda M, Housman DE, Graybiel AM (1998) A family of cAMP-binding proteins that directly activate Rap1. Science 282:2275-2279

Kiss L, LoTurco J, Korn SJ (1999) Contribution of the selectivity filter to inactivation in potassium channels. Biophys J 76:253-263

Koch W-H, Stryer L (1988) Highly cooperative feedback control of retinal rod guanylate cyclase by calcium ions. Nature 334:64-66

Kolesnikov SS, Zhainazarov AB, Kosolapov AV (1990) Cyclic nucleotide-activated channel in the frog olfactory receptor plasma membrane. FEBS Lett 266:96-98

Komatsu H, Mori I, Rhee J-S, Akaike N, Ohshima Y (1996) Mutations in a cyclic nucleotide-gated channel lead to abnormal thermosensation and chemosensation in *C. elegans*. Neuron 17:707-718

Körschen HG, Beyermann M, Müller F, Heck M, Vantler M, Koch K-W, Kellner R, Wolfrum U, Bode C, Hofmann KP, Kaupp UB (1999) Interactions of glutamic-acid-rich proteins with the cGMP signaling pathway in rod photoreceptors. Nature 400:761-766

Körschen HG, Illing M, Seifert R, Sesti F, Williams A, Gotzes S, Colville C, Müller F, Dosé A, Godde M, Molday L, Kaupp UB, Molday RS (1995) A 240 kDa protein

represents the complete β-subunit of the cyclic nucleotide-gated channel from rod photoreceptors. Neuron 15:627-636

Koutalos Y, Yau K-W (1996) Sensitivity regulation in rod photoreceptors by calcium. Trends Neurosci 19:73-81

Kramer RH, Siegelbaum SA (1992) Intracellular Ca^{2+} regulates the sensitivity of cyclic nucleotide-gated channels in olfactory receptor neurons. Neuron 9:897-906

Krieger J, Strobel J, Vogl A, Hanke W, Breer H (1999) Identification of a cyclic nucleotide- and voltage-activated ion channel from insect antennae. Insect Biochem Mol Biol 29:255-267

Krizek BA, Merkle DL, Berg JM (1993) Ligand variation and metal ion binding specificity in zinc fingers peptides. Inorganic Chemistry 32:937-940

Krovetz HS, VanDongen HMA, VanDongen AMJ (1997) Atomic distance estimates from disulfides and high-affinity metal-binding sites in a K^+ channel pore. Biophys J 72:117-126

Kubo Y, Yoshimichi M, Heinemann SH (1998) Probing pore topology and conformational changes of Kir2.1 potassium channels by cysteine-scanning mutagenesis. FEBS Letts 435:69-73

Kumar VD, Weber IT (1992) Molecular model of the cyclic GMP-binding domain of the cyclic GMP-gated ion channel. Biochemistry 31:4643-4649

Kurahashi T, Menini A (1997) Mechanism of odorant adaptation in the olfactory receptor cell. Nature 385:725-729

Kurz LL, Zuhlke RD, Zhang H-J, Joho RH (1995) Side-chain accessibilities in the pore of a K^+ channel probed by sulfhydryl-specific reagents after cysteine-scanning mutagenesis. Biophys J 68:900-905

Labarca P, Santi C, Zapata O, Morales E, Beltrán C, Liévano A, Darszon A (1996) A cAMP regulated K^+-selective channel from the sea urchin sperm plasma membrane. Dev Biol 174:271-280

Lagnado L, Baylor DA (1994) Calcium controls light-triggered formation of catalitically active rhodopsin. Nature 367:273-277

Laio A, Torre V (1999) Physical origin of selectivity in ionic channels of biological membranes. Biophys J 76:129-148

Li J, Lester HA (1999) Functional roles of aromatic residues in the ligand-binding domain of cyclic nucleotide-gated channels. Mol Pharmacol 55:873-882

Liévano A, Santi CM, Serrano CJ, Treviño CL, Bellvé AR, Hernández-Cruz A, Darszon A (1996) T-type Ca^{2+} channels and alpha1E expression in spermatogenic cells, and their possible relevance to the sperm acrosome reaction. FEBS Lett 388:150-154

Liman ER, Buck LB (1994) A second subunit of the olfactory cyclic nucleotide-gated channel confers high sensitivity to cAMP. Neuron 13:611-621

Liu M, Chen T-Y, Ahamed B, Li J, Yau K-W (1994) Calcium-calmodulin modulation of the olfactory cyclic nucleotide-gated cation channel. Science 266:1348-1354

Liu Y, Holmgren M, Jurman ME, Yellen G (1997) Gated access to the pore of a voltage-dependent K^+ channel. Neuron 19:175-184

Liu Y, Jurman E, Yellen G (1996a) Dynamic rearrangement of the outer mouth of a K^+ channel during gating. Neuron 16:859-867

Liu DT, Tibbs GR, Paoletti P, Siegelbaum SA (1998) Constraining ligand-binding site stoichiometry suggests that a cyclic nucleotide-gated channel is composed of two functional dimers. Neuron 21:235-248

Liu DT, Tibbs GR, Siegelbaum SA (1996b) Subunit stoichiometry of cyclic nucleotide-gated channels and effects of subunit order on channel function. Neuron 16:983-990

Lolley RN, Racz E (1982) Calcium modulation of cyclic GMP synthesis in rat visual cells. Vision Res 22:1481-1486

Lowe G, Nakamura T, Gold GH (1989) Adenylate cyclase mediates olfactory transduction for a wide variety of odorants. Proc Natl Acad Sci USA 86:5641-5645

Lu Q, Miller C (1995) Silver as a probe of pore-forming residues in a potassium channel. Science 268:304-307

Ludwig J, Margalit T, Eismann E, Lancet D, Kaupp UB (1990) Primary structure of cAMP-gated channel from bovine olfactory epithelium. FEBS Lett 270:24-29

Ludwig A, Zong X, Hofmann F, Biel M (1999a) Structure and function of cardiac pacemaker channels. Cell Physiol Biochem 9:179-186

Ludwig A, Zong X, Jeglitsch M, Hofmann F, Biel M (1998) A family of hyperpolarization-activated mammalian cation channels. Nature 393:587-591

Ludwig A, Zong X, Stieber J, Hullin R, Hofmann F, Biel M (1999b) Two pacemaker channels from human heart with profoundly different activation kinetics. EMBO J 18:2323-2329

Luehring H, Hanke W, Simmoteit R, Kaupp UB (1990) Cation selectivity of the cyclic GMP-gated channel of mammalian rod photoreceptors. In "Sensory transduction" (Borsellino L, Cervetto L, Torre V). Plenum Press, NY 169-174

Lüthi A, McCormick DA (1998a) Periodicity of thalamic synchronized oscillations: the role of Ca^{2+}-mediated upregulation of I_h. Neuron 20:553-563

Lüthi A, McCormick DA (1998b) H-current: properties of a neuronal and network pacemaker. Neuron 21:9-12

Lüthi A, McCormick DA (1999) Modulation of a pacemaker current through Ca^{2+}-induced stimulation of cAMP production. Nat Neurosci 2:634-641

Lynch JW, Lindermann B (1994) Cyclic nucleotide-gated channels of rat olfactory receptor cells: divalent cations control the sensitivity to cAMP. J Gen Physiol 103:87-106

Maccaferri G, Mangoni M, Lazzari A, DiFrancesco D (1993) Properties of the hyperpolarization-activated current in rat hippocampal CA1 pyramidal cells. J Neurophysiol 69:2129-2136

Magee JC (1998) Dendritic hyperpolarization-activated currents modify the integrative properties of hippocampal CA1 pyramidal neurons. J Neurosci 18:7613-7624

Martell AE, Smith RM (1974) Critical Stability Constants. Plenum Press, New York

Marten I, Hoshi T (1998) The N-terminus of the K channel KAT1 controls its voltage-dependent gating by altering the membrane electric field. Biophys J 74:2953-2962

Marx T, Gisselmann G, Stoertkuhl KF, et al. (1999) Molecular cloning of a putative voltage- and cyclic nucleotide-gated ion channel present in the antennae and eyes of *Drosophila melanogaster*. Invert Neurosci 4:55-63

Matthews G, Watanabe S-I (1987) Properties of ion channels closed by light and opened by 3', 5'-cyclic monophosphate in toad retinal rods. J Physiol 389:691-715

Matthews G, Watanabe S-I (1988) Activation of single ion channels from toad retinal rod inner segments by cyclic GMP: concentration dependence. J Physiol (Lond) 403:389-405

McCormick DA, Bal T (1997) Sleep and arousal: thalamocortical mechanisms. Annu Rev Neurosci 20:185-215

McCormick DA, Huguenard JR (1992) A model of the electrophysiological properties of thalamocortical relay neurons. J Neurophysiol 68:1384-1400

McCormick DA, Pape H-C (1988) Acetylcholine inhibits identified interneurons in the cat lateral geniculate nucleus. Nature 334:246-248

McCormick DA, Pape H-C (1990) Properties of a hyperpolarization-activated cation current and its role in rhythmic oscillation in thalamic relay neurones. J Physiol 431:291-318

McGeoch JEM, McGeoch MW, Guidotti G (1995) Eye CNG channel is modulated by nicotine. Biochem Biophys Res Commun 214:879-887

McKay DB, Steitz TA (1981) Structure of catabolite gene activator protein at 2.9 Å resolution suggests binding to left-handed B-DNA. Nature 290:744-749

McLatchie LM, Matthews HR (1992) Voltage-dependent block by *l-cis*-diltiazem of the cyclic GMP-activated conductance of salamander rods. Proc R Soc Lond (B) 247:113-119

Menini A (1990) Currents carried by monovalent cations through cyclic GMP-activated channels in excised patches from salamander rods. J Physiol 424:167-185

Menini A, Rispoli G, Torre V (1988) The ion selectivity of the light-sensitive current in isolated rods of the tiger salamander. J Physiol 402:279-300

Miledi R, Parker I (1984) Chloride currents induced by injection of Ca^{2+} into *Xenopus* oocytes. J Physiol (Lond) 357:173-183

Miller AG, Aldrich RW (1996) Conversion of a delayed rectifier K^+ channel to a voltage-gated inward rectifier K^+ channel by three amino acid substitutions. Neuron 16:853-858

Misaka T, Kusakabe Y, Emori Y, Gonoi T, Arai S, Abe K (1997) Taste buds have a cyclic nucleotide-activated channel, CNGgust. J Biol Chem 272:22623-22629

Molday RS (1996) Calmodulin regulation of cyclic nucleotide-gated channels. Curr Opin Neurobiol 6:445-452

Moosmang S, Biel M, Hofmann F, Ludwig A (1999) Differential distribution of four hyperpolarization-activated cation channels in mouse brain. Biol Chem 380:975-980

Moroni A, Barbuti A, Altomare C, Viscomi C, Morgan J, Baruscotti M, DiFrancesco D (2000) Kinetic and ionic properties of the human HCN2 pacemaker channel. Eur J Physiol 439:618-626

Munsch T, Pape H-C (1999) Modulation of the hyperpolarization-activated cation current of rat thalamic relay neurones by intracellular pH. J Physiol 519:493-504

Nakamura T, Gold GH (1987) A cyclic nucleotide-gated conductance in olfactory receptor cilia. Nature 325:442-444

Nakatani K, Koutalos Y, Yau K-W (1995) Ca^{2+} modulation of the cGMP-gated channel of bullfrog retinal rod photoreceptors. J Physiol 484:69-76

Nakatani K, Yau K-W (1988) Calcium and magnesium fluxes across the plasma membrane of the toad rod outer segment. J Physiol 395:695-729

Nizzari M, Sesti F, Giraudo MT, Virginio C, Cattaneo A, Torre V (1993) Single-channel properties of cloned cGMP-activated channels from retinal rods. Proc R Soc Lond (B) 254:69-74

Noble D, Tsien RW (1968) The kinetics and rectifier properties of the slow potassium current in calf Purkinje fibers. J Physiol 195:185-214

Noma A, Irisawa H (1976) Membrane currents in the rabbit sinoatrial node cell as studied by the double microelectrode method. Pflügers Arch 366:45-52

North A (1995) Handbook of receptors and channels. CNC Press, 1-151

Numa S (1989) A molecular view of neurotransmitter receptors and ionic channels. In: Kaback HR, Kirschner MW, Numa S, et al., editors. The Harvey lectures, Series 1983. New York: Liss, pp. 121-165

Nunn BJ (1987) Ionic permeability ratios of the cyclic GMP-activated conductance in the outer segment membrane of salamander rods. J Physiol 394, 17P

Oda Y, Timpe LC, McKenzie RC, Sauder DN, Largman C, Mauro T (1997) Alternatively spliced forms of the cGMP-gated channel in human keratinocytes. FEBS Lett 414:140-145

Pallanck L, Ganetzky B (1994) Cloning and characterization of human and mouse homologs of the *Drosophila* calcium-activated potassium channel gene, slowpoke. Hum Mol Gen 3:1239-1243

Paoletti P, Young EC, Siegelbaum SA (1999) C-linker of cyclic nucleotide-gated channels controls coupling of ligand binding to channel gating. J Gen Physiol 113:17-33

Papazian DM, Schwarz TL, Tempel BL, Jan YN, Jan LY (1987) Cloning of genomic and complementary DNA from Shaker, a putative potassium channel gene from *Drosophila*. Science 237: 749-753

Pape HC (1992) Adenosine promotes burst activity in guinea-pig geniculocortical neurons through two different ionic mechanisms. J Physiol 447:729-753

Pape HC (1996) Queer current and pacemaker: the hyperpolarization-activated cation current in neurons. Annu Rev Physiol 58:299-327

Pare D, Llinas R (1995) Conscious and pre-conscious processes as seen from the standpoint of sleep-waking cycle neurophysiology. Neuropsychologia 33:1155-1168

Pascual JM, Shieh CC, Kirsch GE, Brown AM (1995) K^+ pore structure revealed by reporter cysteines at inner and outer surfaces. Neuron 14:1055-1063

Pedarzani P, Storm JF (1995) Protein kinase A-independent modulation of ion channels in the brain by cyclic AMP. Proc Natl Acad Sci USA 92:11716-11720

Picco C, Menini A (1993) The permeability of the cGMP-activated channel to organic cations in retinal rods of the tiger salamander. J Physiol 460:741-758

Picones A, Korenbrot JI (1995a) Permeability and interaction of Ca^{2+} with cGMP-gated ion channels differ in retinal rod and cone photoreceptors. Biophys J 69:120-127

Picones A, Korenbrot JI (1995b) Spontaneous, ligand-independent activity of the cGMP-gated ion channels in cone photoreceptors of fish. J Physiol 485:699-714

Pittler SJ, Lee AK, Altherr MR, Howard TA, Seldin MF, Hurwitz RL, Wasmuth JJ, Baehr W (1992) Primary structure and chromosomal localization of human and mouse rod photoreceptor cGMP-gated cation channel. J Biol Chem 267:6257-6262

Pongs O, Kecskemethy N, Müller R, Krah-Jentgens I, Baumann A, Kiltz HH, Canal I, Llamazares S, Ferrus A (1988) *Shaker* encodes a family of putative potassium channel proteins in the nervous system of *Drosophila*. EMBO J 7:1087-1096

Prystowsky EN, Grant AO, Wallace AG, Strauss HC (1979) An analysis of the effects of acetylcholine on conduction and refractoriness in the rabbit sinus node. Circ Res 44:112-120

Quandt FN, Nicol GD, Schnetkamp PPM (1991) Voltage-dependent gating and block of the cyclic GMP-dependent current in bovine rod outer segments. Neurosci 42:629-638

Rieke F, Schwartz EA (1994) A cGMP-gated current can control exocytosis at cone synapses. Neuron 13:863-873

Root MJ, MacKinnon R (1993) Identification of an external divalent binding site in the pore of a cGMP-activated channel. Neuron 11:459-466

Root MJ, MacKinnon R (1994) Two identical noninteracting sites in an ion channel revealed by photon transfer. Science 265:1852-1856

Ruiz ML, Karpen JW (1997) Single cyclic nucleotide-gated channels locked in different ligand-bound states. Nature 389:389-392

Ruiz ML, Karpen JW (1999) Opening mechanism of a cyclic nucleotide-gated channel based on analysis of single channels locked in each liganded state. J Gen Physiol 113:873-895

Ruiz ML, London B, Nadal-Ginard B (1996) Cloning and characterization of an olfactory cyclic nucleotide-gated channel expressed in mouse heart. J Molec Cell Cardiol 2828:1453-1461

Sambrook J, Fritsch EF, Maniatis T (1989) Molecular cloning: a laboratory manual. 2nd ed. Cold Spring Harbor Laboratory Press, Cold Spring Harbor, New York.

Santoro B, Grant SGN, Bartsch D, Kandel ER (1997) Interactive cloning with the SH3 domain of N-src identifies a new brain specific ion channel protein, with homology to Eag and cyclic nucleotide-gated channels. Proc Natl Acad Sci USA 94:14815-14820

Santoro B, Liu DT, Yao H, Bartsch D, Kandel ER, Siegelbaum SA, Tibbs GR (1998) Identification of a gene encoding a hyperpolarization-activated pacemaker channel of brain. Cell 93:717-729

Santoro B, Tibbs GR (1999) The HCN gene family: molecular basis of the hyperpolarization-activated pacemaker channels. Ann NY Acad Sci 868:741-764

Sautter A, Biel M, Hofmann F (1997) Molecular cloning of cyclic nucleotide-gated cation channel subunits from rat pineal gland. Brain Res Mol Brain Res 48:171-175

Sautter A, Zong X, Hofmann F, Biel M (1998) An isoform of the rod photoreceptor cyclic nucleotide-gated channel β-subunit expressed in olfactory neurons. Proc Natl Acad Sci USA 95:4696-4701

Schreiber M, Wei A, Yuan A, Gaut J, Saito M, Salkoff L (1998) Slo3, a novel pH-sensitive K^+ channel from mammalian spermatocytes. J Biol Chem 273:3509-3516

Schempf H, Schmidt O, Kummerlen R, Hinnah S, Muller D, Betzler M, Steinkamp T, Wagner R (1995) A procaryotic potassium ion channel with two predicted transmembrane segments from *Streptomyces lividans*. EMBO J 14:5170-5178

Scott SP, Harrison RW, Weber IT, Tanaka JC (1996) Predicted ligand interactions of 3', 5'-cyclic nucleotide-gated channel binding sites: comparison of retina and olfactory binding site models. Protein Eng 4:333-344

Seifert R, Eismann E, Ludwig J, Baumann A, Kaupp UB (1999a) Molecular determinants of a Ca^{++}-binding site in the pore of cyclic nucleotide-gated channels: S5/S6 segments control affinity of intrapore glutamates. EMBO J 18:119-130

Seifert R, Scholten A, Gauss R, Mincheva A, Lichter P, Kaupp UB (1999b) Molecular characterization of a slowly gating human hyperpolarization-activated channel

predominantly expressed in thalamus, heart, and testis. Proc Natl Acad Sci USA 96:9391-9396

Sentenac H, Bonneaud N, Minet M, Lacroute F, Salmon JM, Gaymard F, Grignon C (1992) Cloning and expression in yeast of a plant potassium ion transport system. Science 256:663-665

Sesti F, Eismann E, Kaupp UB, Nizzari M, Torre V (1995) The multi-ion nature of the cGMP-gated channel from vertebrate rods. J Physiol (Lond) 487:17-36

Sesti F, Nizzari M, Torre V (1996) Effect of changing temperature on the ionic permeation through the cyclic GMP-gated channel from vertebrate photoreceptors. Biophys J 70:2616-2639

Sesti F, Straforini M, Lamb TD, Torre V (1994) Properties of single channels activated by cyclic GMP in retinal rods of the tiger salamander. J Physiol (Lond) 474:203-222

Shabb JB, Corbin JD (1992) Cyclic nucleotide binding domains in proteins having diverse functions. J Biol Chem 267:5723-5726

Shabb JB, Ng L, Corbin JD (1990) One amino acid change produces a high affinity cGMP-binding site in cAMP-dependent protein kinase. J Biol Chem 265:16031-16034

Shapiro MS, Zagotta WN (1998) Stoichiometry arrangement of heteromeric olfactory cyclic nucleotide-gated ion channels. Proc Natl Acad Sci USA 95:14546-14551

Shen J, Watanabe S-I, Kaneko A (1995) Cell dissociation with papain reduces the density of cGMP-activated channels of the retinal rod. Jpn J Physiol 45:151-164

Shi W, Wymore R, Yu H, Wu J, Wymore RT, Pan Z, Robinson RB, Dixon JE, McKinnon D, Cohen IS (1999) Distribution and prevalence of hyperpolarization-activated cation channel (HCN) mRNA expression in cardiac tissues. Circ Res 85:e1-16

Singer W, Gray CM (1995) Visual feature integration and the temporal correlation hypothesis. Annu Rev Neurosci 18:555-586

Sklar PB, Anholt RRH, Snyder SH (1986) The odorant-sensitive adenylate cyclase of olfactory receptor cells. Differential stimulation by distinct classes of odorants. J Biol Chem 261:15538-15543

Smith PL, Baukrowitz TM, Yellen G (1996) The inward rectifier mechanism of the HERG cardiac potassium channel. Nature 379:833-836

Solomon JS, Nerbonne JM (1993) Hyperpolarization-activated currents in isolated superior colliculus-projecting neurons from rat visual cortex. J Physiol 462:393-420

Soltesz I, Lightowler S, Leresche N, Jassik-Gerschenfeld D, Pollard CE, Crunelli V (1991) Two inward currents and the transformation of low-frequency oscillations of rat and cat thalamocortical cells. J Physiol 441:175-197

Starkus JG, Kuschel L, Rayner MD, Heinemann SH (1997) Ion conduction through C-type inactivated *Shaker* channels. J Gen Physiol 110:539-550

Steriade M, Deschênes M (1984) The thalamus as a neuronal oscillator. Brain Res 320:1-63

Steriade M, McCormick DA, Sejnowski TJ (1993) Thalamocortical oscillations in the sleeping and aroused brain. Science 262:679-685

Stern JH, Kaupp UB, MacLeish PR (1986) Control of the light regulated current in rod photoreceptors by cyclic GMP, calcium and *l-cis*-diltiazem. Proc Natl Acad Sci USA 83:1163-1167

Stryer L (1987) Visual transduction: design and recurring motifs. Chem Scr 27B:161-171

Su Y, Dostmann WR, Herberg FW, Durick K, Xuong NH, Ten Eyck L, Taylor SS, Varughese KI (1995) Regulatory subunit of protein kinase A: structure of deletion mutant with cAMP binding domains. Science 269:807-813

Suarez SS, Varosi SM, Dai X (1993) Intracellular calcium increases with hyperactivation in intact, moving hamster sperm and oscillates with the flagellar beat cycle. Proc Natl Acad Sci USA 90:4660-4664

Sudlow LC, Huang R-C, Green DJ, Gilette R (1993) cAMP-activated Na^+ current of molluscan neurons is resistant to kinase inhibitors and is gated by cAMP in the isolated patch. J Neurosci 13:5188-5193

Sun Z-P, Akabas MH, Goulding EH, Karlin A, Siegelbaum SA (1996) Exposure of residues in the cyclic nucleotide-gated channel pore: P region structure and function in gating. Neuron 16:141-149

Sunderman ER, Zagotta WN (1999a) Mechanism of allosteric modulations of rod cyclic nucleotide-gated channels. J Gen Physiol 113:601-619

Sunderman ER, Zagotta WN (1999b) Sequence of events underlying the allosteric transition of rod cyclic nucleotide-gated channels. J Gen Physiol 113:621-640

Tang CY, Papazian DM (1997) Transfer of voltage independence from a rat olfactory channel to the *Drosophila* ether-a-go-go K^+ channel. J Gen Physiol 109:301-311

Taylor SS, Buechler JA, Yonemoto W (1990) cAMP-dependent protein kinase: framework for a diverse family of regulatory enzymes. Annu Rev Biochem 59:971-1005

Tempel BL, Papazian DM, Schwartz TL, Jan YN, Jan LY (1987) Sequence of a probable potassium channel component encoded at the *Shaker* locus of *Drosophila*. Science 237:770-775

Tibbs GR, Goulding EH, Siegelbaum SA (1997) Allosteric activation and tuning of ligand efficacy in cyclic nucleotide-gated channels. Nature 386:612-615

Torre V, Menini A (1994) Selectivity and single channel properties of the cGMP-activated channel in amphibian retinal rods. In "Handbook of membrane channels", Academic Press, 345-358

Torre V, Straforini M, Sesti F, Lamb TD (1992) Different channel-gating properties of two classes of cyclic GMP-activated channels in vertebrate photoreceptors. Proc R Soc B 250:209-215

Trudeau MC, Warmke JW, Ganetzky B, Robertson GA (1995) Herg, a human inward rectifier in the voltage-gated potassium channel family. Science 269:92-95

Vaca L, Stieber J, Zong X, Ludwig A, Hofmann F, Biel M (2000) Mutations in the S4 domain of a pacemaker channel alter its voltage dependence. FEBS Lett 479:35-40

Vaccari T, Moroni A, Rocchi M, Gorza L, Bianchi ME, Beltrame M, DiFrancesco D (1999) The human gene coding for HCN2, a pacemaker channel of the heart. Biochim Biophys Acta 1446:419-425

Varnum MD, Black KD, Zagotta WN (1995) Molecular mechanism for ligand discrimination of cyclic nucleotide-gated channels. Neuron 15:619-625

Varnum MD, Zagotta WN (1996) Subunits interactions in the activation of cyclic nucleotide-gated ion channels. Biophys J 70:2667-2679

Vassalle M (1966) Analysis of cardiac pacemaker potential using a voltage clamp technique. Am J Physiol 210:1335-1341

von Krosigk M, Bal T, McCormick DA (1993) Cellular mechanisms of a synchronized oscillation in the thalamus. Science 261:361-364

Ward CR, Kopf GS (1993) Molecular events mediating sperm activation. Dev Biol 158:9-34

Warmke JW, Drysdale R, Ganetzky B (1991) A distinct potassium channel polypeptide encoded by the *Drosophila eag* locus. Science 252:1560-1562

Warmke JW, Ganetzky B (1994) A family of potassium channel genes related to *eag* in *Drosophila* and mammals. Proc Natl Acad Sci USA 91:3438-3442

Watanabe S-I, Matthews G (1988) Regional distribution of cGMP-activated ion channels in the plasma membrane of the rod photoreceptor. J Neurosci 8:2334-2337

Watanabe S-I, Shen J (1997) Two opposite effects of ATP on the apparent sensitivity of the cGMP-gated channel of the carp retinal cone. Vis Neurosci 14:609-615

Weber I, Shabb J, Corbin J (1989) Predicted structures of cGMP-binding domains of the cGMP-dependent protein kinase: a key alanine/threonine difference in evolutionary divergence of cAMP and cGMP binding sites. Biochemistry 28:6122-6127

Weber IT, Steitz TA (1987) Structure of a complex of catabolite gene activator protein and cyclic AMP refined at 2.5 Å. J Mol Biol 198:311-326

Weber IT, Steitz TA, Bubis J, Taylor SS (1987) Predicted structures of cAMP binding domains of type I and II regulatory subunits of cAMP-dependent protein kinase. Biochemistry 26:343-351

Wei A, Covarrubias A, Butler A, Baker K, Pak M, Salkoff L (1990) K^+ current diversity is produced by an extended gene family conserved in *Drosophila* and mouse. Science 248:599-603

Wei J-Y, Roy DS, Leconte L, Barnstable CJ (1998) Molecular and pharmacological analysis of cyclic nucleotide-gated channel function in the central nervous system. Prog Neurobiol 56:37-64

Weidmann S (1951) Effect of current flow on membrane potential of cardiac muscle. J Physiol 115:227-236

Weitz D, Zoche M, Müller F, Beyermann M, Körschen HG, Kaupp UB, Koch K-W (1998) Calmodulin controls the rod photoreceptor CNG channel through an unconventional binding site in the N-terminus of the β-subunit. EMBO J 17:2273-2284

West TC (1955) Ultramicroelectrode recording from the cardiac pacemaker. J Pharm Exp Ther 115:283-290

Weyand I, Godde M, Frings S, Weiner J, Müller F, Altenhofen W, Hatt H, Kaupp UB (1994) Cloning and functional expression of a cyclic nucleotide-gated channel from mammalian sperm. Nature 368:859-863

Wissinger B, Müller F, Weyand I, Schuffenhauer S, Thanos S, Kaupp UB, Zrenner E (1997) Cloning, chromosomal localization and functional expression of the gene encoding the alpha-subunit of the cGMP-gated channel in human cone photoreceptors. Eur J Neurosci 9:2512-2521

Wollmuth LP (1995) Multiple ion binding sites in I_h channels of rod photoreceptors in tiger salamander. Pflügers Arch 430:34-43

Wollmuth LP, Hille B (1992) Ionic selectivity of I_h channels of rod photoreceptors in tiger salamanders. J Gen Physiol 100:749-765

Yanagihara K, Irisawa W (1980) Inward current activated during hyperpolarization in the rabbit sino atrial node cell. Pflügers Arch 385:11-19

Yang J, Ellinor PT, Sather WA, Zhang J-F, Tsien RW (1993) Molecular determinants of Ca^{2+} selectivity and ion permeation in L-type Ca^{2+} channels. Nature 366:158-161

Yang N, George AL Jr, Horn R (1996) Molecular basis of charge movement in voltage-gated sodium channels. Neuron 16:113-122

Yang N, Horn R (1995) Evidence for voltage-dependent S4 movement in sodium channels. Neuron 15:213-218

Yau K-W, Baylor D (1989) Cyclic-GMP activated conductance of retinal photoreceptor cells. Annu Rev Neurosci 12:289-327

Yau K-W, Nakatani K (1984) Cation selectivity of light-sensitive conductance in retinal rods. Nature 309:352-354

Yau K-W, Nakatani K (1985a) Light-induced reduction of cytoplasmic free calcium in retinal rod outer segment. Nature 313:579-582

Yau K-W, Nakatani K (1985b) Light-suppressible, cyclic GMP-sensitive conductance in the plasma membrane of a truncated rod outer segment. Nature 317:252-255

Yellen G (1998) The moving parts of voltage-gated ion channels. Q Rev Biophys 31:239-295

Yellen G, Sodickson D, Chen T-Y, Jurman ME (1994) An engineered cysteine in the external mouth of a K^+ channel allows inactivation to be modulated by metal binding. Biophys J 66:1068-1075

Yoshizawa T, Wald G (1963) Nature 197:1279-1286

Yu H, Chang F, Cohen IS (1995) Pacemaker current i_f in adult canine cardiac ventricular myocites. J Physiol 485:469-483

Yu WP, Grunwald ME, Yau KW (1996) Molecular cloning, functional expression and chromosomal localization of a human homolog of the cyclic nucleotide-gated ion channel of retinal cone photoreceptors. FEBS Lett 393:211-215

Yusaf SP, Wray D, Sivaprasadarao A (1996) Measurement of the movement of the S4 segment during the activation of a voltage-gated potassium channel. Eur J Physiol 433:91-97

Zagotta WN, Siegelbaum SA (1996) Structure and function of cyclic nucleotide-gated channels. Annu Rev Neurosci 19:135-263

Zhang Q, Pearce-Kelling S, Acland GM, Aguirre GD, Ray K (1997) Canine rod photoreceptor cGMP-gated channel protein α-subunit: studies on the expression of the gene and characterization of the cDNA. Exp Eye Res 65:301-309

Zimmermann AL, Baylor DA (1986) Cyclic GMP-sensitive conductance of retinal rods consists of aqueous pores. Nature 321:70-72

Zimmermann AL, Baylor DA (1992) Cation interactions within the cyclic GMP-activated channel of retinal rods from the tiger salamander. J Physiol 449:759-783

Zong X, Zucker H, Hofmann F, Biel M (1998) Three amino acids in the C-linker are major determinants of gating in cyclic nucleotide-gated channels. EMBO J 17:353-362

Zufall F, Firestein S (1993) Divalent cations block the cyclic nucleotide-gated channels of olfactory receptor neurons. J Neurophys 69:1758-1768

Zufall F, Firestein S, Shepherd GM (1994) Cyclic nucleotide-gated ion channels and sensory transduction in olfactory receptor neurons. Annu Rev Biophys Biomol Struct 23:577-607

Zufall F, Leinders-Zufall T (1997) Identification of a long-lasting form of odor adaptation that depends on the carbon monoxide/cGMP second messenger system. J Neurosci 17:2703-2712